[American Journal of Science, Vol. 307, October, 2007, P. 1051–1139, DOI 10.2475/08.2007.01]

American Journal of Science

OCTOBER 2007

INSIGHTS INTO MANTLE MELTING FROM GRAPHICAL ANALYSIS OF ONE-COMPONENT SYSTEMS

EDWARD STOLPER and PAUL ASIMOW

Division of Geological and Planetary Sciences, California Institute of Technology
Pasadena, California 91125 USA; ems@gps.caltech.edu

1. ABSTRACT. Decompression melting can be approximated as an isentropic (that is, reversible adiabatic) process. In such a process, specific entropy (S) and pressure (P) are the independent variables and equilibrium is achieved when the specific enthalpy (H) of the system reaches a minimum. We present a largely graphical analysis of decompression melting in one-component systems based on phase equilibria in H-P-S space. Although mantle sources contain more than one component, use of one-component model systems provides insights into several aspects of mantle melting that can be generalized to more complete and complex systems (for example, batch vs. fractional fusion; the influence of pressure-dependent solid-solid reactions on melting; melting of multilithologic mixtures such as peridotite plus eclogite; advection of heat and melting by rising magmas) and places these insights into the visualizable framework of simple phase diagrams.

2. INTRODUCTION

Igneous activity is one of the most important of all planetary phenomena: It is the principal mechanism by which planetary interiors differentiate chemically; the generally upward motion of magmas relative to solids can advect significant energy toward planetary surfaces; intrusion of magma at shallow levels and extrusion on the surface are the principal mechanisms by which planetary crusts form; these processes ultimately provide the raw material that is weathered, reworked, and remobilized by near-surface geologic processes; and the eruption of magma at the surface has geomorphic expression and in many cases can have substantial influence on climate.

As with most geological phenomena, igneous processes are complex and, as a result, geologists (students and professionals alike) have long relied on phase diagrams in compositionally simple model systems as frameworks for visualizing, understanding, and analyzing igneous phenomena in more complex natural systems. Thus, for example, given a particular magma composition at a constant pressure (P), generations of geologists have learned to follow crystallization paths on cooling using temperature (T) versus composition (X) diagrams in binary systems (with their familiar eutectics, peritectics, phase loops, azeotropes, solvi, *et cetera*) and polythermal liquidus diagrams in ternary systems (with their familiar configurations of isotherms traversing primary liquidus fields, cotectics leading to ternary eutectics, minima, critical end points, *et cetera*). These same simple diagrams can be used to analyze aspects of isobaric melting and more complex processes such as metasomatism, magma mixing, and assimilation. Although these simple phase diagrams are incomplete models of actual magmatic systems, many of the processes that occur in natural systems can be understood by analogy with them and, most importantly, these phase diagrams often make it possible to visualize complex processes in relatively simple terms. Their staying power in earth science reflects the easy to understand yet powerful

framework for interpreting and understanding complex natural phenomena that they provide (Bowen, 1928; Morse, 1994).

Decompression melting is generally accepted as the most important process by which magmas form in the earth's mantle. In general terms, decompression melting refers to the process by which parcels of ascending solid mantle (ascending, for example, in response to plate spreading at a mid-ocean ridge, as part of a regional upwelling in the overall mantle circulation pattern, or in buoyant plumes) first intersect the solidus during decompression and then undergo progressive melting with further ascent. To our knowledge, the first clear, modern description of the process is due to Verhoogen (1954), although the possibility that decompression in the earth's interior could lead to melting dates from the mid-1800s (see Sigurdsson, 2000), and Bowen (1928, Chapter XVII) articulated clearly the likely adiabatic nature of such a process and its consequences. Although this is arguably the most significant of all terrestrial igneous processes and it has a very long history in the geological literature, it cannot be modeled or readily visualized within the framework of familiar phase diagrams. The problem is basically that familiar binary and ternary phase diagrams are constructed based on the choice of P, T, and X as the independent variables. For processes in which P, T, and composition are "specified" (that is, in which they are *independent* variables — imagine these variables as "knobs" that we can turn to drive the system along a path, while the conditions of equilibrium within the system determine all the remaining, *dependent*, variables), these familiar phase diagrams are useful for evaluating equilibrium assemblages and how they evolve with changes in these variables. So, if we consider a magma cooling at constant pressure (we set the pressure by adjusting one of our knobs) in which we want to evaluate the phases that crystallize and the evolving liquid composition as a function of temperature (a second knob that we can adjust at will), these diagrams are very useful, and it is for this reason that there is so much focus on these diagrams, since processes such as isobaric crystallization are important for understanding the observed compositional diversity of igneous rocks. However, P, T, and composition are *not* the independent variables during decompression melting, and thus the familiar phase diagrams — designed to evaluate processes in which they are — are incomplete as frameworks for modeling or visualizing this process.

The limitations of thinking about P and T as the "knobs" that are independently turned during decompression melting can be understood with figure 1, which shows the usual portrayal of adiabatic decompression melting. The concept of adiabaticity is critical: that is, the region of ascending mantle is assumed to be sufficiently large and ascending sufficiently fast that the flow of heat into or out of it can be neglected (there are other assumptions built into this analysis; these will be explained in more detail below). Imagine a parcel of mantle starting at point *1*. The way to envision its decompression is that we have one hand on the knob for pressure, and we turn it, decreasing the pressure continuously; however, we keep our other hand off of the temperature knob. From *1*→*2*, as we decrease the pressure by turning its knob, the temperature decreases slightly by an amount that depends on the decrease in pressure (even though we have not turned the temperature knob; it is as if the temperature knob turns on its own in response to our turning of the pressure knob). In other words, pressure is an independent variable in this process, but temperature, although a well-defined function of the pressure, is a dependent variable; the curve describing their relationship is called an adiabat (because we have specified that no heat can flow in or out of our mantle parcel). Because the solidus is steeper in P-T space than the adiabat of the solid, the ascending solid mantle intersects the solidus at *2*, and the mantle begins to melt. From *2*→*3*, the ascending mantle melts progressively, and the rate at which the temperature decreases as we turn the pressure knob is higher than it

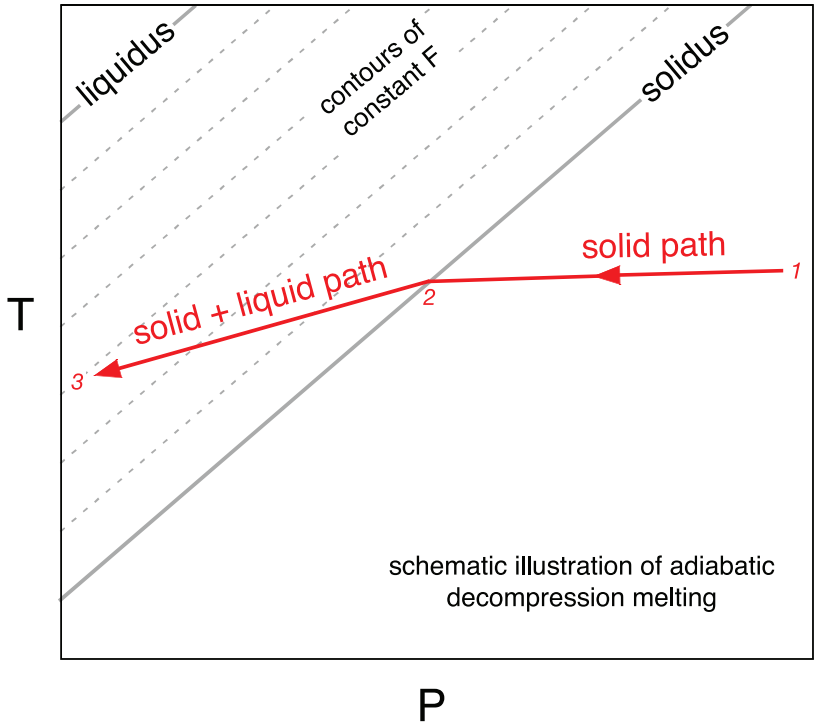

Fig. 1. Schematic P-T diagram showing a representative decompression melting path of a mantle source. The parallel solidus, liquidus, and contours of constant degree of melting are schematic.

was from *1*→*2* because, given the adiabatic constraint, the heat of fusion must be supplied by cooling of the ascending material. It is generally accepted that this simple picture explains melt production under mid-ocean ridges (Klein and Langmuir, 1987) and "hot spot" volcanoes such as Hawaii and Iceland (Watson and McKenzie, 1991; Thompson and Gibson, 2000); it may also play an important role in island arc magmatism (Plank and Langmuir, 1988; Sisson and Bronto, 1998) and in the generation of continental flood basalts and other so-called "large igneous provinces" (McKenzie and Bickle, 1988; Richards and others, 1989; Campbell and Griffiths, 1990; Basu and others, 1998; Thompson and Gibson, 2000).

What is important at this point are not the details but that temperature is a dependent rather than an independent variable for this process; that is, it is well defined at each pressure on the path *1*→*2*→*3* given the starting point *1*, but it is neither constant nor independently variable (that is, set by an arbitrary turn of the temperature knob at each pressure along the path). Consequently, phase diagrams in which temperature is an independent variable are not very useful for understanding or visualizing this process, and it is for this reason that figure 1 and the description we have given of it is usually where the analysis ends. The kinds of questions that phase diagrams are so useful at answering, such as how the proportions of solid and liquid change as the parcel of mantle ascends from *2*→*3*, how batch and fractional melting differ during decompression melting, and so forth, cannot be addressed with this presentation or with any of the simple phase diagrams we ordinarily use since they all are based on the choice of temperature as an independent variable. To answer these and related questions with the usual binary T-X diagrams or polythermal ternary

liquidus diagrams would require a series of diagrams at different pressures, with an independent calculation of the appropriate T at the pressure of each diagram. The fact that this has not been widely done reflects how difficult and uninformative this approach would be.

As we show below, the independent variables for the idealized adiabatic decompression path shown in figure 1 are P, specific entropy (S)[1], and X. Thus, we can anticipate that, just as phase diagrams in which P, T, and X are the independent variables are useful as a framework for understanding processes such as isobaric crystallization, phase diagrams in which P, S, and X are the independent variables would be similarly valuable for analyzing decompression melting. The focus of this paper is to introduce and develop such phase diagrams for one-component systems and to illustrate how they can provide insights into melting processes. Although treatments of igneous processes using phase diagrams typically pass over one-component systems quickly, these deceptively simple systems offer valuable perspectives on many aspects of mantle melting. Indeed, the richness of one-component systems for understanding melting processes has been masked by the usual treatments of these systems using P and T as the independent variables; when the more appropriate variables P and S are taken as independent, the utility of one-component systems for analyzing a wide range of processes believed to be relevant to understanding petrogenesis (for example, batch vs. fractional melting; melting of heterogeneous mantle sources; the impact of solid-solid reactions on melting; interaction of ascending melts with their surroundings) becomes apparent. Although by neglecting composition as a variable we necessarily lose the opportunity to address issues related to compositional variability of the mantle and the important role played by compositional differences between coexisting phases in natural melting phenomena (in which P, S, and X must all be treated as independent variables — see the treatments in Asimow and others, 1997; Hirschmann and others, 1998a, 1998b, 1999a, 1999b; Smith and others, 2003), we hope to show in this paper that many of the most critical insights needed for thinking about mantle melting in thermodynamic terms can be gleaned from study of one-component systems.

Our objectives are two-fold: The first is pedagogical; we hope to provide a comprehensive introduction to the graphical analysis of mantle melting that will be accessible to graduate and advanced undergraduate students in the earth sciences. The second is to emphasize those aspects of melting phenomena that can be illustrated and illuminated by these phase diagrams and thereby to provide researchers in the field with a simple yet rigorous set of graphical tools than can serve as a useful framework for thinking about (and for better calibrating their intuitions about) these phenomena.

In this paper, we focus on the graphical analysis of phase diagrams to provide a basis for understanding melting processes. Although these diagrams and the graphical analysis we present all have straightforward analytic descriptions based on the underlying thermodynamics and in various places we present the relevant equations, we have banished the detailed derivations to an Appendix (section 14). The reasoning behind this is to make the presentation compatible with and comparable to the standard analysis of P-T-X phase diagrams for binary systems, to which the diagrams we present have topological similarities. Although such binary P-T-X diagrams also have rigorous analytic underpinnings, they are not usually critical to (and can even get in the way of) developing the powerful graphical insights that have made such phase diagrams so useful to generations of geologists, and the same is true for the phase diagrams

[1] We use italicized symbols to refer to total entropy (S), volume (V), *et cetera* (that is, to extensive properties) and regular text (S, V, *et cetera*) to refer to specific or molar properties (that is, to intensive properties).

presented here. Readers interested in the analytical aspects of the phase diagrams presented here are referred to Asimow and others (1995, 1997), where some of these details are presented, and to the complete treatments in the Appendix to this work. Note that some aspects of the graphical analysis of phase equilibria presented here were introduced in these previous papers, but the focus there was on the specific issue of melt productivity during decompression melting.

3. definition of the independent variables for decompression melting

As described above, decompression mantle melting is generally envisioned to be approximately adiabatic; that is, on the time scale of ascent, the heat (q) that flows into or out of the ascending source is assumed to be negligible. The following simple calculations based on McKenzie and Bickle (1988) demonstrate that this is likely to be a reasonable approximation. During melting under ridges there are no significant lateral temperature gradients, so we are not concerned with horizontal heat flow. The importance of vertical heat flow relative to advection is parameterized by the thermal Peclet number $Pe_T = vL/\kappa$, where v is upwelling velocity, L is the length scale of interest (the vertical extent of the melting regime), and κ is thermal diffusivity; processes for which $Pe_T \gg 1$ can be approximated as adiabatic. Taking a depth interval of melting under ridges of order 100 km and an ascent velocity of 5 cm/y (such that the time scale for traversing the depth interval over which melting takes place is ~2 million years) and assuming a thermal diffusivity of $\sim 10^{-2}$ cm^2/s, the Peclet number is ~100. A step function in temperature, which is an extreme case for driving thermal diffusion, would spread out by roughly 10 km while being advected 100 km upwards. Hence, the approximation of an adiabatic source is reasonable over most of the melting interval of mantle melting beneath mid-ocean ridges. Under hot spots, where the depth interval for melting is similar to ridges but estimates of ascent velocities are up to an order of magnitude or more higher, vertical heat flow is even smaller and horizontal heat flow from the margins of a 50 to 100 km plume conduit will only penetrate a few kilometers. Thus although there are interesting exceptions to the adiabatic assumption (for example, cooling by conduction to the overlying ocean floor can be important for slow spreading ridges; fluid or melt flow can advect heat into or out of the source), this is nevertheless an appropriate reference point for thinking about decompression melting.

Thus, from a thermodynamic perspective, adiabatic decompression melting can be described by a system with variable P and $q = 0$. We start with the first law of thermodynamics,

$$\mathrm{d}E = q + w = q - \mathrm{P}\mathrm{d}V, \tag{1}$$

where E is internal energy, w is the work done on the system, and V is volume. Note that this describes the behavior of a closed system (that is, one that can exchange energy but not matter with its environment), and although this could refer either to a multicomponent system of constant mass and composition or to a one-component system (which by definition cannot change composition), we will from this point forward limit our consideration to one-component systems. Differentiating the definition of enthalpy, H,

$$H = E + \mathrm{P}V, \tag{2}$$

we obtain

$$\mathrm{d}H = \mathrm{d}E + \mathrm{P}\mathrm{d}V + V\mathrm{dP}. \tag{3}$$

Substituting this into equation (1), we obtain

$$\mathrm{d}H = q + V\mathrm{dP}. \tag{4}$$

The entropy change in a closed system undergoing a reversible process is defined by

$$q = \mathrm{T}dS; \tag{5}$$

and the second law of thermodynamics states that for a closed system undergoing an irreversible process,

$$q < \mathrm{T}dS. \tag{6}$$

Substituting equations (5) and (6) into equation (4), we obtain the key relationship:

$$dH \leq \mathrm{T}dS + V\mathrm{d}P, \tag{7}$$

where the equality refers to a reversible process and the inequality refers to an irreversible or natural process. As mentioned above, V, S, H, and E in these equations all refer to total volume, entropy, *et cetera*, but we can divide both sides of equation (7) by total mass, yielding the equivalent expression in terms of specific enthalpy, specific entropy, and specific volume. Equation (7) then becomes:

$$\mathrm{dH} \leq \mathrm{TdS} + \mathrm{VdP}, \tag{8}$$

where the non-italicized symbols refer to properties per unit mass (that is, S is the total entropy of a system or phase, and S is the specific entropy).

We showed at the start of this section that upwelling mantle can be approximated as adiabatic for all but the smallest of diapirs (that is, as long as the upwelling region is at least about 5 – 10 km in diameter), but how close to reversible are processes such as melting that occur in these upwellings likely to be? This question is critical for the identification of the independent variables that describe decompression melting because if the melting process is both adiabatic and reversible, then the process is isentropic; that is, $\mathrm{dS} = \mathrm{q}/\mathrm{T} = 0$ for such a process based on equation (5), which would reduce the thermodynamic problem to the relatively straightforward one of evaluating the behavior of a system with two independent variables, S and P, one of which (S) is held constant. It is simple to see that in the limit of very slow ascent, adiabatic decompression melting can approach a reversible process: that is, if an adiabatic parcel of mantle that is at equilibrium rises an infinitesimal amount at a very slow rate and undergoes internal reactions such as melting to a new equilibrium state in response to the changing pressure, it is clear that if we recompressed it, we could return to the original condition on precisely the reverse of the original path. Any larger decompression could be broken down into a succession of infinitesimal decompressions, each of which reach equilibrium but could be undone by simply re-increasing the pressure. Although not all processes can be idealized in this way, any changes that can be broken down into a succession of equilibrium states can be treated as reversible phenomena (Prigogine and Defay, 1954) and thus, provided that decompression and melting take place slowly enough that the system is never far from equilibrium, decompression melting can be idealized as reversible and thus isentropic.

There have been several recent attempts to estimate the degree to which equilibrium is likely to be approached during decompression melting (for example, Qin, 1992; Spiegelman and Kenyon, 1992; Hart, 1993; Spiegelman and Elliott, 1993; Lundstrom and others, 1995; Van Orman and others, 1998). These efforts have focused on comparing the time scales for melt generation with the time scale required to wipe out by diffusion the zonation that develops between the cores and rims of residual crystals as melting proceeds. There is no unique answer, as the approach to equilibrium depends not only on the rates of ascent and of melt generation, on the relative velocities of melt and solid in the ascending mantle, and on grain size, but also on diffusion coefficients in the solids and on solid/liquid partition coefficients, which

differ for each element and for different residual phases. Moreover, difficult-to-quantify processes such as deformation, dissolution, and reprecipitation of the residual phases could result in significantly enhanced rates of exchange between melt and solid relative to the diffusive processes that have been modeled. Available calculations are not all in agreement about what conditions might be required to preserve significant zonation of highly incompatible (for example, solid/liquid partition coefficients of $<$ 0.01), slow-diffusing cations (for example, $D < 10^{-15}$ cm^2/s) such as U and Th in clinopyroxene. However, while these highly incompatible elements are all calculated to be near the boundary between a close approach to equilibrium and significant disequilibrium for reasonable grain sizes and melting rates, major elements have significantly higher bulk partition coefficients ($\sim$0.1 – 10) and can diffuse significantly faster than these trace elements (for example, up to 4 – 6 orders of magnitude faster for Mg in olivine, spinel, and garnet). Both of these factors decrease significantly the time scales required for diffusive equilibrium (Hart, 1993), so conditions under which highly incompatible elements are marginal with respect to diffusive equilibrium are likely to be highly equilibrated for the major elements that constitute most of the mass of the system. We thus consider it likely that at each stage of their ascent, partially molten source regions are close to equilibrium, and we adopt the reversible adiabatic approximation as our starting point for evaluating decompression melting in the mantle. We emphasize, however, that a reversible adiabatic path is only an idealization as there are several sources of irreversibility (for example, viscous dissipation during melt extraction, overstepping of reaction boundaries, diffusion in zoned crystals) that may under some circumstances be significant. Moreover, even if the system as a whole is adiabatic and each increment of melt generation is nearly reversible, there are likely to be important local deviations from adiabaticity and reversibility due to the motion of melt relative to residual solids in regions undergoing melting. McKenzie (1984), Asimow and Stolper (1999), and Asimow (2002) evaluated the impact of several of these sources of irreversibility on melting phenomena and the magnitude of the entropy increases to which they correspond; these quantitative treatments strongly support the adiabatic, reversible approximation as an accurate starting point for modeling decompression melting. We will, however, analyze one of these complexities in detail below (the advection of heat by ascending melt; see section 11) since it is potentially important in mantle melting.

Thus, the independent thermodynamic variables on the path *1→2→3* shown in figure 1 are S, P, and composition; and, in particular, S and composition (assuming batch melting – see below) are held constant on this path as P decreases. The inequality in equation (8) indicates that for a choice of S and P as independent variables, H is minimized at equilibrium subject to infinitesimal perturbations in these variables. The concept of enthalpy minimization at equilibrium is a critical one for the development of the phase diagrams we will use to describe decompression melting: For any choice of S and P, the equilibrium state will be one characterized by a minimum in H, and thus a diagram showing equilibrium states as functions of S and P will be a map of assemblages of minimum H. The Gibbs free energy (G) is the thermodynamic potential minimized for the choice of P, T, and X as independent variables, and thus the more familiar P-T-X phase diagrams are maps of minimum-G assemblages as functions of these variables.

It should be emphasized that although the isentropic path *1→2→3* in figure 1 is often referred to as "*the* adiabat", it is just one of an infinite number of adiabatic paths from the same initial P and T. Shock compression and isenthalpic or Joule-Thomson expansions are also adiabatic but are not isentropic. Although this reversible adiabat (or isentrope) is, as explained above, a useful reference, it is by no means the only useful one in evaluating petrological processes (and indeed, since no real process is

truly reversible, S must in reality increase during decompression melting, and the isentrope is a limiting case never actually achieved). Analogous use of isentropic approximations for adiabatic processes is common in analysis of fluid-dynamic expansions including volcanic eruptions (Kieffer and Delany, 1979), stream flow (Kieffer, 1989), and release from shock states (Ahrens, 1987). Care must be taken to specify the details of the particular adiabat being considered and not to assume that all adiabats are identical or equally applicable. Otherwise, confusion can result: for example, as described below (see section 7), other adiabatic paths have been widely used to model decompression melting (for example, Hess, 1989, 1992; Langmuir and others, 1992). Although not wrong in any sense – they are indeed adiabatic – they include explicitly irreversible steps, so they are not isentropic and not necessarily good descriptions of decompression melting. Some authors have argued that adiabatic decompression melting should be modeled as an irreversible process akin to Joule-Thompson expansion. Waldbaum (1971) made this assumption but arrived at erroneous results by excluding gravitational potential energy from his definition of enthalpy, as pointed out by Ramberg (1971). More recently, Ganguly (2005) has revived this approach with a discussion that assumes that melting induced buoyancy will drive an irreversible accelerating upwelling. However, upwelling mantle flows are generally well approximated as creeping flows with negligible inertia (McKenzie, 1984), and thus we take reversible flow as our starting point. This leads to the well-defined isentropic end-member approximation to the energetic constraints on mantle melting, to which known sources of irreversibility can be added to arrive at an exact description.

An important petrological example of an irreversible adiabatic process that we will deal with in later sections is the achievement of thermal equilibrium between two parts of a system initially at different temperatures. If we specify that the pressure is constant and that no heat flows into or out of the system but allow heat to flow from the hotter to the cooler part of the system in order to achieve thermal equilibrium, then the system is isobaric and adiabatic but the process is irreversible. This is how we might describe thermal equilibration between two magmas at different initial temperatures or between a dike and its country rock. For such a system, $q = 0$ and $dP = 0$, and consequently, $dH = 0$ based on equation (4). Note that H here refers to the system as a whole, and although the total enthalpy of the system does not change, the specific enthalpy of each of the two parts of the system changes as thermal equilibrium is approached. We can rearrange equation (8) as follows:

$$dS > \frac{dH}{T} - \frac{VdP}{T} = 0, \tag{9}$$

Thus, for this system in which P and H are constant, heat flows irreversibly from the hot to the cold part of the system resulting in an increase in S. When the system reaches thermal equilibrium, S reaches a maximum (and is at a maximum relative to infinitesimal variations in H and P). This process, although adiabatic by definition, is clearly irreversible and bears little resemblance to the isentrope used to describe decompression melting. We could, however, develop phase diagrams in which H and P are the independent variables, and these would represent maps of the stable (that is, maximum S) assemblages as functions of H and P. As we shall see, such phase diagrams could be useful for visualizing a variety of processes of importance in mantle and crustal melting.

4. CONSTRUCTION OF A SIMPLIFIED H-S-P PHASE DIAGRAM

We are now ready to develop phase diagrams for one-component systems in which S and P are the independent variables. Based on equation (8), for a system at a given P and S, the equilibrium state is one of minimum H. The simplest way to visualize phase

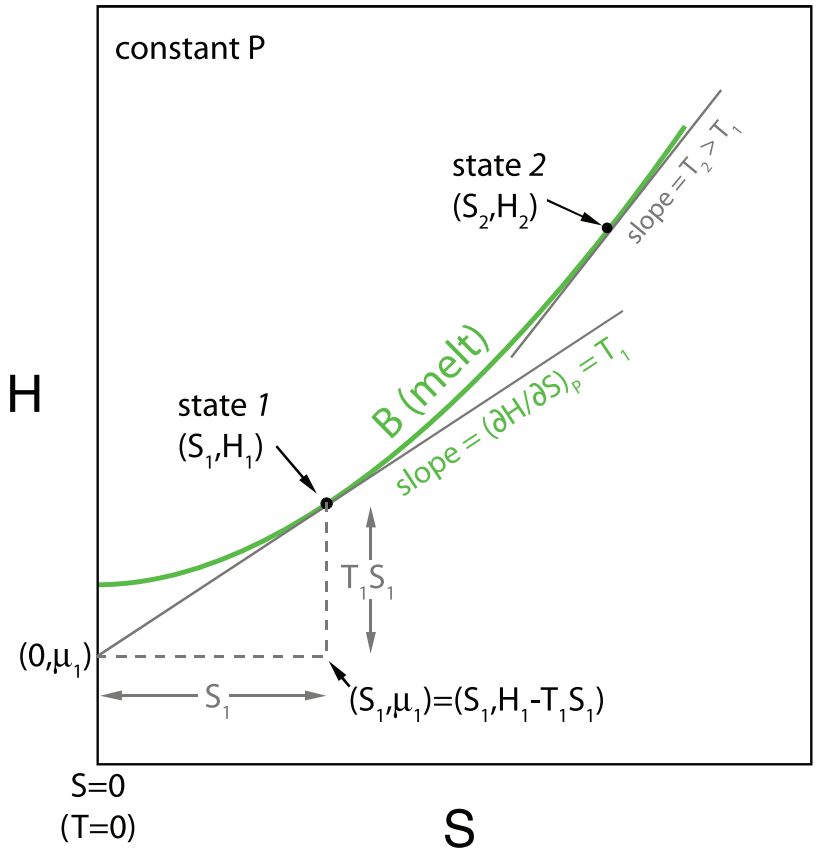

Fig. 2. Schematic isobaric H-S diagram for a single phase (arbitrarily chosen to be melt). The curve represents the locus of (S, H) coordinates for a stable (or metastable) phase at this pressure. Several simple geometric relationships are illustrated: the slope of the tangent to the curve at each point is equal to the temperature (T) and has an H intercept equal to the chemical potential (μ); the curve is drawn as horizontal at S = 0 (that is, T = 0); the stable curve must be concave up (that is, $(\partial^2 H/\partial^2 S)_P = T/C_P > 0$ since both T and C_P are positive), so T increases and μ decreases with increasing S.

equilibria in a one-component system subject to these constraints is with an H-S diagram at constant P (fig. 2). The accessible states of any stable phase (including metastable phases) define a curve on such a diagram; that is, for any stable phase, for a given choice of H and P, there is a well-defined value of S given by the H-S curve. Since the curve defines stable, equilibrium states, dH can be written as a total differential and the equality in equation (8) holds:

$$dH = \left(\frac{\partial H}{\partial S}\right)_P dS + \left(\frac{\partial H}{\partial P}\right)_S dP = TdS + VdP, \tag{10}$$

Thus, the slope of the tangent to this curve describing a stable phase, $(\partial H/\partial S)_P$, is T. Consequently, the H-S curve of a stable phase is positively sloped, except at T = 0, where the curve is horizontal. If Nernst's heat theorem applies, S = 0 at T = 0 (Prigogine and Defay, 1954, Chapter IX); if S ≠ 0 at T = 0 (as, for example, in liquids with residual configurational entropy), the curve terminates horizontally at S > 0. The second derivative of a phase's H-S curve, $(\partial^2 H/\partial S^2)_P$, is given by $(\partial T/\partial S)_P = T/C_P$,

where C_P is the isobaric heat capacity; thus the requirement that $C_P > 0$ for a stable phase (Prigogine and Defay, 1954, p. 213) means that the H-S curve for a stable phase must be concave upward (that is, convex toward the S axis). In other words, starting from any point on the curve, as heat is added to the system, H and S of the phase increase (that is, as the phase slides along the curve to the right) and the slope of the curve (T) increases; if the curve were concave down, it would require that temperature decreased as heat is added to the system, which is not possible. Note that $C_P = \infty$ for a critical phase (for example, Domb, 1996), which is still described by a concave upward H-S curve, but for which $(\partial^2 H/\partial S^2)_P = 0$, and that the H-S curve describing a phase between the spinodes (at each of which C_P is also infinite) for a system with a solvus would be concave down (that is, unstable). The final important aspect of the H-S diagram is that the H-intercept (that is, at S = 0) of the tangent to the curve describing the stable substance, H - TS, is equal to μ, the chemical potential.

As an aside, it is possible to prove graphically that a stable phase must have a concave upward H-S curve (that is, that $C_P > 0$). Suppose the H-S curve describing a phase were concave down as shown in figure 3A. If so, it would be possible to have an initially homogeneous phase at a given H, S and P (state *i*) undergo an isobaric, adiabatic fluctuation (indicated by the red arrow) whereby it would break down into two materials (states *ii* and *iii*) with a higher total S (the red arrow is horizontal since the total H cannot change because the hypothetical fluctuation occurs at constant P and for q = 0). Such an increase in S would occur for any fluctuation, and would correspond to a "natural" (that is, irreversible) process, so the initial state could not have been stable since it would spontaneously and irreversibly break down into a mixture of states *ii* and *iii* with an increase in S. In contrast and as shown in figure 3B, only if the H-S curve is concave up will spontaneous fluctuations from state *i* to a mixture of states *ii* and *iii* lead to a decrease in S; such processes cannot occur naturally and the initial state *i* is stable relative to such fluctuations.

Figure 4 shows an isobaric H-S diagram for a one-component system with two phases, A and B; for convenience, we label phase A as solid and phase B as melt. Each phase is described by a separate concave-up curve. When phases A and B coexist, they must have the same temperature and the same chemical potential; thus, when A and B coexist, a single line must be tangent to the curves for both A and B (that is, such that the same slope, T, and intercept, μ, describes each of the coexisting phases). Examination of figure 4 shows that the two coexisting phases have different entropies and enthalpies [(S_1, H_1) for phase A coexisting with B and (S_2, H_2) for phase B coexisting with A]. This diagram can be used to visualize the stable (that is, minimum H) assemblages for any choice of S and P; likewise, it allows us to visualize the stable (that is, maximum S) assemblages for any choice of H and P. For all choices of S less than or equal to S_1, phase A has the lowest H. Phase B can be made as a metastable phase for such choices of S (that is, its state is well defined by a concave up H-S curve, but its specific enthalpy is higher than stable phase A with the same S). The temperature for stable phase A at values of $S < S_1$ is lower than the temperature at S_1, reflecting the concave upward nature of the stable curve for phase A; in addition, for this range of S, the slope of the B curve, and thus the temperature of metastable B, is lower than that of phase A at the same S for the diagram as drawn. For all values of S between S_1 and S_2, the lowest enthalpy available to the system is achieved by mixtures of phase A with (S_1, H_1) and phase B with (S_2, H_2). The lever rule applies to such mixtures, such that X_B, the mass fraction of phase B in the mixture, is $(S\text{-}S_1)/(S_2\text{-}S_1)$. The temperature is the same (that is, the same tangent applies) for all such mixtures; single-phase A (at higher T) or single-phase B (at lower T) can also exist for any value of S between S_1 and S_2, but their enthalpies are higher than the stable mixture, so they would be metastable. For choices of S greater than or equal to S_2 (and T higher than that at which phases A and

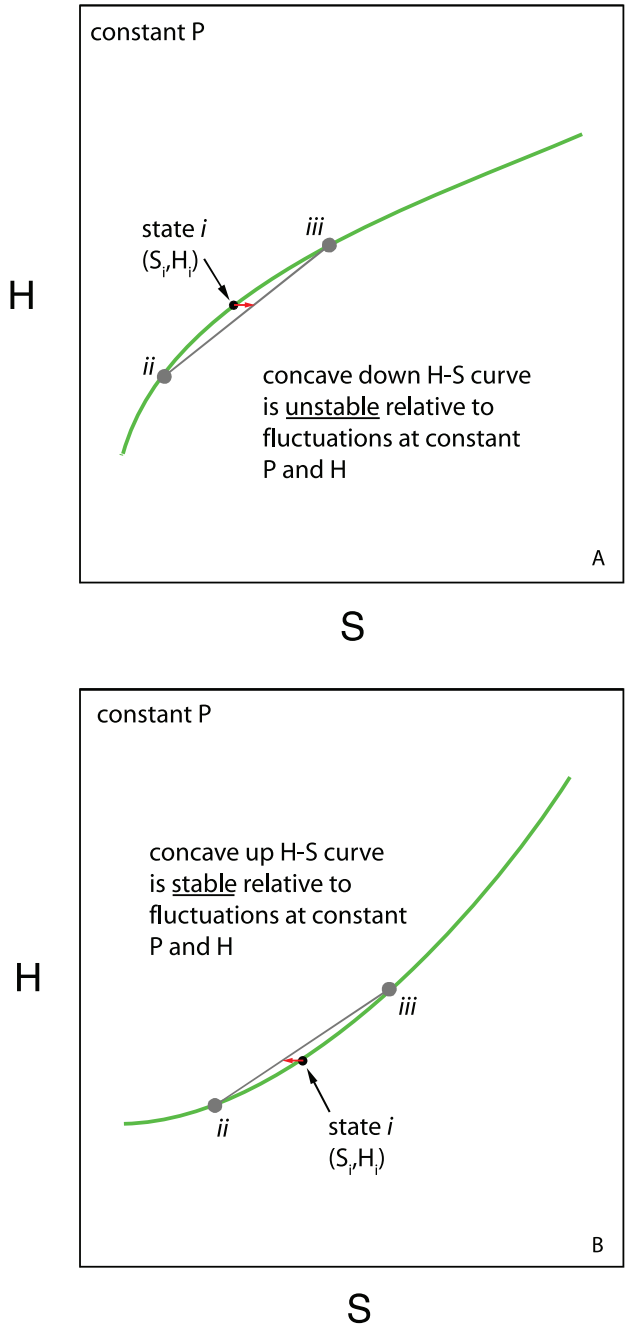

Fig. 3. Graphical demonstration of the requirement that the H-S curve for a stable phase must be concave up (that is, that $C_P > 0$ is a necessary condition for thermodynamic stability). (A) This panel illustrates that if the curve for a phase were concave down, when material at state *i* on the curve experienced a fluctuation at constant P and H, S would increase by spontaneously breaking the single phase at *i* into two phases at *ii* and *iii* on the curve, and thus state *i* could not have been stable. (B) This panel demonstrates that if the curve is concave up, when material at *i* experiences a fluctuation at constant P and H, breaking *i* into *ii* and *iii* would result in a decrease in S, and thus this breakdown would not be a natural process (which requires that S increase in order to proceed); consequently, *i* represents a maximum in S relative to all such fluctuations and thus is stable. See the text for further discussion.

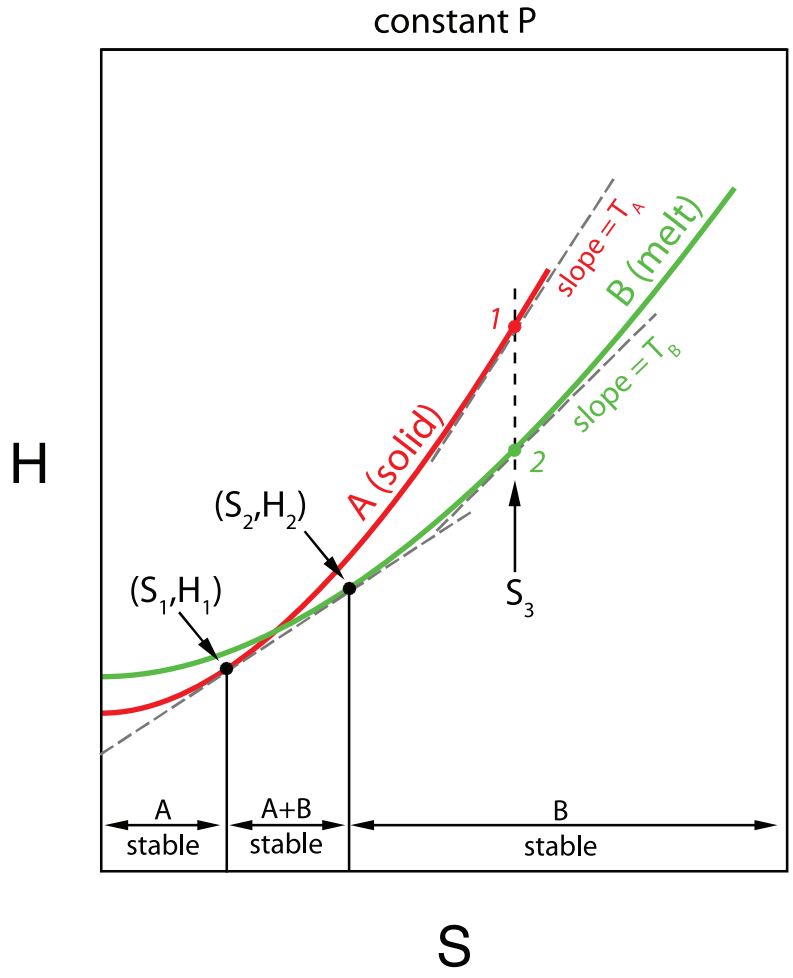

Fig. 4. Schematic isobaric H-S diagram showing relationships for a system with two phases (arbitrarily chosen to be solid and melt). Each curve represents the locus of (S, H) coordinates for a stable (or metastable) phase at this pressure. Equilibrium between melt and solid requires that they have the same T and μ, and thus such a coexistence is represented by a single line tangent to both curves; for the curves shown, this is the dashed line tangent to the solid and melt curves at (S_1, H_1) and (S_2, H_2), respectively. The stable assemblage for this P is the one with the lowest H for a given S. As illustrated on the figure, this is solid (A) for $S \leq S_1$, solid + melt (A + B) for $S_1 < S < S_2$, and melt (B) for $S \geq S_2$. This diagram also illustrates metastable equilibria and their relationships to stable equilibria. For example, for $S \geq S_2$, melt has the lowest possible H and thus represents the stable state. Although there is also a concave-up curve for solid in this entropy range, the fact that its H is higher than that of melt signifies that solid is metastable relative to melt; note that as drawn the slope of the metastable solid curve is higher than that of stable liquid for all such choices of S (that is, the temperature of metastable solid is higher than that of stable melt for a given choice of S at which melt is stable; this can be seen by comparing the tangents to solid *1* and melt *2* at S_3). Note likewise that the temperature of metastable melt is lower than that of stable solid for S in the stable solid field (that is, $S \leq S_1$) and that melt (with lower T) or solid (with higher T) can be metastable relative to the stable solid + melt assemblage at $S_1 < S < S_2$.

B coexist), phase B has the lowest H; again, metastable phase A can also exist, although the temperature is higher than that of the stable phase B at the same S (that is, in fig. 4, the slope of the curve at point *1*, which describes metastable phase A, is higher than that at point *2*, which describes stable phase B at the same S). Note the very close analogy with respect to the construction and reading of the isobaric H-S diagram to the

more familiar isobaric, isothermal G-X diagrams for binary systems (Gibbs, 1961, Chapter III; Morse, 1994) and that as the independent variable (that is, S or X) is increased, stable assemblages of one phase and two phases alternate.

Now consider how the H-S diagram changes with increasing pressure. Based on equation (10), $(\partial H/\partial P)_S = V$: that is, each curve moves up with increasing P, and the amount by which each point moves up with each increment in pressure is proportional to its specific volume. To make things more concrete, suppose that phase A is a solid and phase B is a melt; this is consistent with the construction of figure 4 in that the entropy of fusion ($\Delta S_f = S^{melt} - S^{solid}$, when the two phases coexist) and the enthalpy of fusion ($\Delta H_f = H^{melt} - H^{solid}$) are both positive. Let us further suppose that the specific volume of the melt is greater than that of the coexisting solid: this, of course, is not always true, but it is generally the case for simple silicate systems at the pressures of the shallow upper mantle. In this case, as shown in figure 5, as pressure increases from P_1 to P_2, the stable curves for both phases move upward, but that for the melt phase (B) rises more than that for the solid phase (A). The requirement of upward concavity for each curve means that the stable sequence of phases with increasing S at P_2 is, as at P_1, still solid $\rightarrow$ solid + melt $\rightarrow$ melt, but the higher position of the melt curve compared to the solid curve at P_2 relative to P_1 results in the two-phase region moving to the right: that is, the solid coexisting with melt and the melt coexisting with solid are both at higher S and at positions on the curves with higher slopes (that is, at higher T) at P_2 relative to P_1. This is, of course, related to the simple result that the slope of the solid + melt univariant curve in P-T space is positive if the entropy of fusion and the volume of fusion ($\Delta V_f = V^{melt} - V^{solid}$) are positive (that is, the Clapeyron equation is $(dP/dT)_{2\varphi} = \Delta S_f/\Delta V_f$, where the subscript 2φ indicates that the derivative is for the two-phase solid + melt coexistence).

H-S sections at different pressures can be combined to create a three-dimensional H-P-S diagram, where for a given choice of S and P, there is a surface defining the lowest enthalpy equilibrium assemblage. Just as a P-T phase diagram is the projection of such a G-P-T surface onto the P-T plane, it is simpler to give up quantitative information on the actual H at equilibrium for a given P and S and just to map out the stable assemblages (that is, those corresponding to minimum H) as functions of S and P. Figure 6 shows schematically and in perspective a three-dimensional H-P-S diagram and the projection onto the P-S plane of the stable assemblages; figure 7A reproduces the schematic P-S phase diagram for this system. At low S, there is a region where the solid phase is stable. This one-phase region is separated by a two-phase region (with horizontal tie lines, since the coexisting phases have the same P at equilibrium) from a second one-phase region where liquid is the stable phase. As described above in connection with figure 5, for this particular example, the slopes of the edges of the two-phase region are positive (that is, at higher P, the values of S for both coexisting solid and liquid are higher). At a given P, the projected length of the tie line in the two-phase region is simply the entropy of fusion. In drawing figure 7A, we have for simplicity approximated the edges of the two-phase region as linear and parallel; we shall see below that deviations from this approximation are actually significant and important for understanding decompression melting.

For any choice of S and P as the independent variables, the phase diagram given in figure 7A allows the stable phase assemblage to be determined. Note that although T is a dependent variable, at equilibrium for any choice of S and P the system has a well-defined T; schematic isotherms are shown in figure 7A. In the two-phase region, the isotherms correspond to the tie lines (since the coexisting phases must have the same temperature). The slope of an isotherm in a one-phase region can be readily derived from the appropriate Maxwell relation: $(\partial P/\partial S)_T = -(\partial T/\partial V)_P = -(V\alpha)^{-1}$, where α is the isobaric coefficient of thermal expansion. These isotherms are typically

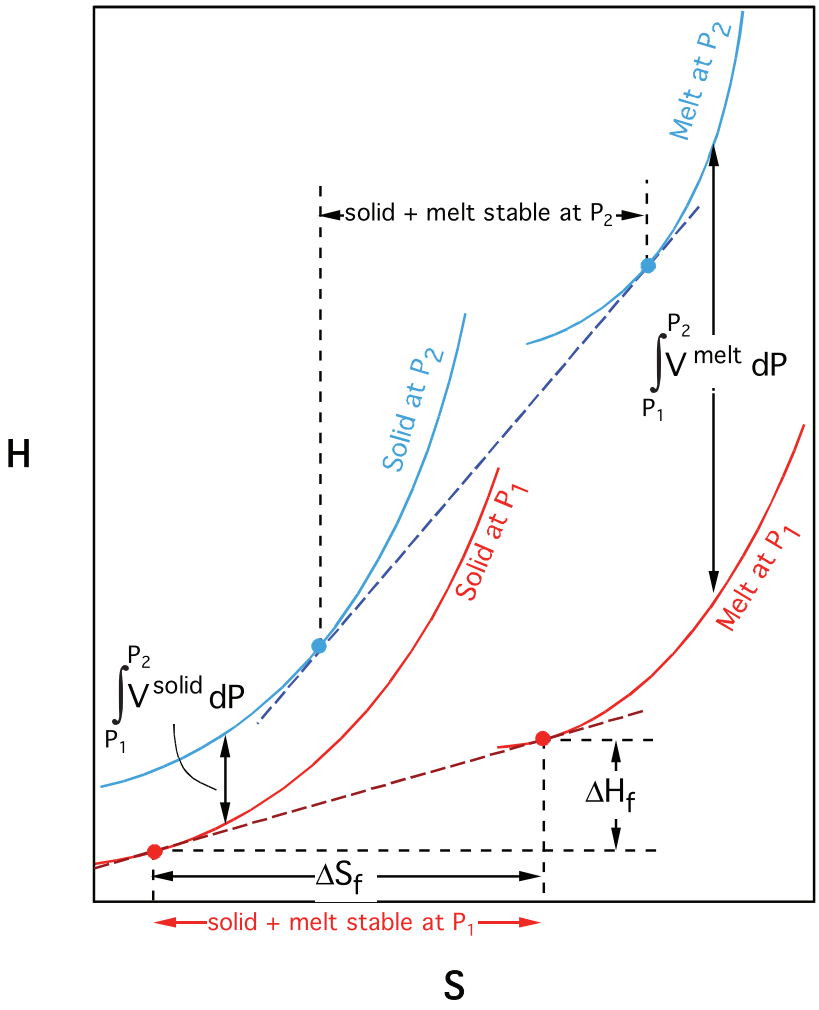

Fig. 5. Schematic H-S diagram for solid and melt at two pressures ($P_2 > P_1$). At each pressure, the stable sequence of assemblages with increasing S is solid → solid + melt → melt. Each curve moves up with increasing P (because $(\partial H/\partial P)_S = V > 0$), but because we assume that $V^{melt} > V^{solid}$, the melt curve moves up more from P_1 to P_2. Consequently, given that the curves are concave upward, the two-phase solid + melt zone shifts to higher S and T at higher P.

negatively sloped (as shown in fig. 7A) since thermal expansion is typically positive. They are likewise usually concave up since $(\partial[V\alpha]/\partial P)_T$ is usually negative.

For a given choice of S and P at minimum H, there are well-defined values of G and T. Thus, there is a P-T phase diagram (that is, mapping the stable assemblage corresponding to minimum G) complementary to the P-S phase diagram shown in figure 7A. Although at this point it is only schematic, such a P-T diagram is shown in figure 7B, adjacent to the P-S diagram. The correspondence between these two phase diagrams is illustrated by comparing the isobar shown as a heavy horizontal red arrow in figure 7A and figure 7B. From low temperature (T_1) up to the solidus at T_2 (the low-entropy boundary of the two-phase region on the P-S diagram; the solid + liquid univariant curve on the P-T diagram), solid is the stable phase. The range of entropies spanning the two-phase region from the solidus to the liquidus on the isobar in figure

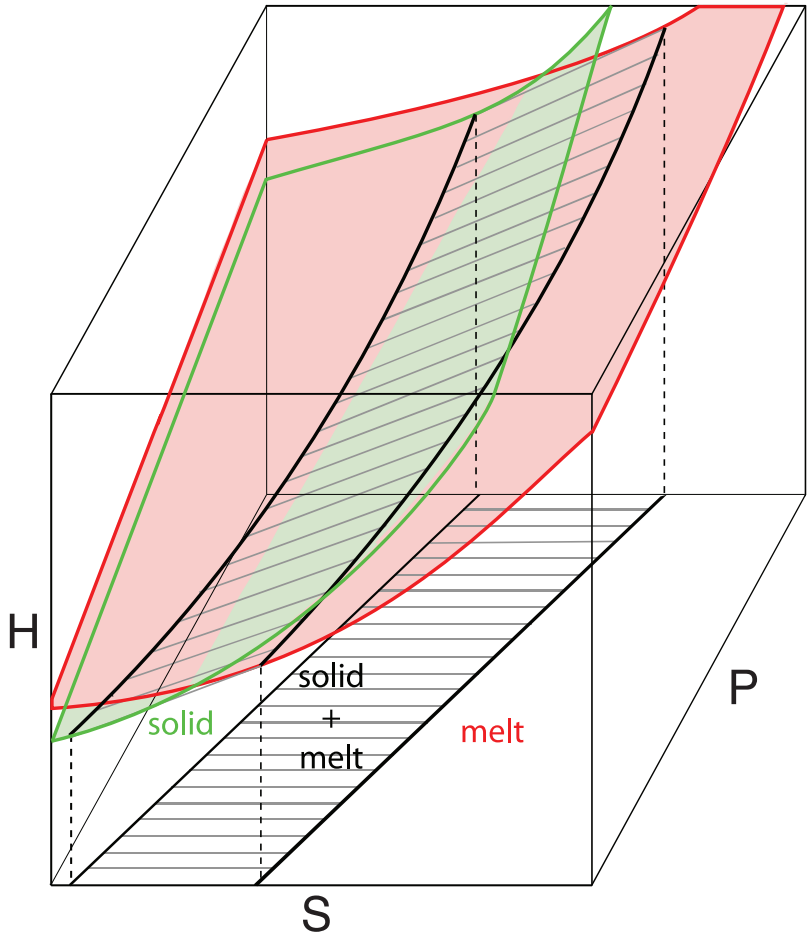

Fig. 6. Schematic three-dimensional representation of stable solid and melt phases in H-P-S space. Solid and melt are each represented by a surface, and for any choice of P and S, the stable assemblage is the lowest H phase or assemblage. The projection of the lowest H assemblages onto the P-S plane is also shown, illustrating the relationship of the P-S diagrams used in this paper to the full three-dimensional enthalpy surfaces. The H-S diagrams (for examples, figs. 2 – 5) are constant P slices through this figure.

7A all correspond to the same T, so all these states where solid + liquid coexist plot as a single point on the univariant curve in figure 7B. From the liquidus (the high-entropy boundary of the two-phase region on the P-S diagram; the univariant curve on the P-T diagram) to higher temperatures (for example, T_3), liquid is the stable phase.

We shall follow melting on the phase diagrams shown in figure 7 in the next section. An obvious point, however, is that, whereas the P-S diagram has one-phase and two-phase regions, the P-T diagram has only one-phase regions; the two-phase region collapses to the familiar univariant melting curve. This illustrates a fundamental difference between phase diagrams in which the two independent variables are the same in coexisting phases at equilibrium (for example, T and P) and those in which one variable is the same and other different (for example, P and S) in coexisting phases. In this respect, the P-S diagram for a one-component system is topologically identical to the isobaric T-X diagrams for binary systems (that is, T is the same in coexisting phases, but composition, X, is typically not); thus, although they may at first

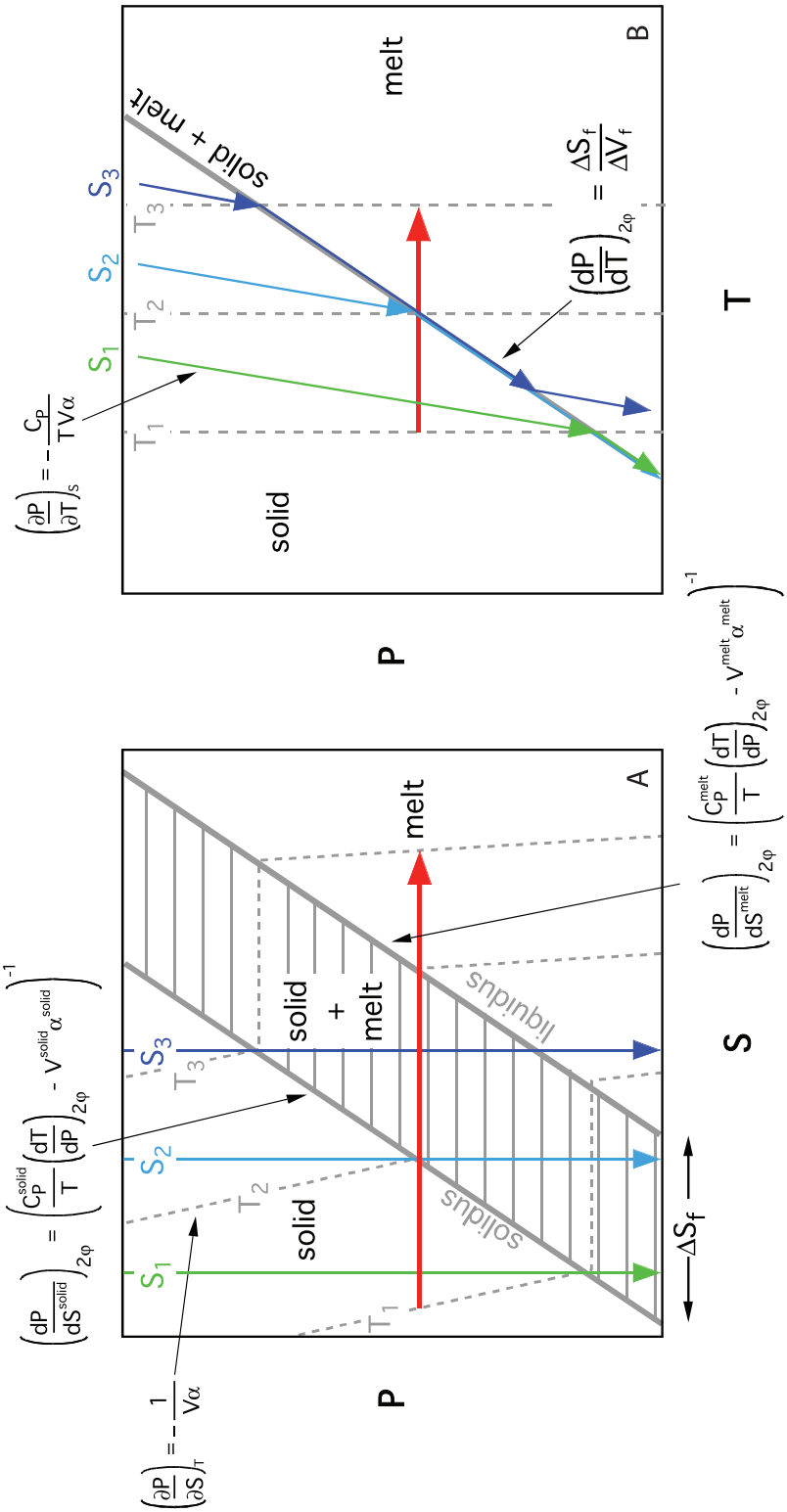

Fig. 7. Schematic (A) P-S and (B) P-T diagrams for a one-component system with solid and melt. Note that the solidus and liquidus in (A) are arbitrarily shown as linear and parallel and the corresponding univariant solid + melt coexistence in (B) is arbitrarily shown as linear. These approximations are used in this and the following diagrams to make them easier to read. Equations for slopes of these boundaries are shown on the figure. Three isotherms (T_1, T_2, T_3) are shown as gray dashed lines/curves in both panels along with the equation for their slope in a single-phase region in panel (A). Three isentropes (S_1, S_2, S_3) are shown as colored lines/curves in both panels along with the equation for their slope in a single-phase region in panel (B). The horizontal solid red arrows are used in the text to illustrate the correspondence between these two diagrams. α is the isobaric coefficient of thermal expansion, $(1/V)(\partial V/\partial T)_P$.

seem rather strange, reading P-S diagrams is essentially identical to reading T-X diagrams — something of which most geologists have considerable experience.

5. ANALYSIS OF DECOMPRESSION MELTING USING THE P-S DIAGRAM

5.1. Batch Melting

We are now ready to use the schematic P-S phase diagram presented in figure 7A to model the simplest case of decompression melting of a solid in a one-component system. We first treat the case of equilibrium or batch melting (also referred to as equilibrium or batch fusion), where solid and liquid remain in contact and in equilibrium as melting proceeds. An equilibrium isentropic decompression path can be followed with a vertical line on a P-S diagram. The red vertical line in figure 8A (which reproduces the phase diagram from fig. 7A) illustrates a representative isentrope for batch melting. Starting as a solid at high P (point *1*), with decreasing pressure at constant S the system reaches the solidus at point *2* (that is, at the upper edge of the two-phase, solid + liquid field) and begins to melt. With continued depressurization from point *2*, the fraction of melt increases (the amount of melt present at any pressure can be determined from the lever rule) until the pressure has decreased to the degree that the liquidus (that is, the lower edge of the two-phase field) is reached (point *4*). At this point the system is totally molten, and further depressurization takes place entirely within the liquid field (for example, to point *5*). For this particular example, the linear and parallel phase boundaries lead to a constant increase in melt fraction per decrement of pressure (this can be seen by the fact that the system is 50 percent molten at point *3* when the pressure is halfway between that at which it begins to melt and that at which it becomes totally molten). As we shall see, this parameter, which we refer to as the isentropic productivity, $-(\partial F/\partial P)_S$ (where F is melt fraction), is not constant in real systems, and its variations could have an impact on petrogenesis. By taking note of the isotherms, figure 8A shows that for this typical case, temperature decreases with decreasing P along the isentrope in the all-solid and all-liquid fields much more slowly than when the system is melting. Note that for an isentrope with lower S (for example, the purple vertical line from *6* to *7*), melting begins at a lower P (and T), but for this simple example, the pressure interval over which melting occurs (and thus the productivity) is the same for all isentropes.

These isentropic paths are also shown on the P-T diagram in figure 8B. Without additional information, however, the variation in melt fraction with pressure, the actual slopes of the isentropes in the one-phase fields, and the pressure range over which melting takes place cannot be read directly from this diagram. This emphasizes the limitations of this choice of variables for evaluating isentropic decompression melting, particularly in comparison to the considerable information available from figure 8A.

5.2. Fractional Fusion

First analyzed in detail by Presnall (1969), fractional fusion, by which is meant that all melt is extracted from the system instantaneously as it is generated, has come to be regarded as an important process – perhaps the dominant one – for melt generation in the mantle. This follows from the expectation based on experiments on textural equilibrium in olivine-rich materials that low-viscosity partial melts will be interconnected at low melt fractions and that they will escape from their sources on time scales that are short relative to the rates at which they are produced (Waff and Bulau, 1979; Johnson and others, 1990; Hart, 1993; Kelemen and others, 1997). Like batch fusion, fractional fusion is an idealized end-member process that can be analyzed readily in a one-component system using a P-S diagram. Fractional fusion is neither reversible nor adiabatic because melt leaves the system carrying entropy with it, but the case can be

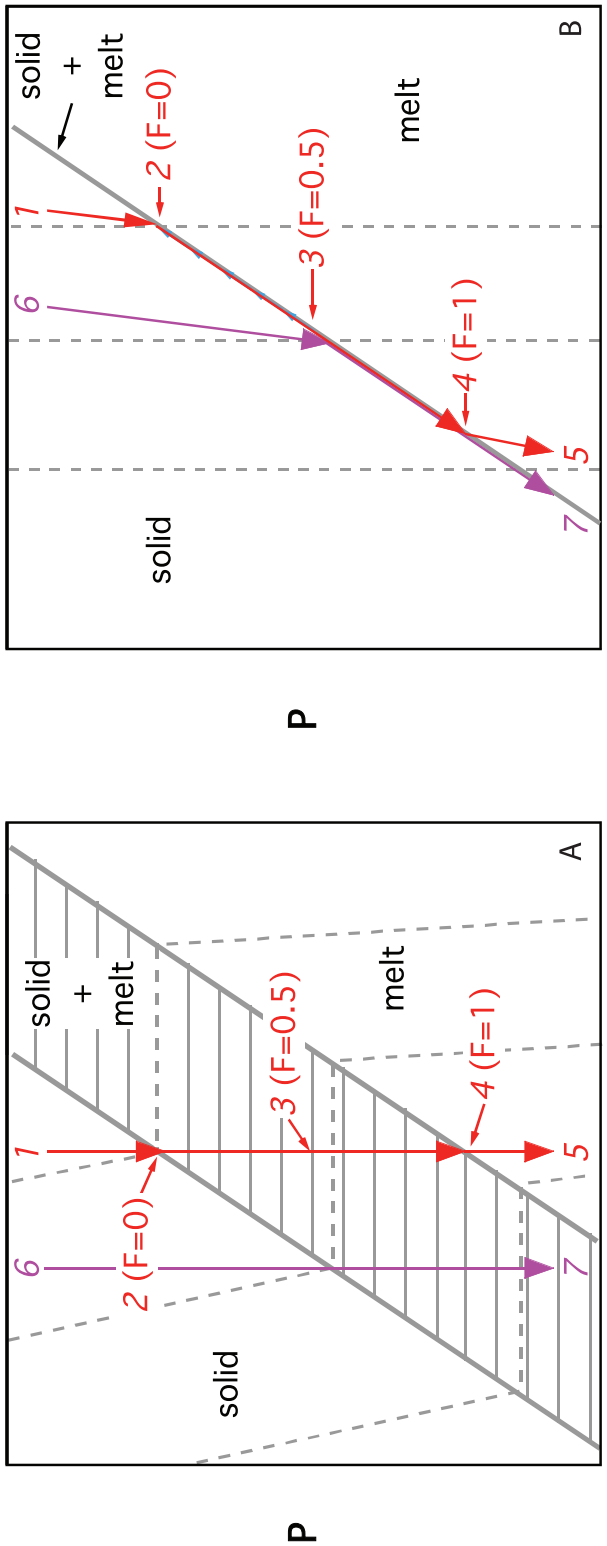

Fig. 8. Schematic (A) P-S and (B) P-T diagrams for a one-component system with solid and melt (from fig. 7). Two isentropic paths (*1*→*2*→*3*→*4*→*5* in red; and *6*→*7* in purple) are shown and used in the text to describe batch isentropic decompression melting. F is the melt fraction (that is, F=0 for 0% melting, 0.5 for 50% melting, and 1 for 100% melting).

considered where each increment of melting is accomplished isentropically, followed by extraction of the melt; we refer to this process as incrementally isentropic fusion. Figure 9A illustrates such a process starting with a specific entropy for the solid identical to that for the batch fusion process described above using figure 8. Here we consider a series of constant decrements of pressure starting from state *2*, right at the solidus. The first pressure decrement is from state *2* (F = 0) to state *i*; at *i*, the stable assemblage is 10 percent melt whose entropy plots at i_{melt} plus residual solid whose entropy plots at i_{solid}. At this point, the melt is removed from the system, leaving a residue at i_{solid} on the solid edge of the two-phase solid + melt field. The next decrement of pressure, equal to the first, acts only on the residual solid, so the path is from i_{solid} to *ii* in figure 9A; the melt (at ii_{melt}) is then removed, leaving a residue at ii_{solid}, and the next decrement of pressure is to *iii*, and so on. Figure 9A shows (in cyan) the resulting stair-step pattern of incrementally isentropic fusion on the P-S diagram for ten equal decrements of pressure (that is, down to the pressure at which, for batch fusion, the system is totally molten) and shows for comparison (in red) the batch-melting (constant S) path from figure 8.

As described earlier, the linear and parallel edges of the two-phase field in figure 9A lead to a constant productivity during batch fusion: that is, for each of the ten decrements in pressure shown in figure 9A, the amount of melt on a vertical (constant S) batch fusion path increases by 10 percent such that after five pressure decrements (that is, at point *3*, halfway between points *2* and *4* at which F = 0 and 1), the melt fraction is 0.5 (50% molten). For each step of incrementally isentropic fusion shown in figure 9A, an amount of melt is generated equal to 10 percent of the mass of the residue, after which the melt is removed from the system, but since the residue decreases in mass after each pressure decrement, the mass of melt produced in each pressure decrement (after the first) is lower than for the equivalent batch melting process over the same pressure interval. For example, starting from an initial mass of solid at state *2* of 1 gram, the mass of residual solid at i_{solid} is 0.9 grams and the mass of melt at i_{melt} is 0.1 gram, the same as for batch fusion by isentropic depressurization from state *2*. However, depressurization from i_{solid} to *ii* melts the solid by 10 percent, such that the amount of melt at ii_{melt} is 0.09 grams and there are 0.81 grams of residual solid at ii_{solid}. Thus whereas isentropic batch fusion to the pressure of *ii* produces 0.2 grams of melt, two equal increments of depressurization followed by melt extraction to the same pressure produces only 0.19 grams. When the pressure has decreased to that of state *4*, where the system is completely molten if the melting process is batch fusion (that is, the mass of melt is 1 gram for this example), incremental melting with ten equal pressure decrements has produced only 0.65 grams of melt. Thus, relative to the original mass of the source region, incrementally isentropic fusion produces less melt than batch fusion during decompression melting.

Figure 9B compares the batch and incremental fusion paths from figure 9A in P-T space. Although the processes and amount of melt produced differ significantly, their paths are indistinguishable in P-T space until the pressure at which batch melting is complete (that is, at the pressure of point *4*), since all melt + solid assemblages are constrained to lie on the two-phase univariant boundary. The fact that the processes can be readily distinguished and analyzed using the P-S diagram in figure 9A illustrates well the greater utility of P-S space for understanding such processes. The incrementally isentropic melting and batch melting paths diverge in P-T space at pressures below that of point *4* because continued decompression on the incrementally isentropic melting path will remain on the two-phase curve (for example, to point *6* and beyond), whereas continued decompression on the batch-melting path diverges into the liquid field (for example, to point *5*).

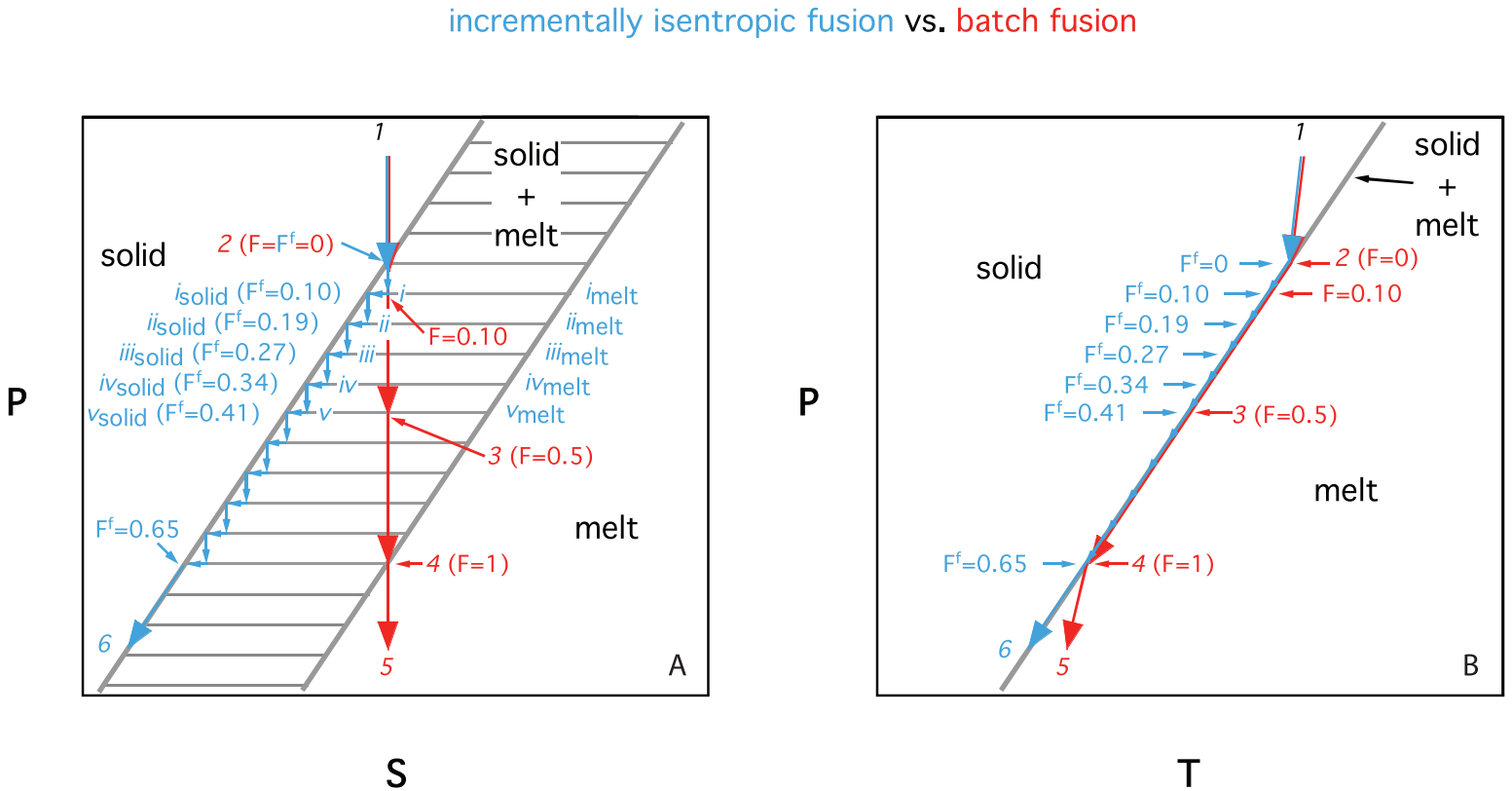

Fig. 9. Schematic (A) P-S and (B) P-T diagrams for a one-component system with solid and melt (from fig. 7). A series of isentropic decompression melting steps, after each of which melt is removed from the system (for example, $2 \rightarrow i \rightarrow i_{solid}$, $i_{solid} \rightarrow ii \rightarrow ii_{solid}$, *et cetera*$\rightarrow 6$, shown as cyan arrows; this process is referred to in the text as incrementally isentropic fusion), is compared to batch isentropic decompression melting from the same initial entropy ($2 \rightarrow 5$, shown as red arrows, from fig. 8). F and F^f are, respectively, the melt fractions for isentropic batch fusion and for incrementally isentropic fusion. See the text for discussion.

The increments of melting for the incrementally isentropic fusion process can be made infinitesimal and to approach zero, in which case the process is a particular class of true fractional fusion that we refer to as incrementally isentropic fractional fusion. As shown in figure 10A, the path of the residual solid in P-S space for this process simply follows the solid edge of the two-phase field, and in P-T space it is constrained to the univariant solid + melt curve, identical to that for batch fusion (until the pressure of point *4*, the point at which complete batch melting is achieved) and to incrementally isentropic fusion where the melting increments are finite. If F and F^f are, respectively, the melt fractions for isentropic batch fusion and for incrementally isentropic fractional fusion, it can be shown (see the final paragraph of section 14.2) that in the fractional fusion limit and given the approximation of linear and parallel solidus and liquidus curves in P-S space used in the simple treatment thus far

$$F^f = 1 - \exp(-F), \tag{11}$$

after the same amount of decompression (this equation is only valid for $0 \leq F \leq 1$). Note by comparison of figure 9 and figure 10 that melt fraction is not significantly different for the fractional fusion end member and for melting increments of 10 percent [for example, melt fraction at the pressure at which $F = 1$ (that is, at the pressure at which batch melting is complete) is 0.65 for the case of 10% increments vs. 0.63 for fractional fusion]. It is important to emphasize that F^f is defined relative to the initial mass of the system (that is, it is the total mass of melt produced in successive increments of decompression melting followed by melt extraction, divided by the initial mass of the system).

One final point is that in each increment of melting followed by separation of the liquid and residue, the total entropy of the system does not change; in this sense, the fractional fusion process as we have defined it is isentropic. Moreover, when the melt and residue are separated after each increment of melting they are in equilibrium, so if they were put back in contact at the same P and T at which they were separated, they would still be at equilibrium and the entropy would be unchanged; again, in this sense, at each step in the process, the process of separation of melt and residue is reversible. And thus, if all the batches of liquid generated in a sequence of isentropic melting increments and the residue were kept separate and we simply added up their total entropy, we retrieve the initial entropy of the system and once more the overall process could be described as isentropic. This is an important point: in our construction the act of separating liquid and residue does not increase the entropy of the system. However, liquids and residues from different increments of melting are all at different temperatures, so if we mixed melts from different increments or allowed melts and residues from different increments to interact thermally (that is, if they are not, as stipulated above, "kept separate"), this interaction would be irreversible and the entropy of the system would increase. Such irreversible interactions of melt and residue during ascent may be important petrologically and we develop tools to analyze them in section 11. As an aside, we note that in this respect, the analysis of fractional fusion during decompression differs from that of isobaric fractional fusion in a binary system analyzed using a conventional T-X loop (for example, Morse, 1994, p. 71-73), despite the topological similarities of the P-S and T-X loops used to analyze these processes: That is, when all the liquids generated during isobaric fractional fusion accompanying increasing T in a binary system are mixed together, composition is conserved (that is, the composition of the integrated liquid is simply the weighted average of the increments, achieving the bulk composition of the system when the system is completely molten — see Morse, 1994), whereas in the case we have considered, S would not be conserved on mixing of the increments of melting with each other (or as deeper increments of melt interact with shallower residues) due to the irreversibility of such processes.

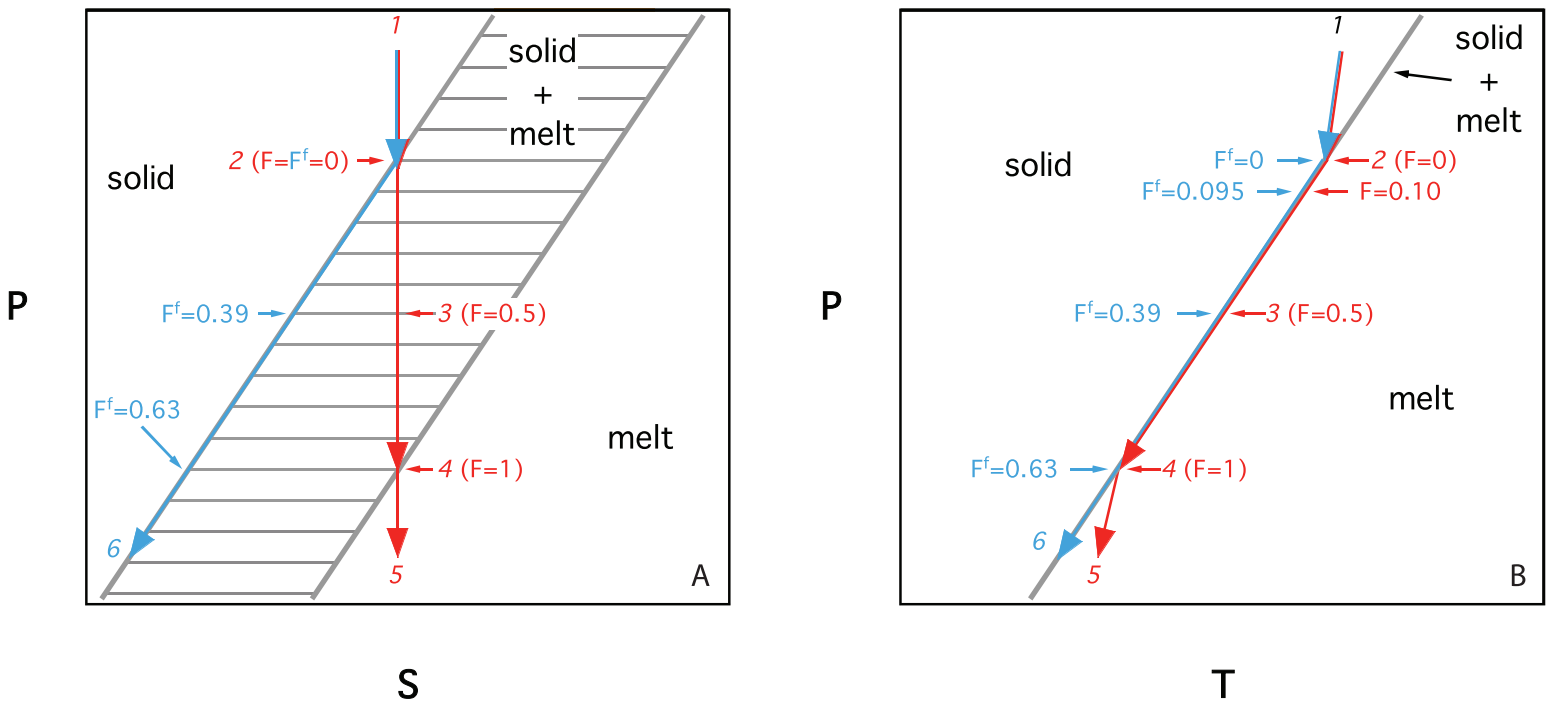

Fig. 10. Schematic (A) P-S and (B) P-T diagrams for a one-component system with solid and melt (from fig. 7). An incrementally isentropic fractional fusion path (2→*6*, shown in cyan; that is, a decompression path made up of a series of isentropic decompression melting steps after each of which melt is removed from the system as shown in figure 9 but in which the increments are infinitesimal) is compared to batch isentropic decompression melting from the same initial entropy (2→*5*, shown as red arrows, from fig. 8). F and F^f are, respectively, the melt fractions for isentropic batch fusion and for incrementally isentropic fractional fusion. See the text for discussion.

5.3. Observations About Fractional Fusion and Its Comparison To Batch Fusion

This simple analysis of incrementally isentropic fusion and its limit of fractional fusion offers several insights into fractional fusion and its comparison with batch fusion:

- For the very first increment of melting (that is, as pressure decreases from state *2* in figure 9 and figure 10), the amounts of melt produced per decrement of pressure by batch and incremental fusion (whether in finite increments or in the limit of fractional fusion) are identical; that is, the productivities of batch and fractional fusion are identical at $F = 0$. Although obvious – each increment of incrementally isentropic melting is itself a batch process, and as the first increment of melt is being produced the system does not yet "know" whether this increment of melting will be followed by melt extraction or not – this simple insight, which holds for more complex systems as well, does not appear to have been noted prior to having been pointed out by Asimow and others (1997) based on the type of analysis presented here. For example, Langmuir and others (1992) assumed that the isobaric productivity of peridotite melting (that is, the amount of melt produced per increment of temperature increase at constant pressure) during fractional fusion is 25 percent lower than that of batch fusion and constant all the way down to the solidus. Likewise, Iwamori and others (1995) estimated the productivity of fractional fusion by uniformly "stretching" the melting interval up to the liquidus of forsterite, thereby lowering the isobaric productivity by 33 percent everywhere, including at the solidus.
- Although the productivities of fractional fusion and batch fusion are identical at the solidus, the productivity of fractional fusion for this simple case decreases continuously with increasing melting (where productivity refers to the change in mass of melt relative to the initial mass of the unmelted source) due to the decreasing mass of the residue relative to the initial mass of the system. Although as we shall see below, other factors play roles such that productivity, even for fractional fusion in a one-component system, will usually initially increase with increasing decompression and degree of melting, the decreasing mass of the residue must ultimately dominate, leading to decreasing (and ultimately vanishingly small) productivity for fractional fusion as the degree of melting of the source approaches 100 percent.

  Note that if productivity were defined relative to the mass of the residue in any given increment of isentropic melting rather than to the initial mass of the system (this was referred to as "local productivity" in Asimow and others, 1997), then for the particular construction used in figure 9A, with linear and parallel solidus and liquidus curves, there would be no difference between the productivities of batch, incremental, or fractional fusion. However, in considerations of petrogenesis, the degree of melting of a source is usually referenced to its initial, unmelted mass (best tracked with the aid of a hypothetical, perfectly compatible tracer, see Asimow and Stolper, 1999), so in the absence of other factors, the productivity will decrease for fractional fusion with increasing melt fraction.
- A critical feature of incrementally isentropic fusion is that a source can never melt completely by this process (provided the decompression steps are less than the pressure drop needed to melt fully the residue in a single step). This contrasts with isentropic batch fusion and can be readily understood by the incremental melting example shown in figure 9A: For each constant decrement of pressure, the solid in the source melts by 10 percent; obviously, if 90 percent of the mass remains after each increment, although the amount of residual

solid left (0.9^n times the initial mass, where n is the number of melting increments) approaches zero when the number of increments is very large, it never actually reaches zero. This is a general result for incremental isentropic fusion and its limit of fractional fusion (that is, it is valid for multicomponent systems). The reason for this behavior is clear from figure 9A: A given pressure decrement less than that required to produce complete melting (that is, especially infinitesimal melting increments) will after melt removal leave a solid residue with S constrained by the solid edge of the two-phase solid + melt region; each subsequent step must therefore also leave a solid residue with ever decreasing S on the solid edge of two-phase field, and so on forever, with the result that there will always be a solid residue and complete melting is impossible regardless of the pressure drop available to the system. Note that this behavior contrasts with that of isobaric fractional fusion described by Presnall (1969). In the isobaric case for a one-component system, melt is generated reversibly as heat (q) flows into the system and the total amount of melt generated, regardless of whether it is removed instantaneously as it is produced, is $q/\Delta H_f$. Thus, under isobaric conditions, a one-component solid will be totally molten ($F = F^f = 1$) when $q = m\Delta H_f$ (where m is the total mass of the system; see the end of section 8.5 for a fuller discussion of this).

Some aspects of the behavior of the model one-component system shown graphically in figure 9A are unique to one-component systems or artifacts of the unrealistic simplification of linear, parallel solidus and liquidus curves bounding the two-phase region. However, the equality of the productivities of batch and fractional fusion at the solidus, the fact that the productivity (relative to the original mass of the system) of incrementally isentropic fractional fusion must approach zero at sufficiently high melt fractions, and the impossibility of complete melting of the system by incrementally isentropic fractional fusion are general results. Thus, although at intermediate melt fractions in multicomponent systems the productivity of incrementally isentropic fractional fusion can exceed that of batch fusion (see Asimow and others, 1997; Hirschmann and others, 1999a), averaged over a sufficiently large pressure interval the productivity of fractional fusion will always be lower than that of batch fusion. Moreover, a lower productivity for incrementally isentropic fractional fusion relative to batch fusion immediately following the initial melting increment appears to be general. As a result, for a given amount of decompression relative to the solidus during ascent (ΔP), even for those cases in which the productivity of fractional fusion exceeds that of batch fusion at intermediate melt fractions, the actual melt fraction (and thus the average productivity, $-F/\Delta P$ or $-F^f/\Delta P$) is always less for fractional relative to batch fusion. It is generally accepted that the amount of melting for fractional fusion after a given degree of decompression will be less than for batch fusion, but the usual explanations of this are related to factors unique to multicomponent systems with solid solution. Phipps Morgan (2001), for example, reasoned that the progressive depletion of the residue in low-melting components leads to an increase in the solidus for fractional fusion relative to batch fusion and that amount of melting is related to the amount by which the solidus temperature is exceeded. Since the fractional fusion case exceeds its solidus temperature by a smaller interval, the amount of melting must be less (Phipps Morgan, 2001). The fact that this behavior is displayed by one-component systems unaffected by such factors demonstrates that a lower average productivity of fractional fusion is a more general feature of decompression melting, related to the decreasing mass of the residue and the impossibility of complete melting by incrementally isentropic fractional fusion.

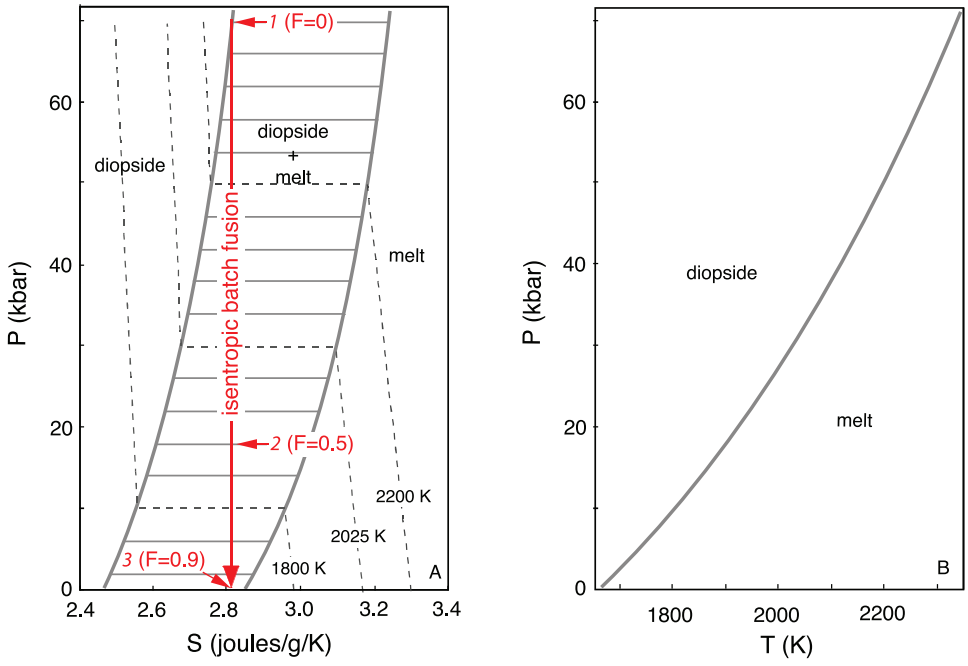

Fig. 11. (A) P-S and (B) P-T diagrams for the one-component system $CaMgSi_2O_6$ (diopside) from Asimow and others (1997), assuming diopside melts congruently (but see Kushiro, 1972). As described in the text, the solidus and liquidus curves in (A) are concave up and not parallel (that is, ΔS_f is not independent of P and T) rather than linear and parallel as assumed in previous figures, and the univariant diopside + melt curve in (B) is concave up rather than linear as previously assumed. The vertical red arrow shows the isentropic decompression path (*1*→*2*→*3*) described in the text. The thermodynamic parameters used to calculate these diagrams are given in Asimow and others (1997).

6. CURVATURE OF THE SOLIDUS AND LIQUIDUS IN P-S SPACE

6.1. Diopside + Melt as a Model System – The Important Influence of Curvature on Productivity

Figure 7 and the figures based on it are entirely schematic, having been drawn with linear, parallel edges to the two-phase solid + melt field on the P-S diagram and with a constant slope for the solid + melt univariant curve on the P-T diagram. Figure 11A shows the diagram for a system with the composition of diopside ($CaMgSi_2O_6$), calculated based on available thermochemical parameters for solid and melt of this composition (Asimow and others, 1997). The most important feature of this "real" system is that the edges of the two-phase field in P-S space are neither linear nor parallel. As indicated in figure 7A, the slopes of these edges are given by

$$\left(\frac{dP}{dS^{\varphi}}\right)_{2\varphi} = \left[\frac{C_P^{\varphi}}{T}\left(\frac{dT}{dP}\right)_{2\varphi} - V^{\varphi}\alpha^{\varphi}\right]^{-1}, \qquad (12)$$

where the superscript φ refers to the properties of either the solid or melt, and the subscript 2φ on the two derivatives indicates that these derivatives apply to the solid + melt coexistence; that is, $(dT/dP)_{2\varphi} = \Delta V_f/\Delta S_f$, the slope of the univariant curve in P-T space for coexistence of solid plus melt. Equation (12) can be obtained simply by rearrangement of equations (34) or (35) and equation (36) (see section 14.1).

The two principal factors contributing to the non-linearity of the edges of the two-phase field (that is, the solidus and the liquidus in figure 11A) are the variations of T and $(dT/dP)_{2\varphi}$ with pressure along the diopside + melt univariant curve. As shown in figure 11B, T decreases with decreasing P on the diopside solidus (reflecting the fact that ΔV_f and ΔS_f for diopside melting are both positive). Likewise, the slope of the univariant curve, $(dT/dP)_{2\varphi}$, increases with decreasing P on the diopside solidus (Boyd and England, 1963) because ΔV_f increases in this direction (reflecting the significantly greater compressibility of the melt relative to solid diopside under these conditions — for example, Rigden and others, 1989). Both of these factors lead to an increase in the first term inside the brackets on the right-hand side of equation (12), and as a result $(dP/dS^{\varphi})_{2\varphi}$ decreases with decreasing pressure in figure 11A for both the solidus and liquidus (that is, both edges of the two-phase field are concave up).

Although less obvious from figure 11A, the edges of the two-phase field are not parallel; that is, ΔS_f may increase or decrease with decreasing P on the diopside solidus. The pressure dependence of ΔS_f along the solidus is:

$$\frac{d\Delta S_f}{dP} = \frac{C_P^l - C_P^s}{T}\left(\frac{dT}{dP}\right)_{2\varphi} - [V^l\alpha^l - V^s\alpha^s]. \qquad (13)$$

This expression can be obtained simply by combining the difference between equations (35) from (34) with equation (36) (see section 14.1). Here and elsewhere, the s and l superscripts refer to the properties of solid or liquid. Liquids generally have both a higher heat capacity and a higher thermal expansion coefficient than coexisting solids, so for positive $(dT/dP)_{2\varphi}$ the two terms are of opposite sign and there is no general rule for increase or decrease of ΔS_f with pressure.

The upward curvature of the edges of the two-phase field in figure 11A leads to an important but unexpected insight into decompression melting that was not discernible from the schematic P-S diagrams in figures 7 – 10 in which the phase boundaries were artificially forced to be linear and parallel. The vertical red arrow in figure 11A illustrates a typical isentropic path. In this case, batch melting begins at 70 kbar and is nearly complete at 1 bar ($F \approx 0.9$). Note, however, that because of the curvature of the boundaries (and to a smaller extent, their non-parallel nature), a decompression of more than 50 kbar is required to go from 0 to 50 percent melting (*1*→*2*), whereas a further decompression of less than 20 kbar is then required to go from 50 percent to almost 100 percent melting (*2*→*3*). Inspection of figure 11A shows that this is simply a geometric requirement of the curvature of the phase boundaries (and the fact that they are nearly parallel) and the lever rule. This result is quite general: due to the curvature of the solidus and liquidus in P-S space (reflecting decreasing T and increasing $(dT/dP)_{2\varphi}$ during decompression melting of a one-component system), the rate at which melt is generated increases with progressive decompression: that is, the isentropic productivity for batch melting, $-(\partial F/dP)_S$, increases with decreasing pressure. It is clear in the case of diopside that this is not a small effect: that is, the average productivity from 0→50 percent melting is ~1%/kbar, increasing to > 2%/kbar from 50→90 percent melting. The same factors influence the productivity of incrementally isentropic fractional fusion, and for the case of diopside, they actually overwhelm the effect discussed above of the progressive decrease in the mass of the residue over much of the melting interval such that the productivity under these conditions also increases with progressive decompression (although it is always less than that of batch isentropic fusion, except right at the solidus). Asimow and others (1997) demonstrated that, although other factors influence melt productivity of multicomponent systems, this unanticipated result generalizes to petrologically important systems and has a number of implications for understanding petrogenesis of mantle-derived magmas.

The analytical expression for productivity for isentropic batch melting in a one-component system is

$$-\left(\frac{\partial F}{\partial P}\right)_S = \frac{1}{\Delta S_f}\left[\overline{\frac{C_P}{T}}\left(\frac{dT}{dP}\right)_{2\varphi} - \overline{V\alpha}\right], \tag{14}$$

(see, section 14.1, equation (38) and Asimow and others (1997) for a derivation) where $\overline{C_P} = FC_P^l + (1 - F)C_P^s$ and $\overline{V\alpha} = FV^l\alpha^l + (1 - F)V^s\alpha^s$ are weighted by the proportions of solid and liquid in the system. Right at the solidus ($F = 0$), these mean values are replaced by those of pure solid, and at the liquidus, those of pure liquid replace them. The comparable expression for incrementally isentropic fractional fusion is [see section 14.2, equation (43)]

$$-\frac{dF^f}{dP} = \frac{(1 - F^f)}{\Delta S_f}\left[\frac{C_P^s}{T}\left(\frac{dT}{dP}\right)_{2\varphi} - V^s\alpha^s\right]. \tag{15}$$

Note the similarities between the expressions for batch and fractional fusion. The fractional fusion expression corresponds to that for batch fusion of a system at its solidus (that is, C_P^s and $V^s\alpha^s$ replace the weighted parameters that appear in the batch fusion expression), weighted by the factor ($1–F^f$) to account for the continuously decreasing mass of the system during fractional fusion described previously. Both expressions confirm what we inferred from graphical analysis of the P-S diagram in figure 11A: that is, like the slopes of the solidus and liquidus in this figure, these productivity expressions vary primarily due to variations in T and $(dT/dP)_{2\varphi}$ and in particular, T decreases and $(dT/dP)_{2\varphi}$ increases with decreasing P on the diopside solidus, and as a consequence, productivity in both cases increases steadily with decompression. The two expressions are identical at $F = F^f = 0$, confirming our previous conclusion that at the solidus, the productivities of batch and fractional fusion are identical.

Figure 12A shows quantitatively the melt fraction as a function of P for isentropic batch fusion of diopside for the isentrope shown in figure 11A. Also shown is the melt fraction versus P for fractional fusion of diopside with the same initial specific entropy. These curves were calculated based on integration of equations (14) and (15), respectively, and the thermochemical parameters for solid and liquid diopside given in Asimow and others (1997). The productivities for batch and fractional melting (that is, the derivatives of the curves in fig. 12A) were calculated directly from equations (14) and (15) and are shown in figure 12B.

The calculated melt fraction and productivity curves shown in figure 12 confirm the qualitative discussion presented above in connection with figure 11. The F versus P curve is concave up: that is, productivity for batch melting increases with increasing F as deduced graphically from figure 11A. This effect is surprisingly large: from $F = 0$ to $F \approx 0.9$, productivity increases by more than a factor of 6, from ~0.5 %/kbar to > 3 %/kbar (fig. 12B). Figure 12 shows that over this same pressure range, the F^f versus P and productivity versus P curves for fractional fusion are lower than the batch melting curve (as anticipated based on the graphical analysis given above), but still concave up: for the same pressure interval over which F goes from 0 to 0.9 and productivity increases by about a factor of six for batch melting, F^f goes from 0 to ~0.6 and productivity increases by about a factor of two. This increase in productivity signifies that the effects of decreasing T and increasing $(dT/dP)_{2\varphi}$, which contribute to increasing $-dF^f/dP$ in equation (15) with decreasing P, initially overwhelm the effect of decreasing mass of the residue [manifested by the $1–F^f$ term in equation (15)], which, as discussed above, contributes to decreasing the productivity of fractional

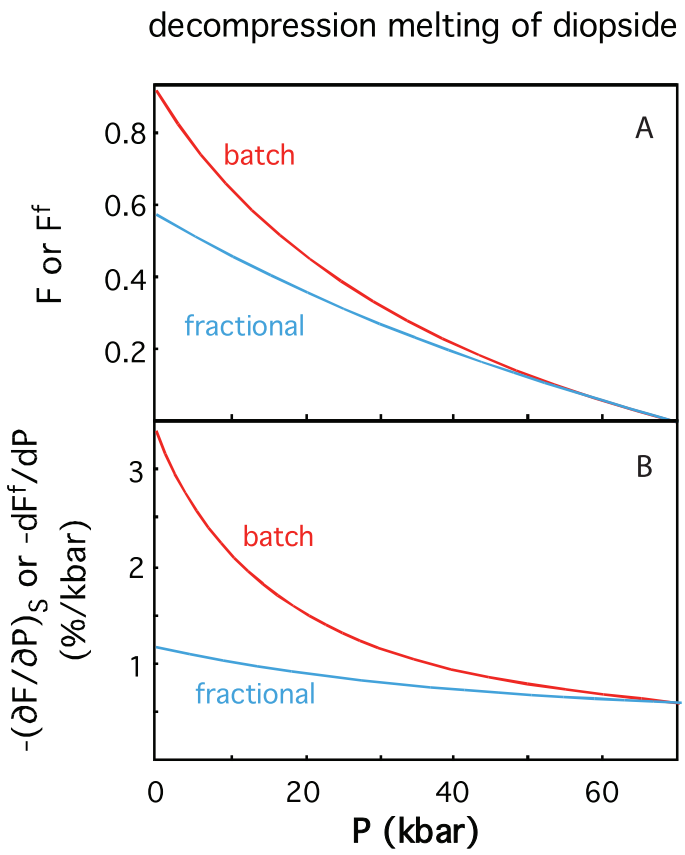

Fig. 12. (A) Melt fraction (F for batch fusion; F^f for fractional fusion) vs. P and (B) productivity vs. P for the diopside one-component system (see fig. 11) for batch (isentropic) and fractional (incrementally isentropic) decompression melting starting from the same initial entropy (*1* in fig. 11). This figure demonstrates the progressive increase in productivity with decompression (related to the curvature of the solidus and liquidus in fig. 11) for both batch and fractional fusion and the lower productivity of fractional relative to batch fusion, except at the solidus, where the two processes have the same productivities. Note that F^f is defined relative to the initial mass of the system. From Asimow and others (1997).

relative to batch fusion with progressive melting (although the $1–F^f$ term must dominate as $F^f \rightarrow 1$). Figure 12B also emphasizes the point made previously that at $F = F^f = 0$, the productivity of batch and fractional fusion are identical. Finally, we note that although diopside is a far simpler system that natural peridotites, the calculated productivities shown in figure 12 compare favorably to estimates for peridotite from Hess (1992) (1.0 % per kilobar) and Langmuir and others (1992) (2.2 % per kilobar).

Although obvious from an analysis of the P-S diagram in figure 11A or equations (14) and (15), the increase in productivity with progressive decompression was unexpected prior to the development of this kind of treatment of decompression melting by Asimow and others (1997). Although a wide range of productivity functions had been implied by various analyses of partial melting (Turcotte and Ahern, 1978; McKenzie, 1984; Klein and Langmuir, 1987; McKenzie and Bickle, 1988; Scott and Stevenson, 1989; McKenzie and Bickle, 1990; McKenzie and O'Nions, 1991; Miller and others, 1991; Niu and Batiza, 1991; Sparks and Parmentier, 1991; Kinzler and Grove, 1992; Langmuir and others, 1992; Longhi, 1992; Iwamori and others, 1995), the

expectation was that in a simple one-component system, the productivity would be approximately constant. This result reemphasizes the point made in the Introduction about how poorly petrological intuition has been calibrated for this key process and how much even a very simple treatment using the proper variables can inform and provide a framework. As discussed in several papers by Asimow, Hirschmann, and others (for example, Asimow and others, 1997; Hirschmann and others, 1998a, 1998b, 1999a, 1999b), there are additional factors in multicomponent systems that can significantly influence productivity, such as phase exhaustion or addition during melting, the compositional differences between melt and residue, and the effects of incompatible components. These authors showed that for peridotitic systems in particular, the latter two factors will tend to reinforce (substantially, under some circumstances) the increase in productivity with progressive decompression deduced for one-component systems. This behavior has several potentially important implications for petrogenesis, including the weighting toward melts produced at lower pressures of magma compositions derived by blending of melts from the full depth interval over which melting occurs and the possibility of a low-productivity "tail" extending to much greater depths than those at which most of the melting occurs, imprinting high-pressure geochemical signatures on magmas derived primarily from low-pressure melting (for example, Galer and O'Nions, 1986; Asimow and others, 1997; Hirschmann and others, 1998a, 1998b, 1999a, 1999b; Asimow and others, 2001; Ito and Mahoney, 2005).

6.2. Maxima on the Solidus and Liquidus

A potentially interesting consequence of the non-linearity of the solidus and liquidus illustrated in figure 11 is the possibility that these two-phase boundaries have maxima in S at some elevated pressure. This is illustrated in figure 13A and is a simple consequence of equation (12). As described above, the increase in T and decrease in $(dT/dP)_{2\varphi}$ with increasing P on the solidus and liquidus both contribute to a decrease in the first term inside the brackets on the right-hand side of equation (12). At low pressure, the second term within the brackets is typically much smaller than the first, and as a result the decrease in the first term dominates and $(dP/dS^{\varphi})_{2\varphi}$ increases with increasing pressure. If this continues indefinitely, for each of the two-phase boundaries in figure 13A the first term inside the brackets in equation (12) will have decreased sufficiently that it equals the second, at which point the two-phase boundary will be vertical; further increases in pressure will decrease the first term even further, and the slope of the two-phase boundary will become negative. At the maximum on the solidus in P-S space, equation (12) reduces to

$$\frac{C_P^s}{T}\left(\frac{dT}{dP}\right)_{2\varphi} - V^s\alpha^s = 0, \tag{16}$$

which on rearrangement becomes

$$\left(\frac{dT}{dP}\right)_{2\varphi} = \frac{TV^s\alpha^s}{C_P^s}. \tag{17}$$

The expression on the right-hand side is the equation for the slope of the solid adiabat (that is, the isentrope), and thus the maximum on the solidus in P-S space corresponds to a tangency between the solid adiabat and the slope of the solidus in P-T space (as well as, obviously, in P-S space, where both are vertical); likewise, the maximum on the liquidus corresponds to such a tangency between the liquidus (coincident with the solidus in P-T space for the one-component system) and the liquid adiabat. Note that the maxima on the P-S solidus (point *9* in fig. 13A) and liquidus (point *15*) do not

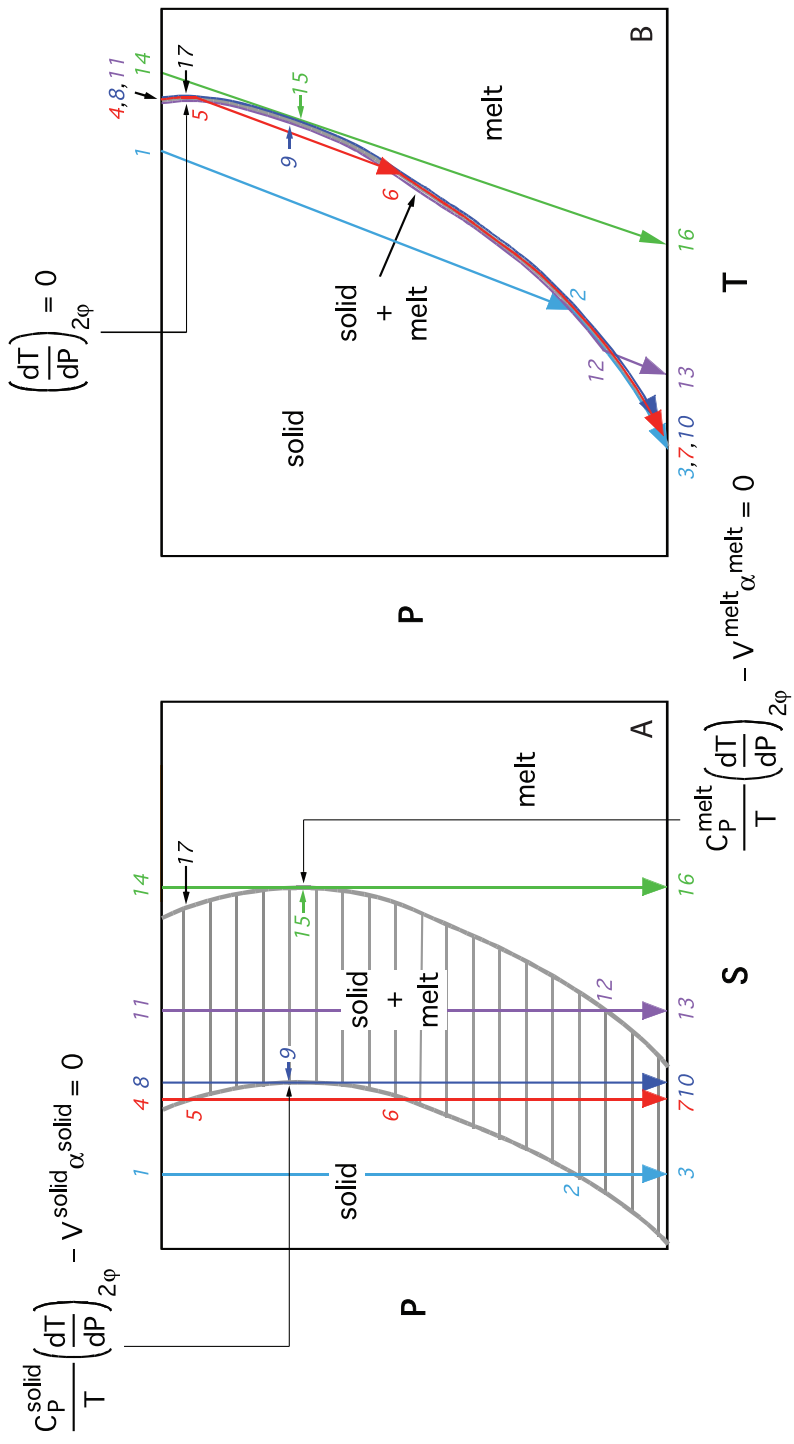

Fig. 13. Schematic (A) P-S and (B) P-T diagrams for a one-component system with maxima in S on the solidus (point *9*) and liquidus (point *15*). These points are where the solidus and liquidus are vertical in P-S space; they correspond to tangencies between the solid and liquid isentropes and the solid + melt univariant curve in P-T space. Note that these maxima are distinct from a maximum on the P-T solidus (point *17*), at which point solid and melt have the same density ($\Delta V_r = 0$). Several isentropes are shown, and the details of decompression on these isentropes are discussed in the text.

occur at the same pressure, since V, α, and C_P for the solid and liquid generally differ. The schematic example shown in figure 13A shows the liquidus maximum occurring at lower pressure than the solidus maximum; there is no thermodynamic constraint on this topology, but this is the generally expected relationship because Vα is generally larger for melts than solids.

Figure 13 shows several isentropes and allows the consequences of this particular topology on mantle melting to be visualized. The path labeled *1→2→3* is the "normal" one: that is, upwelling solid begins to melt when the isentrope reaches the solidus (*2*), and the melt fraction and productivity increase progressively with further decompression. Material following the path labeled *4→5→6→7* on figure 13A has the contrasting behavior of being partially molten at the highest pressure (*4*), initially crystallizing on ascent until at *5* it is completely crystalline, traversing the solid field (*5→6*), then reintersecting the solidus at *6* and melting progressively with further decompression; when examined in P-T space (fig. 13B), this path initially follows the two-phase univariant curve for solid + melt (*4→5*), then crosses the solid field for a short pressure interval (*5→6*), then again coincides with the univariant curve after melting recommences (*6→7*). Material on the unique isentrope that intersects the maximum on the solidus follows the path *8→9→10*, with melt fraction decreasing to zero from *8→9*, then increasing again with depressurization (*9→10*); in P-T space, this path follows the univariant curve over the entire pressure interval. Paths such as *11→12→13* begin partially molten (but with higher initial melt fractions than *4* and *8*), and with decompression the melt fraction initially decreases but reaches a minimum at $F > 0$; then it increases again, until complete melting is reached (*12*), after which the material follows an isentropic path through the liquid field. The minimum in melt fraction on this path occurs at the pressure at which the following relationship is satisfied:

$$-F\left(\frac{dS^l}{dP}\right)_{2\varphi} = (1 - F)\left(\frac{dS^s}{dP}\right)_{2\varphi}; \tag{18}$$

thus, this minimum depends on the specific entropy of the system and occurs at a pressure between the maximum in S on the solidus (*9*) and that on the liquidus (*15*). In P-T space, this path follows the univariant curve from *11* to *12*, after which it follows a liquid adiabat (*12→13*). Path *14→15→16* follows a single liquid adiabat, but is tangent to the maximum on the P-S liquidus at *15*.

As emphasized previously, there is considerable information and complexity contained in the P-S diagram in figure 13A that is not apparent in the corresponding P-T diagram in figure 13B. In particular, there need be no indication from the shape of the univariant curve in figure 13B that the maxima on the P-S solidus and liquidus are even present, and the complex variations in F with decompression that are possible (for example, on paths such as *11→12*) and their variations with the specific entropy of the system are not apparent since these paths all simply follow the univariant curve for solid + liquid. It is important to note that the maximum on the univariant curve in P-T space (point *17*), which occurs for $\Delta V_f = 0$ (and which must occur, if at all, at higher pressures than the P-S maxima, provided $\alpha^{\varphi} > 0$, such that the single phase isentropes have positive slopes in P-T space), is independent of maxima in P-S space and reflects entirely different phenomena.

The possibility of maxima in S on the solidus and liquidus of mantle peridotite was suggested by Asimow and others (2001) based on extrapolation of the MELTS thermodynamic model of the solidus of fertile peridotite to pressures of 60 to 80 kbar. It is also present in the treatment of Miller and others (1991), where the melt fractions along hot isentropes appropriate for komatiite genesis have minima in melt fraction

between 60 kbar (near the liquidus) and 110 kbar (near the solidus). It will be difficult to determine directly whether such a topology actually exists, since P-S diagrams are constructed by calculation based on thermodynamic properties, but it is a simple consequence of a concave downward solidus (which is difficult to avoid given the greater compressibility of liquids relative to solids), the increasing solidus temperature with pressure, and the assumption that αV remains positive for solid and liquid.

The analysis presented here for a one-component system provides a useful framework for evaluating the consequences of this topology on mantle melting (although "cusps" on the solidus due to solid-solid transitions could make this topology metastable; see section 9). Up to this point, our treatment (for example, fig. 7 and fig. 11) has been in accord with the conventional wisdom that solids will intersect the solidus upon isentropic decompression, and that higher specific entropies (or "potential temperatures", see McKenzie and Bickle, 1988) result in the initiation of melting at higher pressures. The maximum in S on the solidus, however, would lead to deep as well as shallow melting on a single adiabat and to the possibility that in the absence of solid-solid phase transformations, there is a value of S above which, no matter the depth from which upwelling begins, the source material will never be fully solidified. It is important to emphasize again, however, that these phenomena do not require a maximum on the solidus in P-T space.

One problem to which the topology shown in figure 13 could apply is the solidification of a planetary-scale magma ocean (Miller and others, 1991). Starting from a totally molten state, the crystallization of a convecting magma ocean can be envisioned as a series of stages characterized by a succession of isentropes at progressively lower values of specific entropy. If the pressure at the base of the ocean is high enough that the topology in figure 13A applies, crystallization begins at *15*, the maximum on the liquidus in P-S space. Thus, contrary to the usual expected behavior, crystallization could commence in the interior rather than at the boundaries of the magma ocean, and this behavior does not require a maximum on the P-T solidus. Although assuming $\alpha^l > 0$ (such that the liquid adiabat has a positive slope), point *15* must be at lower pressure than any maximum on the P-T solidus, it is not possible to say in general for multicomponent systems whether the crystals that grow will be denser than the coexisting liquid (see Walker and others, 1988).

7. An alternative approach to visualizing adiabatic melting

The use of P-S diagrams provides a straightforward and rigorous approach to visualizing adiabatic decompression melting. There is, however, an alternative approach that has been more widely used to analyze adiabatic melting paths (Ramberg, 1972; Cawthorn, 1975; Hess, 1992; Langmuir and others, 1992; Longhi, 1992; Hart, 1993). Although this alternative approach is not as general as the one developed above, it is worth analyzing because it is so widely used, because it is conceptually slightly different from our approach, and because it provides additional insights into some of the points we have made.

Figure 14A illustrates this approach for a one-component system. The path begins in the solid field at point *1*. The solid then decompresses adiabatically and reversibly past the solidus [point *2* (P_i, T_i)], following the metastable solid isentrope to point *3* (P_f, $T_{i'}$). It is important to emphasize that at *3*, the solid is metastable relative to a molten or partially molten state. The next step is to allow the solid at *3* to convert isobarically to the stable assemblage at point *4* (P_f, T_f). We will assume that the overstepping of the melting reaction (that is, *2*→*3*) is small enough that the solid only partially melts and therefore that the stable assemblage at *4* is solid + melt; that is, state *4* is on the univariant solidus.

A key point is the nature of the isobaric conversion of the metastable solid at *3* to the stable, partially molten assemblage at *4*. Although previous treatments of this step

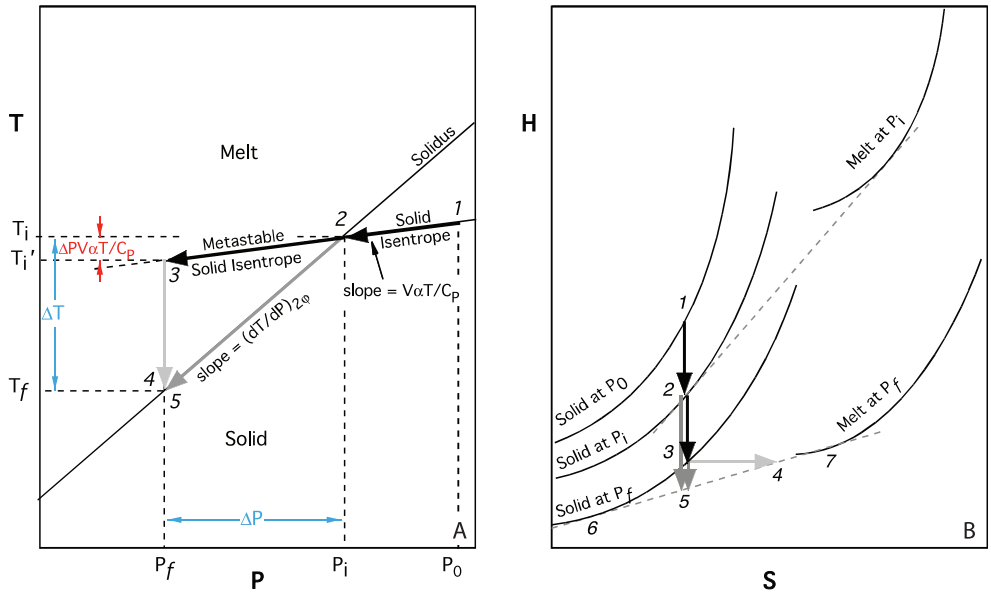

Fig. 14. Schematic comparison of enthalpy- and entropy-conservation during adiabatic melting using (A) P-T and (B) H-S diagrams (after Asimow and others, 1997). (A) In P-T space, a parcel of adiabatically upwelling solid intersects its solidus at state *2* (P_i, T_i). If the solid crosses the solidus without melting, it continues on the metastable extension of the isentrope from *2*→*3*, reaching state *3* (P_f, $T_{i'}$). The stable partially molten state *4* (P_f, T_f) is obtained by an adiabatic, isobaric (that is, isenthalpic) process whereby the enthalpy recovered by cooling from state *3* to state *4* (that is, from $T_{i'}$ to T_f at P_f) equals that required to melt up to some degree of melting F_H. Stable state *5* can be reached either by reversible, adiabatic (that is, isentropic) melting from state *2* to state *5* along the solidus or by an isentropic (but non-adiabatic) isobaric process whereby the entropy recovered by cooling from state *3* to state *5* (that is, again from $T_{i'}$ to T_f at P_f) equals that required to melt up to some degree of melting F_S. (B) The same processes can also be visualized in H-S space. Metastable decompression of solid from *2* to *3* is illustrated by the vertical black arrow from the stable solid curve at P_i to the metastable part of the solid curve at P_f. Adiabatic, isobaric isenthalpic conversion of the metastable solid at *3* to a stable partially molten assemblage is represented by the horizontal (that is, constant H) light gray arrow from *3*→*4*. The alternative of isobaric isentropic conversion of the metastable solid at *3* to a stable partially molten assemblage is represented by the vertical (that is, constant S) gray arrow from *3*→*5*. It is clear from this construction that the amount of melting at *4* (F_H) is greater than that at *5* (F_S). Note that point *5* can also be reached by reversible adiabatic (that is, isentropic) melting on the vertical path from *2*→*5* passing reversibly through a succession of partially molten states (for example, as we would read for isentropic batch partial melting on a P-S diagram).

assume it is adiabatic (Ramberg, 1972; Cawthorn, 1975; Hess, 1992; Langmuir and others, 1992; Longhi, 1992; Hart, 1993), it is important to emphasize that such an isobaric, adiabatic conversion from a metastable solid to a stable solid + melt assemblage is *not* reversible. Thus, $dS_{3\to4} \neq 0$; instead, this process is isenthalpic ($dH_{3\to4} = 0$; recall our previous demonstration in section 3 that this is the case for an isobaric adiabatic process). Because this step is irreversible, $dS > 0$: that is, for such a process at constant H and P, equilibrium is reached when entropy is maximized. Thus, we make the important distinction that although the path as described from *1*→*2*→*3*→*4* is adiabatic, it is not isentropic. Consequently, the final partially molten state on the solidus at point *4* (P_f, T_f) reached on this path must differ from that of material that reached (P_f, T_f) by the reversible adiabatic path *1*→*2*→*5* (that is, for material that does not overstep the solidus metastably, but instead melts reversibly and progressively for each infinitesimal decrement of pressure).

How does melt production for the adiabatic process with an irreversible isenthalpic melting step (*1*→*2*→*3*→*4*) differ from reversible adiabatic (that is, isentropic) melt

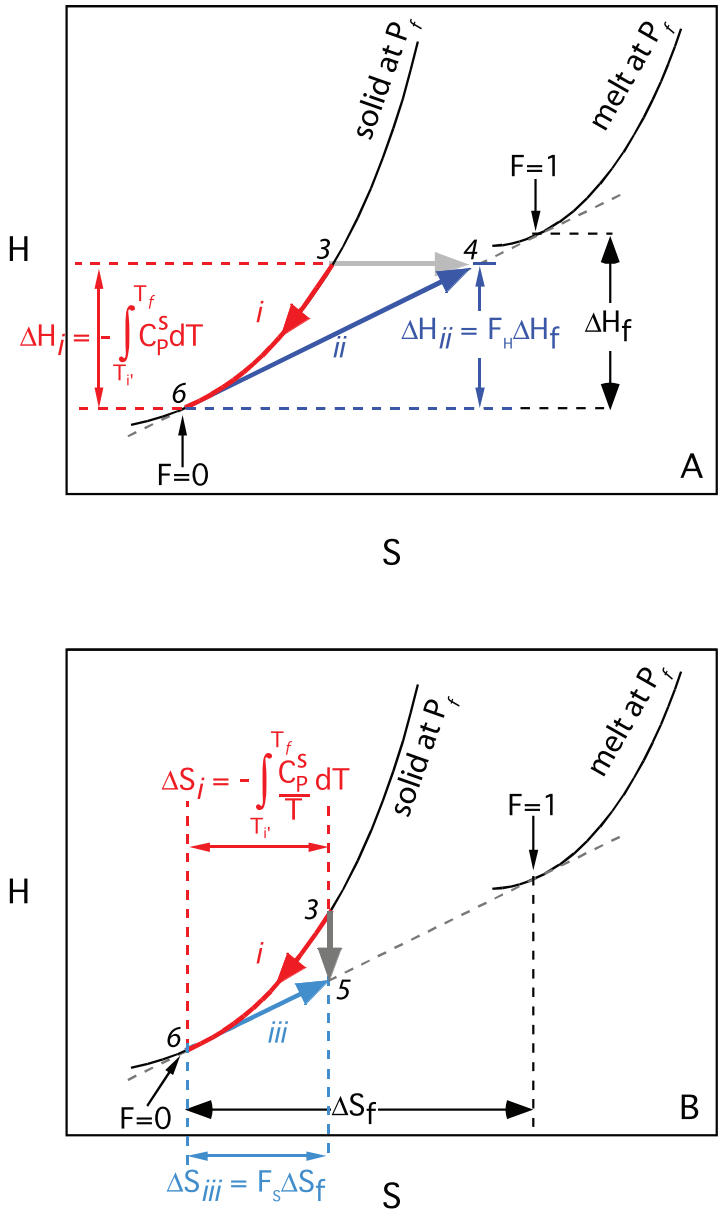

Fig. 15. H-S diagrams after figure 14 illustrating the enthalpy-balanced [*3→4*; equation (19)] and entropy-balanced [*3→5*; equation (20)] conversions of metastable solid to the stable partially molten assemblages at P_f. In (A), the enthalpy-balanced conversion is broken into *3→6→4*, illustrating graphically the significance of equation (19). Likewise, in (B), the entropy-balanced conversion is broken into *3→6→5*, illustrating graphically the significance of equation (20).

production (*1→2→5*)? Figure 14B and figure 15 illustrate this difference using the H-S diagrams developed above (see figs. 2 – 5). Curves describing stable (and metastable) states of solid and liquid are shown in figure 14B at several pressures. P_0 is the pressure of the initial state *1*. P_i is the pressure at state *2*: that is, the pressure at which the

isentrope for the solid crosses the solidus (at higher pressure the solid is stable, whereas it is metastable relative to solid + melt at lower pressure). P_f is the pressure of states *3* and *4*: that is, the pressure at which the irreversible, adiabatic transformation from metastable solid to stable solid + melt occurs; it is also the pressure of state *5*. The isentropic path from stable state *2* on the solidus at P_i to the stable, partially molten state *5* at P_f is vertical in H-S space (fig. 14B and fig. 15B). The irreversible adiabatic path, however, corresponds to a path on figure 14B and figure 15A from the stable state *2* at P_i to the metastable solid state *3* at P_f (reached by a reversible adiabatic decompression), followed by a second, horizontal path to the stable partially molten state *4* at P_f (which has the same enthalpy as state *3*). It is clear from figure 14B and figure 15 that state *4* is at a higher melt fraction and higher S than state *5* (reflecting the fact that during the isobaric, isenthalpic conversion from solid to solid + melt, equilibrium is achieved when S is maximized); note, however, that given the univariant nature of the solid + melt coexistence in this one-component system, the temperature is the same for states *4* and *5*.

The amount of melting along the *3*→*4* path with its irreversible isenthalpic melting step can be quantified by breaking it into the non-adiabatic reversible path *3*→*6*→*4*, as illustrated in figure 15A. The amount of melting for this isenthalpic conversion, F_H, can be quantified as follows,

$$-\int_{T_{i'}}^{T_f} C_P^s dT = \Delta H_f F_H, \tag{19}$$

where the integral on the left-hand side is the enthalpy "released" by cooling the metastable solid reversibly and isobarically at P_f from state *3* ($T_{i'}$) to state *6* (T_f) (that is, on path *i* on fig. 15A), and the product on the right-hand side is the enthalpy "consumed" during reversible melting at (P_f,T_f) going from state *6* to state *4* (that is, on path *ii* in fig. 15A).

The same approach can be used to quantify the amount of melting for isentropic melting provided that S rather than H is conserved in converting the metastable solid assemblage (state *3*) to the stable partially molten assemblage on the solidus. We can do this by breaking the isentropic path from state *2* to state *5* illustrated in figure 14 into the sum of paths *2*→*3* and *3*→*5*. Note that isobaric conversion of the metastable solid at state *3* to the final partially molten condition at state *5* would be an irreversible and non-adiabatic process, whereas the direct isentropic, polybaric path from *2*→*5* is accomplished in a series of infinitesimal, reversible, adiabatic steps. Nevertheless, an entropy-balanced calculation comparing states *3* and *5* is still valid since state *5* is on the isentrope, and its properties are independent of the path by which it is reached (Miller and others, 1991).

The required entropy balance can be visualized by breaking the irreversible isentropic path from *3*→*5* into the non-adiabatic reversible path *3*→*6*→*5*, as illustrated in figure 15B. The amount of melting for this isentropic conversion, F_S, can be quantified by the following expression, analogous to equation (19) for the enthalpy-balanced case

$$-\int_{T_{i'}}^{T_f} \frac{C_P^s}{T} dT = \Delta S_f F_S, \tag{20}$$

where the integral on the left-hand side is the entropy "released" by cooling the metastable solid reversibly and isobarically at P_f from state *3* ($T_{i'}$) to state *6* (T_f) (that is, on path *i* on fig. 15B), and the product on the right-hand side is the entropy

"consumed" during reversible melt production at (P_f,T_f) in going from state *6* to state *5* (that is, on path *iii* on fig. 15B). We emphasize that this is conceptually identical to the balancing implicit in equation (19), except entropy rather than enthalpy is conserved. The construction shown in figure 15 can also be used to understand what would be required to reach the stable isentropic state *5* (P_f, T_f) from metastable state *3* (P_f, $T_{i'}$). In H-S space, this is a simple vertical (that is, constant S) process, but we have seen that a "natural" or spontaneous isobaric process moves horizontally, that is, with an increase in S. The only way to achieve state *5* from state *3* would be to extract heat from the system (equal to $\Delta F \Delta H_f$, where $\Delta F = F_H - F_S$ is the difference in melt fraction between states *4* and *5*) to compensate for the irreversible entropy production on melting of the metastable solid.

It is simple to show that the amount by which the enthalpy-balanced calculation overestimates the total melt production relative to the true isentropic path is small. We first integrate the left-hand side of equation (19) assuming C_P^s is a constant, and then rearrange the resulting expression to give

$$F_H \approx \frac{C_P^s}{\Delta S_f} \frac{\Delta T}{T_f}, \tag{21}$$

using the fact that, for univariant melting, $\Delta H_f = T_f \Delta S_f$ and defining the temperature difference between the metastable solid isentrope and the solidus as $\Delta T = T_{i'} - T_f$. We can similarly integrate and rearrange equation (20), again assuming constant C_P^s, which gives the following after rearrangement:

$$F_S \approx \frac{C_P^s}{\Delta S_f} \ln\left[\frac{\Delta T}{T_f} + 1\right]. \tag{22}$$

Using a series expansion for the logarithmic term and neglecting the terms higher than quadratic, we get

$$F_S \approx \frac{C_P^s}{\Delta S_f} \frac{\Delta T}{T_f}\left[1 - \frac{1}{2}\left(\frac{\Delta T}{T_f}\right)\right]. \tag{23}$$

Comparing equations (21) for F_H and equation (23) for F_S, we obtain

$$F_S \approx F_H\left[1 - \frac{1}{2}\left(\frac{\Delta T}{T_f}\right)\right]. \tag{24}$$

This approximation confirms what we determined graphically previously: that is, the enthalpy-balanced approximation overestimates melt production compared to the entropy-balanced form. Using the example of diopside, assuming melting begins at 70 kbar and 2337 K, after 20 kbar of decompression ΔT =105 K, or $\Delta T/T_f \approx 0.05$, producing an overestimate in melt production based on the isenthalpic approximation of 2.4 percent relative. Note that this overestimate increases with melt fraction (since ΔT becomes a progressively larger fraction of T_f with increasing decompression (and melting), as ΔT increases and T_f decreases), reaching a maximum overestimate of 15 percent relative for the diopside case after 69 kbar of decompression, where the enthalpy-balance model reaches complete melting and the isentropic model is at F = 0.87. On the other hand, as $F \to 0$ (that is, $\Delta T \to 0$), the enthalpy- and entropy-balanced cases become indistinguishable. We note in this regard that the irreversible treatment of Ganguly (2005), which continuously conserves gravity-compensated enthalpy, differs from the irreversible treatment arising from finite steps and enthalpy balance; that is, productivity in the Ganguly (2005) formulation is different even in the limit $F \to 0$.

Although the quantitative difference in melt production between the isenthalpic and isentropic conversion from the metastable solid to a stable partially molten state is small, particularly at low degrees of melting, this discussion illustrates the importance of a precise definition of the thermodynamics governing the melting process. Thus, the treatment involving an isenthalpic melting step is not "wrong"; it does follow an adiabatic path, just not the reversible one. It is also possible that such a path could be of petrologic or geophysical interest: for example, such an analysis would apply at a solid-solid phase transformation for which the transition might plausibly be kinetically inhibited such that a metastable state persists well into the stable field of the reaction products, followed by a rapid, irreversible transformation to the stable assemblage (Solomatov and Stevenson, 1994).

Finally, we note that this approach to thinking about decompression melting provides a straightforward explanation of why decreasing T and increasing $(dT/dP)_{2\varphi}$ lead to increases in the productivity of isentropic fusion: that is, although we emphasized the importance of these two parameters in the equations for productivity [equations (14) and (15) for batch and fractional fusion], we offered no simple explanation for why this was so other than the curvature of the solidus and liquidus in P-S space. As shown in figure 14 and figure 15 and equation (20), the amount of melting for a given isentropic decrement of P is approximately proportional to the integral of C_P^s/T over the T drop associated with the pressure decrement. Since C_P^s/T is larger at lower T (assuming C_P^s is roughly constant), its integral over a given ΔT is larger at lower T, and thus the amount of melting will be larger. For example, if we compare the entropy balance for equal pressure decrements from B and A in figure 16, the integral of C_P^s/T from T_3 to T_4 (that is, starting from B) and thus the amount of melting is larger than from T_1 to T_2 (that is, starting from A) even though the temperature drop is the same in both cases. Similarly, to evaluate the importance of the slope of the solidus, $(dT/dP)_{2\varphi}$, we compare the entropy balances for equal pressure decrements from B and C in figure 16. The amount of melting on decompression is again approximately proportional to the integral of C_P^s/T over the T drop associated with the pressure decrement, but since the slope of the solidus is higher for C, the temperature drop starting from C is larger for a given pressure decrement than starting from B, and this larger T interval over which C_P^s/T is integrated leads to a larger value of the integral in equation (20). In other words, for the same value of ΔP and mean T, if the slope of the solidus is higher, the integral of C_P^s/T is higher due to a larger ΔT, so F (and productivity) is higher. Although in principle no different than the explanation given in section 6.1 of why T and solidus slope influence the slopes of the two-phase boundaries in P-S space and consequently the productivity, this explanation based on the entropy balance during melting of the metastable solid may be more intuitive because it can be visualized directly in P-T space.

8. WHY THE MANTLE PARTIALLY MELTS

8.1. P-S as the Independent Variables

The treatment of isentropic melting based on P-S diagrams in one-component systems helps to explain why the mantle partially rather than totally melts. Although this might seem like an odd statement, as we show in the next section, if P and T were the independent variables for melting in a one-component system, partially molten systems would not occur. Indeed, this would be the case for any choice of independent variables in which both variables must be equal in coexisting phases at equilibrium (such as P, T, or chemical potential); that is, an arbitrary choice of values for two such variables will nearly always yield only one phase since it is essentially impossible that such a choice would produce conditions right on the univariant curve where both phases would be stable (see fig. 8B). However, the situation is different for one-

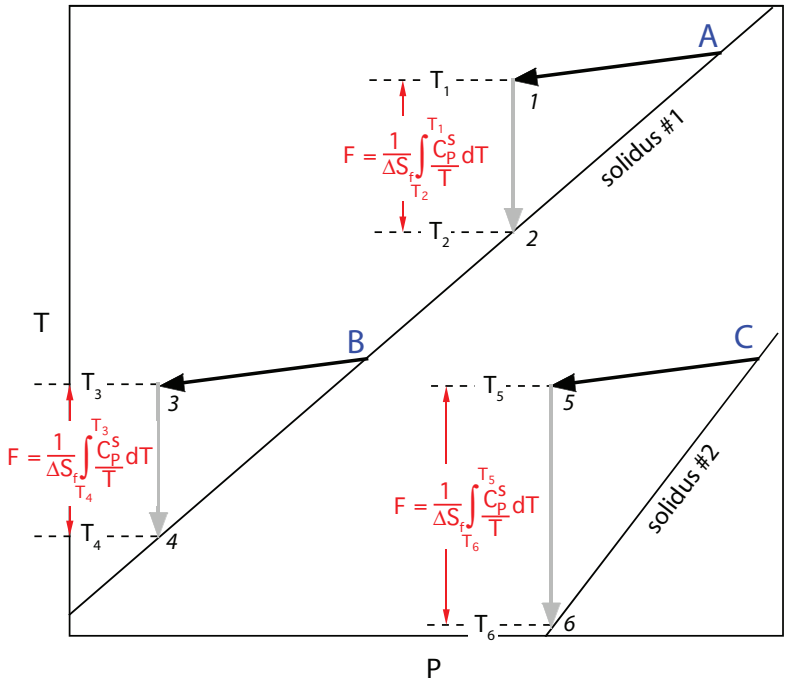

Fig. 16. P-T diagram illustrating the amount of melting based on the entropy-balance calculation [fig. 14 and fig. 15; equation (20)] for different conditions. Although the temperature interval of the integration to calculate the entropy balance is the same at high temperature (A) and low temperature (B) for a given solidus slope, the 1/T term inside the integral means that the integral and therefore the total amount of melting for a given pressure decrease is higher at B than A. Similarly, although B and C are at the same temperature, the higher solidus slope at C means that for the same pressure decrement, the integral is taken over a larger ΔT, so the integral and total amount of melting for a given pressure decrease is higher at C than B. These comparisons illustrate why melt productivity increases with decreasing T and increasing solidus slope.

component systems in which P and S are the independent variables, or indeed for any choice of independent variables for which one of the independent variables (P in this case) must be the same in all phases in the equilibrium assemblage and the other independent variable (S in this case) differs in the coexisting phases; that is, an arbitrary choice of values for the two variables can produce an equilibrium assemblage either in one of the one-phase fields or in the two-phase field (see fig. 8A). Although not shown, if the independent variables were S and V, both of which differ in coexisting phases, an arbitrary choice of these variables can produce one-, two-, or three-phase assemblages.

Our analysis shows that an isentropic decompression that produces melting must pass through the two-phase field over a finite pressure interval: that is, it must *partially* melt as it decompresses. This reflects entirely the nature of the independent variables in the process: that is, because the S of coexisting solid and melt differ (by ΔS_f), a significant P and T interval is required at constant total S to transform from solid to liquid; P and T must change by a sufficient amount that at the end of the process, the S of the liquid when melting is complete is equal to the S of the solid just as melting begins. The usual way of stating this is that for every increment of melting of the solid at constant total entropy, entropy is required (equal to the entropy of fusion) to produce the higher entropy liquid phase; this entropy is provided by cooling (see the analysis

associated with fig. 15B) so that melting must take place over a T (and P) interval (Hess, 1989).

8.2. P-T as the Independent Variables

Figure 17 illustrates the contrasting situation for the choice of P and T as the independent variables. The dotted lines in this figure correspond to isotherms. Figure 17A shows in green an *isothermal* (as opposed to an isentropic) decompression (*8→2→9→10*) in P-S space; this same path is vertical in P-T space, as shown in figure 17B. The path of an isentropic decompression (*1→2→3→4→5*) that starts to melt at the same pressure and temperature (that is, at point *2*) is shown in P-S and P-T space in red on these same figures for comparison. For the isothermal decompression, the system passes from a totally solid state to a totally liquid state at the P and T corresponding to the intersection of the isotherm with the solidus and liquidus (points *2* and *9* in figs.17A and 17B): that is, total rather than partial melting must occur in this case. As the pressure decreases from infinitesimally higher than that of the solidus to infinitesimally lower, the solid goes from 0 to 100 percent molten at constant temperature. We can imagine that the system is immersed in an infinite heat bath at constant T and that as the solidus is crossed on decompression, the heat bath provides sufficient heat ($q = mT\Delta S_f$) to increase the entropy by the amount required to melt the solid reversibly. This is illustrated clearly in figure 17A where the system goes from being totally solid (point *2*) to totally molten (point *9*) by crossing the two-phase field at constant P and T (that is, increasing S by ΔS_f). In contrast to the isentropic case, the entropy of fusion does not have to be supplied by cooling of the system, so the system does not have to cool as melting proceeds, and complete melting occurs at much higher temperature than in the isentropic case (compare the temperatures at points *4* and *9* in fig. 17B). The same reasoning applies to the more commonplace process of isobaric melting in a one-component system with increasing temperature: that is, complete melting occurs at a single temperature.

8.3. Heterogeneous Mantle Sources

Although it might at first appear based on the previous paragraph that the choice of P and T as independent variables would never apply to mantle melting, the analysis presented above is similar to that applicable to the limiting case of a heterogeneous mantle with an infinitesimal amount of a low-melting source rock. This would be the case, for example, for a mantle source with minor eclogitic or pyroxenitic veins in a dominantly peridotitic mantle (Wood, 1979; Allègre and others, 1984; Langmuir and Bender, 1984; Zindler and others, 1984; Allègre and Turcotte, 1986; Prinzhofer and others, 1989; Ben Othman and Allègre, 1990; Langmuir and others, 1992; Chabaux and Allègre, 1994; Lundstrom and others, 1995; Hirschmann and Stolper, 1996). Suppose that a parcel of largely peridotitic mantle is well below the solidus of the peridotite, and it ascends along a continuous and nearly reversible P-T path. Suppose further, however, that the peridotite contains as veins or pods a small fraction of material that melts at much lower temperature than the dominant peridotitic assemblage. In this case, providing the chemical interaction between the vein material and the surrounding mantle are minimal but they are always in thermal equilibrium (Sleep, 1984; Hirschmann and Stolper, 1996; Phipps Morgan, 2001) and the amount of vein material is infinitesimal relative to the enclosing solid, the P-T path of the low-melting vein material would be constrained to the continuous isentrope of the dominant, subsolidus material. Thus, although P and S are the independent variables for the enclosing solid, P and T are externally imposed on the vein material. This is illustrated in figure 18. Solid A is the dominant material, and we assume it is a one-component material. Thus, upwelling mantle follows the isentrope of solid A. This isentrope crosses the solidus of solid B, approximated as a second one-component

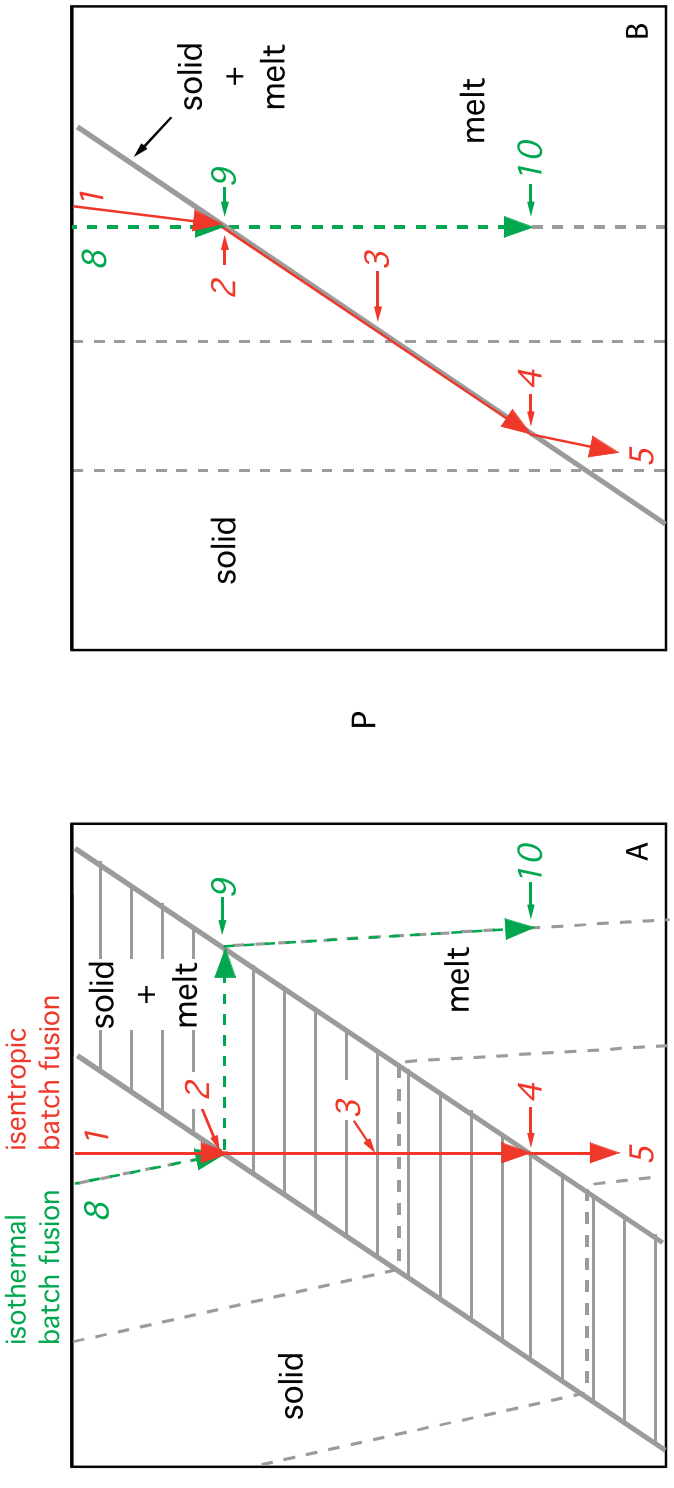

Fig. 17. Schematic (A) P-S and (B) P-T diagrams for a one-component system with solid and melt (from fig. 7). An isothermal decompression path (*8*→*2*→*9*→*10*) is compared with an isentropic decompression path (*1*→*5* from fig. 8). See the text for discussion.

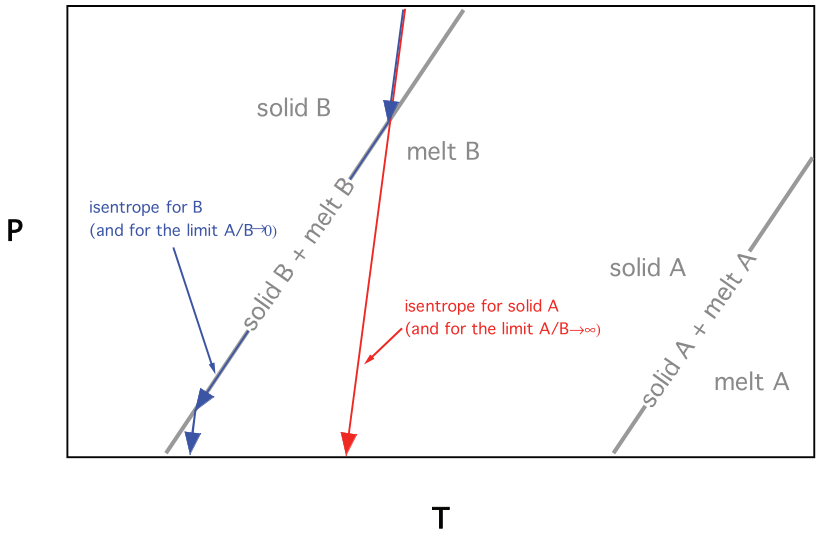

Fig. 18. Schematic P-T diagram illustrating melting of sources containing two one-component systems that interact thermally but not chemically. The solidus of B is at lower temperature than that of A. Two cases of isentropic decompression melting are shown: first, in red, a source with A » B, in which the system essentially follows an isentrope for pure solid A, and the minor component B melts completely at the single temperature and pressure at which the solidus of B is crossed; second, in blue, a source with B » A, in which the system essentially follows an isentrope of B, undeflected by the small amount of entrained A. See the text and sections 8.3 and 10 for details.

solid with a lower solidus than A. Clearly, the P-T path defined by the isentrope of the dominant material, solid A, crosses the solidus of solid B at a single P and T, and total melting of B occurs at this point; thus this situation closely approximates one in which, from the standpoint of the enclosed pyroxenite veins, P and T are externally imposed (that is, independent) variables. In reality, the entropy of fusion of B is supplied by heat flow from the enclosing solid A, so the actual P-T path, although still adiabatic, must deviate, even if only infinitesimally, from the isentrope of solid A, following the solidus of B until B is completely molten. A fuller analysis of upwelling, including cases in which the amount of B is not infinitesimal, is presented in section 10.

8.4. The Importance of Additional Chemical Components

The explanation we have given for why the mantle melts partially during decompression melting is incomplete: that is, because the real mantle is a polymineralic, multicomponent assemblage (rather than a single, one-component phase), the melting interval at constant P (that is, the temperature difference between the solidus and liquidus) is non-zero, so that in contrast to the situation for a one-component system, when P and T are chosen as the independent variables, the system melts over a T (or P) interval. This is readily understandable in terms of the nature of the independent variables, as described above. Consider isothermal decompression melting of a binary solid solution (for example, forsterite-fayalite or anorthite-albite) along the path *1→2→3→4→5* in figure 19. Obviously, this binary solid melts over a range of pressures (that is, it partially melts), in contrast to the behavior of a one-component system, even though P and T are the independent variables, and they are the same in the coexisting solid and melt. However, there are, in fact, three independent variables in this process – P, T, *and* X_b – and like S in the one-component cases described above, X_b is not the same in the coexisting phases. Thus, for a binary system in which P, T, and X are the

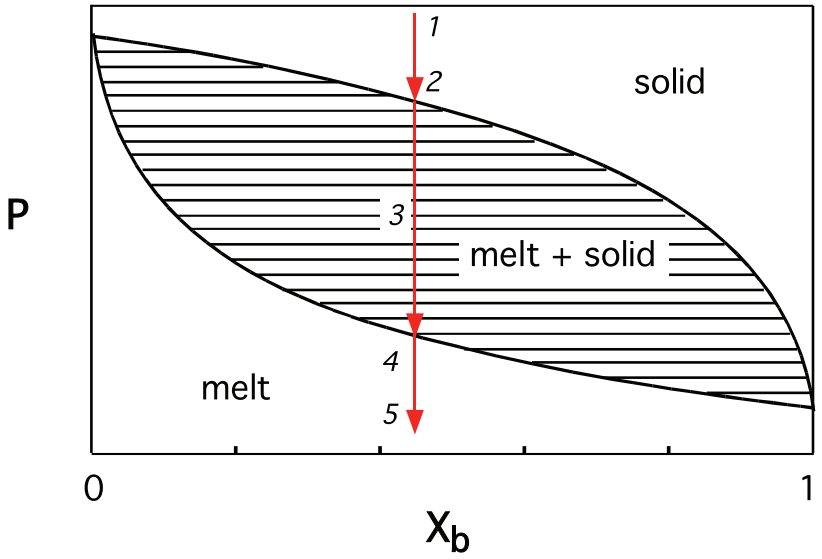

Fig. 19. Schematic isothermal P-X diagram for batch melting of a binary solid, demonstrating that systems with more than one component typically melt partially on decompression even when P and T are chosen as the independent variables. X_b is the mass (or mole) fraction of one of the two components. The path 1→5 illustrates progressive melting as pressure is decreased at constant temperature.

independent variables, both one- and two-phase assemblages are possible for an arbitrary choice of the independent variables, and isothermal decompression melting or isobaric melting with increasing T leads to partial melting. However, note that with P, T, and X_b as the independent variables, three-phase assemblages are practically impossible, whereas with T, S, and X_b as the independent variables, such assemblages are easy to achieve (Asimow and others, 1997). Likewise, as mentioned above, if S and V are the independent variables for a one-component system, three-phase assemblages are possible for arbitrary choices of these variables. The general rule is that for each substitution of a variable such as P, T, and μ_i (which are the same in all phases in an equilibrium assemblage; the subscript i refers to the "i^{th}" component of a multicomponent system) with a variable such as S, V, and X_i, (which are not the same in coexisting phases), the number of phases that can be present in an equilibrium assemblage for an arbitrary choice of the independent variables increases by one. Thus, although it is true that the multicomponent nature of real mantle sources does indeed lead to partial rather than total melting of the mantle regardless of the melting process, the important point is that because the process under consideration is an adiabatic decompression, it would lead to partial melting even in a one-component system.

8.5. Isobaric Heating: The Case of P and H as the Independent Variables

Another melting process that can be illustrated with simple diagrams in a one-component system is the commonplace one of isobaric heating. This is important petrologically in crustal environments where, for example, hot, mantle-derived basaltic magmas underplate cooler, more felsic rocks and, as the basalt cools and crystallizes, heat flows into the crustal rocks and they melt (Huppert and Sparks, 1988b, 1988a; Bergantz, 1989, 1992). Similarly, juxtaposition of hot asthenospheric mantle against colder, volatile-rich continental lithosphere, associated for example with rifting, lithospheric delamination, and/or ascent of mantle plumes, has been suggested as a

heat source for the production of continental and ocean island magmas (Gallagher and Hawkesworth, 1992; Turner and others, 1992; McKenzie and O'Nions, 1995; Turner and others, 1996a, 1996b).

The melting processes in these cases are obviously not adiabatic because heat is added to the part of the system that is melting: that is, $q > 0$, so even if the process is reversible, $dS > 0$. If melting and achievement of equilibrium in the source takes place rapidly relative to the rate at which heat flows into it, we can envision the process as a reversible one in which the independent variables are P and H, such that $dP = 0$ and $dH = q = TdS$. Figure 20A shows an H-P diagram for a simple one-component system. This phase diagram, like the P-S diagram in figure 7A, is based on a series of isobaric H-S sections, except that it maps out the phase assemblages with maximum S for a given choice of H and P (rather than minimum H for a given S and P as in fig. 7A). The topology is similar to the P-S diagram; the slopes of the isotherms, isenthalps, and edges of the two-phase field are simple to derive and are given in the figure. The edges of the two-phase field are demonstrably non-parallel in this case because the second term in brackets in the equation for the slope of each edge is approximately the specific volume of the phase at that edge, and the liquid and solid volumes are typically significantly different. It should also be emphasized that H in this diagram is the specific enthalpy, without correction for the effects of gravitational potential, and thus decompression paths at constant H correspond to decompression at constant gravitational potential and cannot be used as a framework for modeling decompression due to ascent from the earth's interior (Ramberg, 1971; Waldbaum, 1971; Ramberg, 1972).

The path *1→2→3→4→5* illustrates reversible isobaric batch melting under these conditions. In the solid field from *1→2*, H increases as heat is added to the system ($dH = q$), and the temperature increases ($dT = dH/C_P^s$). Once the edge of the solid + melt field (point *2*; that is, the solidus) is reached, additional heat flow produces melt at constant temperature according to $dF = dH/\Delta H_f$. When sufficient heat has been added to the system (that is, equal to ΔH_f), the system is completely molten (point *3*). Further additions of heat then lead to increasing temperature according to the heat capacity of the liquid ($dT = dH/C_P^l$). As with the isentropic melting process, again because of the nature of the independent variables (that is, H is not the same in coexisting phases at equilibrium), the system partially melts with continuous changes in the independent variables. The corresponding P-T diagram for this process is shown in figure 20B, and the partially molten segment of the path (*2→3*) is compressed to a single point on the two-phase curve. A multicomponent system undergoing this same process will melt over a range of temperatures (that is, the solidus and liquidus do not usually coincide in a multicomponent system), but the one-component system nevertheless captures the essence of this process.

In this simple case, fractional fusion (that is, where each increment of melt is removed from the system as it is generated — Presnall, 1969) is not distinguishable from batch melting: that is, the residual solid is always at point *2* and the liquid at point *3* from the onset to the completion of melting, and melting in both cases is complete when the total amount of heat added to the system is equal to $m\Delta H_f$, where m is the initial mass of the system. It is important to note that the simple case of isobaric heating in a one-component system illustrated in figure 20 differs in this respect from isentropic decompression melting processes in which, as we showed above, fractional and batch fusion paths differ.

9. THE EFFECTS OF SOLID-SOLID PHASE TRANSITIONS ON ISENTROPIC MELTING

9.1. Solidus "Cusps"

The discussion thus far has focused on the melting of a single phase in a one-component system. Natural systems differ in that they consist of a larger number of

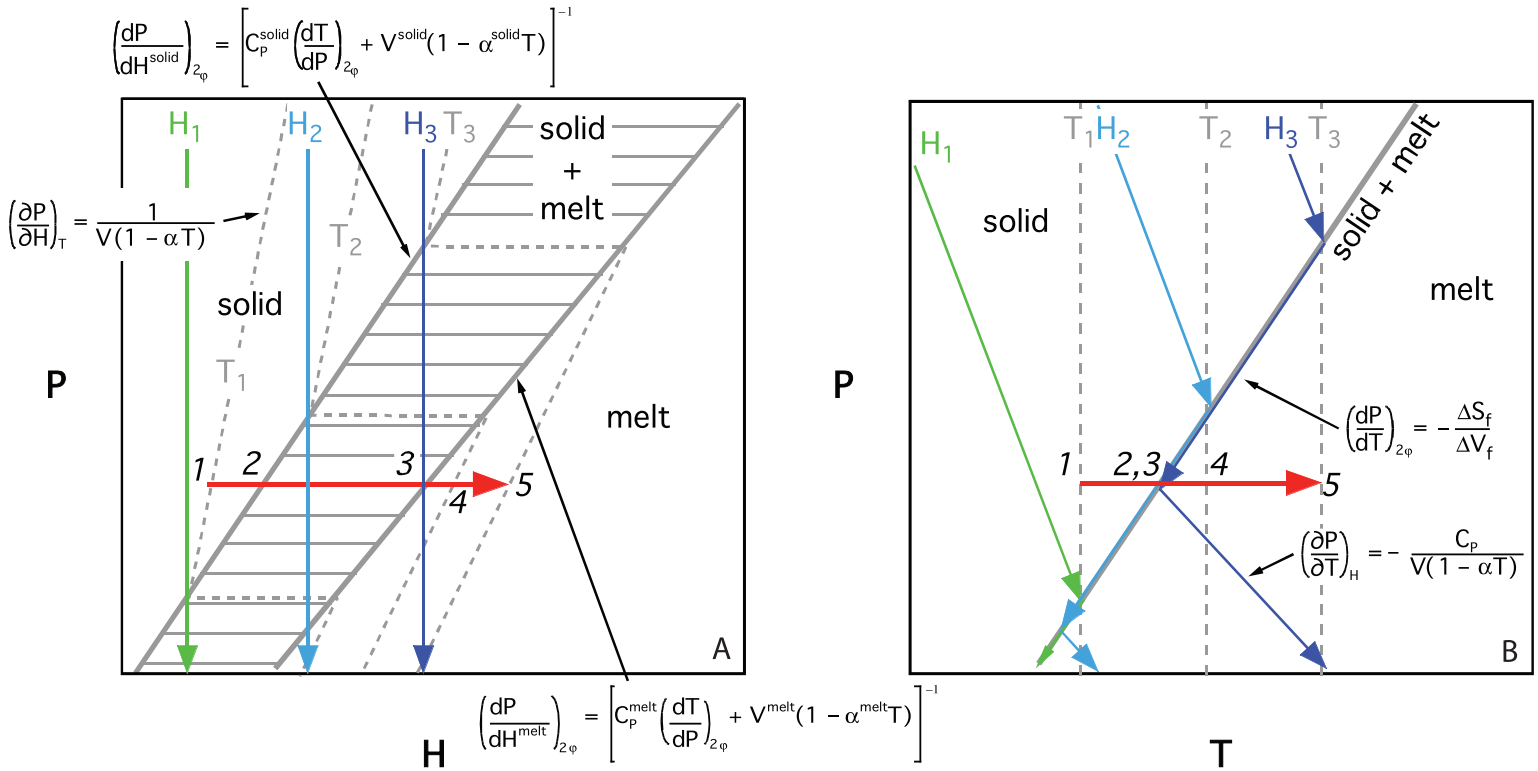

Fig. 20. Schematic (A) P-H and (B) P-T diagrams for a one-component system with solid and melt. The P-H diagram is a projection of the stable (that is, maximum S) assemblages as functions of P and H. Note that the solidus and liquidus in (A) are arbitrarily shown as linear and the corresponding univariant solid + melt coexistence in (B) is shown as linear. Equations for slopes of these boundaries are shown on the figure. Three isotherms (T_1, T_2, T_3) are shown as gray dashes lines/curves in both panels along with the equation for their slope in a single-phase region in panel (A). Three isenthalps (H_1, H_2, H_3) are shown as colored lines/curves in both panels along with the equation for their slope in a single-phase region in panel (B). The horizontal solid red arrows are used in the text to describe isobaric melting in which enthalpy is chosen as the independent variable and increased progressively by addition of heat to the system.

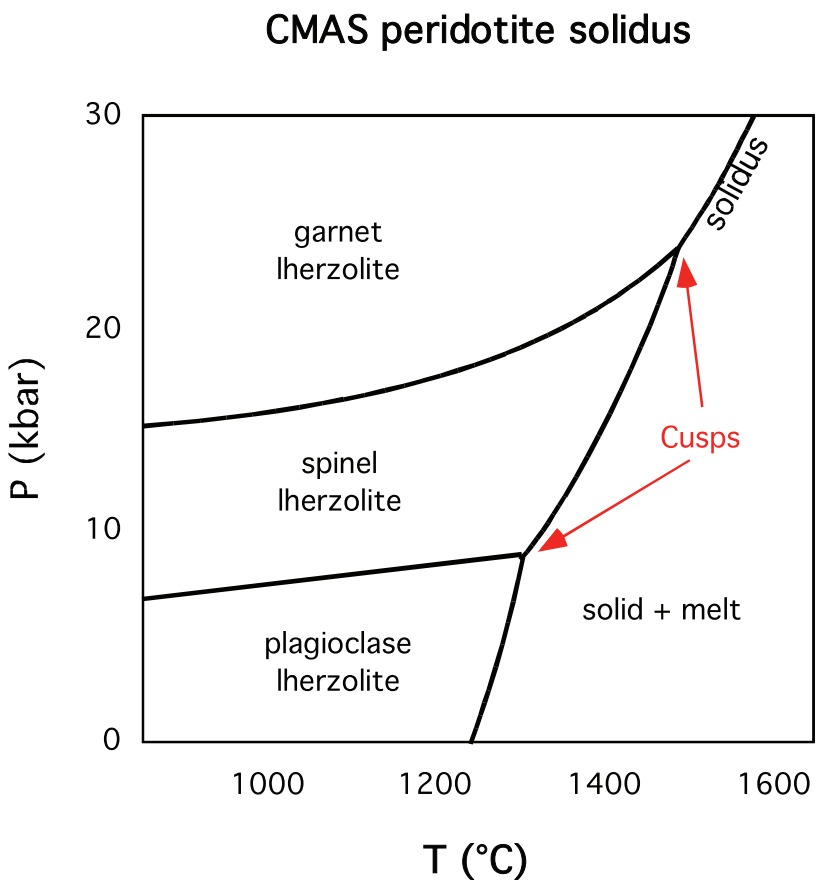

Fig. 21. Forsterite+enstatite+diopside-saturated solidus and subsolidus phase equilibria in the system CaO-MgO-Al_2O_3-SiO_2 (after Figure 3.3.4, in the Basaltic Volcanism Study Project, 1981), showing slope changes, or "cusps", on the solidus. These are invariant points in this system, and the slope changes in the solidus relate primarily to the volume changes associated with the intersections of the model plagioclase⟶spinel lherzolite and spinel⟶garnet lherzolite subsolidus transitions with the solidus. Note that the plagioclase⟶spinel lherzolite and spinel⟶garnet lherzolite subsolidus transitions have positive slopes in P-T space.

components and they usually contain several solid phases. During decompression melting, continuous and discontinuous reactions involving the various solid phases occur. These reactions either consume or release entropy and thus affect the entropy balance underlying isentropic decompression melting. Continuous reactions cannot be modeled in a one-component system, but discontinuous reactions in multicomponent systems have simple analogues in one-component systems, and in this section we explore the influence of such reactions on isentropic melting.

Figure 21 shows the near-solidus P-T diagram for olivine+orthopyroxene+clinopyroxene-bearing assemblages in the system CaO-MgO-Al_2O_3-SiO_2 (after Figure 3.3.4 in the Basaltic Volcanism Study Project, 1981), a useful model for natural mantle peridotites. The subsolidus assemblage transforms with increasing pressure from plagioclase- to spinel- to garnet-lherzolite via univariant solid-solid reactions. The stable segments of the univariant curves separating these distinct divariant fields terminate at the solidus in two invariant points. The topology of these invariant points is identical to that of a triple

point in a one-component system. In particular, the requirement that the metastable extensions of each of the three univariant curves meeting at such invariant points must project into the divariant field bordered by the other two univariant curves means that the slope of the solidus is discontinuous at its intersection with these solid-solid reactions. Presnall and others (1979) called these sharp changes in slope on the solidus "cusps", and they suggested that they would be sites of enhanced melt production in the mantle. The transitions between the different subsolidus assemblages in natural peridotite systems are not univariant, so transition intervals replace simple cusps on the solidus; nevertheless, these transitions still influence the shape of the solidus, and more significantly, these reactions must have an effect on isentropic melting because they have entropy changes associated with them.

9.2. The Case of a Solid-Solid Transition with a Positive dT/dP

To evaluate the effects of discontinuous reactions (and pressure-dependent solid-solid reactions in particular) on isentropic melting we consider two different one-component system topologies, following Asimow and others (1995). The first is shown in P-S space in figure 22A and P-T space in figure 22B. For this example we use calculated phase diagrams in the vicinity of the coesite-quartz-melt triple point in the system SiO_2. As shown in figure 22B, the calculated solidus has a well-defined "cusp" at the triple point and the univariant quartz-coesite equilibrium has a positive P-T slope: the topology of the P-T diagram in the vicinity of the cusp is thus similar to that of the cusps at the plagioclase-spinel and spinel-garnet transitions in the quaternary model peridotite system shown in figure 21 and is likely to be a useful model for thinking about the effects of such transitions on melting.

The topology of the P-T phase diagram in figure 22B is a familiar one. Although the coordinates of the P-S diagram in figure 22A are not widely used, such diagrams, as discussed above, are topologically quite familiar to petrologists in that, since the diagram plots stable assemblages (minimum H) for a choice of variables, one of which (P) is the same in coexisting phases and the other (S) is not, the diagram looks like and can be read like widely used isobaric T-X diagrams in binary systems. Thus, for example, the diagram in figure 22A looks very much like a T-X diagram for a system with a peritectic. The three-phase coexistence of coesite, quartz, and melt, which is a "triple point" in P-T space, is a horizontal line in P-S space because the three phases, all at the same pressure, have different values of specific entropy. The positive Clapeyron slope of the quartz-coesite curve, given the higher density of coesite, requires that the S of quartz is greater than that of coexisting coesite; the entropy of liquid is always greater than either of the coexisting solid phases. The correspondence to a binary T-X diagram is emphasized by the fact that the rules of metastable extensions (shown as dotted lines in figure 22A) for the P-S diagram at the triple point are the same as those for a binary T-X diagram. Note that the two-phase fields shown in figure 22A (three of which come together at the triple point) are topologically similar to that described in detail for the diopside + melt system shown in figure 11A; in particular, the upward curvatures of the edges of the two-phase fields involving melt again reflect the effects of changing T and $(dT/dP)_{2\varphi}$ with decreasing pressure for these univariant equilibria.

Figure 23 shows a series of schematic H-S diagrams corresponding to the P-S diagram shown in figure 22A. At the pressure of the triple point, a single line is tangent to the concave up H-S curves of all three phases; at higher pressure, the quartz curve has moved up relative to the coesite and liquid curves such that the tangent to these two curves has a lower H than the quartz curve and quartz is everywhere metastable; at lower pressure, the quartz curve is lower than the metastable coesite + melt tangent, and quartz has a stability field at intermediate values of S (and T). This sequence of H-S diagrams with increasing P in the vicinity of the triple point is topologically similar to the more familiar sequence of binary G-X diagrams with increasing T (at constant P)

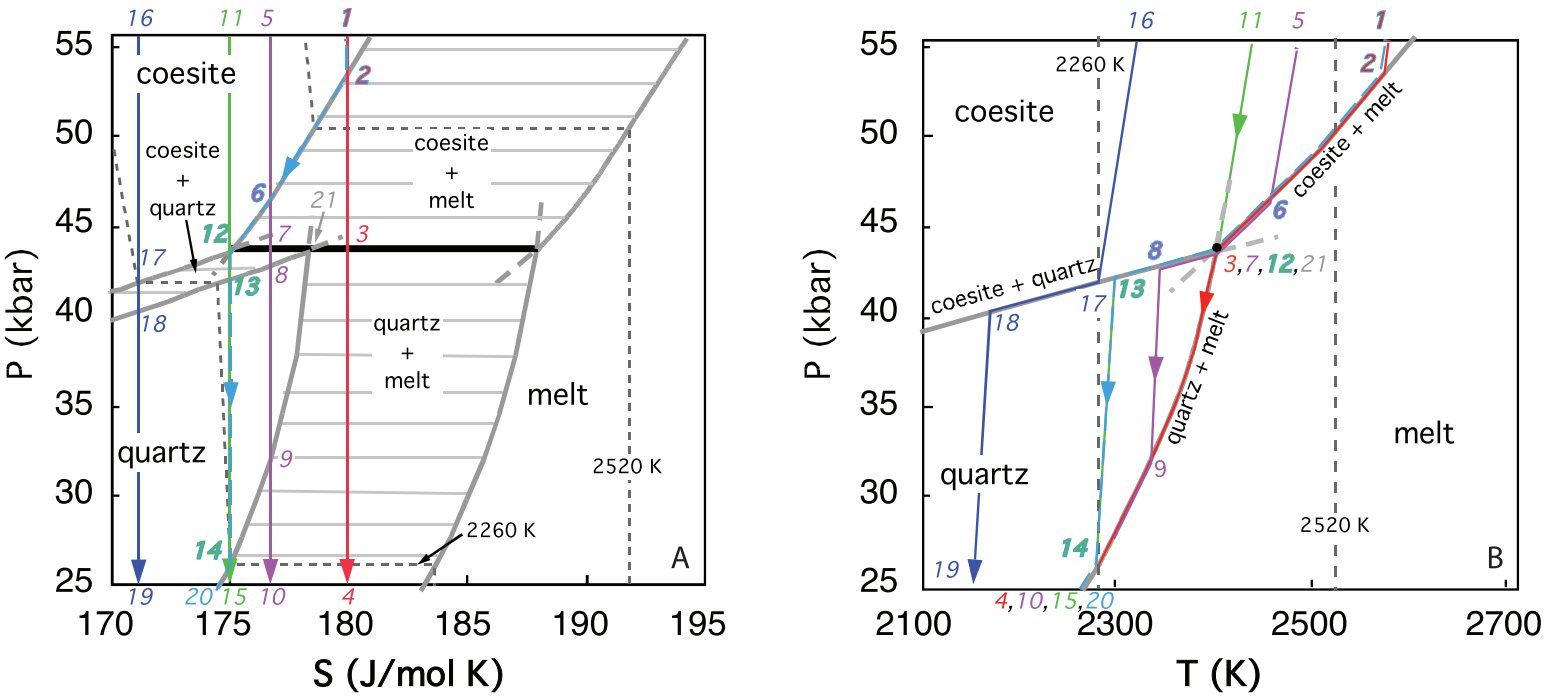

Fig. 22. (A) P-S and (B) P-T phase diagrams for the system SiO_2 in the vicinity of the coesite, quartz, liquid triple point after Asimow and others (1995) and calculated using the thermochemical parameters and phase equilibria referred to therein. The heavy black horizontal line at 43.6 kbar in (A) is the triple point where β-quartz, coesite, and melt coexist; this same point is shown in (B) as the invariant point where these three phases coexist. Two representative isotherms (2260 and 2520 K) are shown in each panel as dashed lines/curves. Isentropic decompression paths are vertical lines in (A) and more complex paths in (B); several are shown in various colors and described in the text. One fractional fusion path is shown (*1→2→12→13→14→20*) and described in the text.

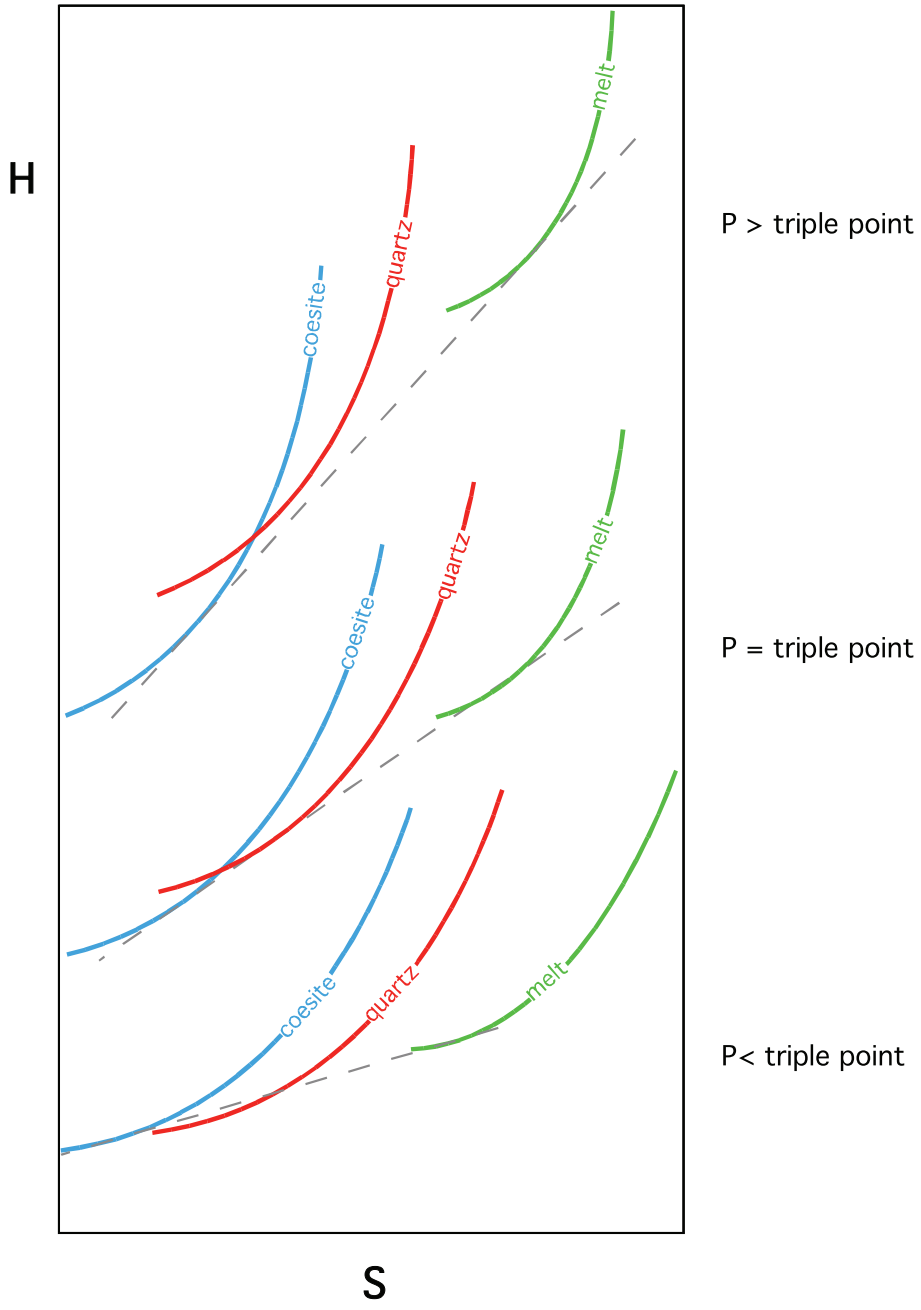

Fig. 23. Schematic H-S diagrams at three pressures near the coesite-quartz-melt triple point. At the pressure of the triple point (the middle set of curves), the H-S curves for the three phases have a common tangent line and the stable sequence of phases with increasing S is coesite → coesite + quartz + melt → melt. At higher pressure (the upper set of curves), the quartz curve is everywhere metastable relative to the coesite and melt curves or to the stable coesite + melt two-phase coexistence, and the stable sequence of phases with increasing S is coesite → coesite + melt → melt. At pressures lower than the triple point (the lowest set of curves), the quartz curve protrudes below the coesite + melt two-phase coexistence (that is, this two-phase coexistence is metastable) and the stable sequence of phases with increasing S at such a pressure is coesite → coesite + quartz → quartz → quartz + melt → melt. This sequence of H-S figures is topologically similar to a sequence of isobaric G-X curves with decreasing T across a peritectic in a binary system (for example, Morse, 1994, Figure 10.3).

for two solids + liquid in the vicinity of the temperature of a peritectic (for example, Morse, 1994, fig. 10.3).

9.2.1. Batch fusion paths.—Isentropic batch and fractional fusion paths can be read simply from figure 22A following the approach described earlier in connection with figure 8 and figure 9. Consider first the path described by the vertical red line (1→2→3→4). From 1 to 2, solid coesite decompresses at constant S. At 2, the coesite begins to melt, and from 2 to 3, the amount of melt increases progressively; using the lever rule, we read from figure 22A that at a pressure just above the triple point, the system is ~35 percent melt and 65 percent coesite. However, at a pressure just below the triple point, the stable assemblage is quartz + melt, and the phase proportions are ~10 percent melt and 90 percent quartz. Continued depressurization (3→4) then leads to a progressive increase in the amount of melt relative to quartz. The corresponding path is shown in P-T space in figure 22B, and from 2→3→4 it simply follows the solidus, with no indication of a substantial, instantaneous decrease in melt fraction at the triple point. The actual F-P and productivity-P curves calculated using equation (14) and the thermodynamic properties of these phases (Asimow and others, 1995) are shown in figure 24. Note the superposition of the freezing event at the triple point on an overall trend that illustrates the same features as for the quantitative treatment of diopside melting: the F versus P curves, first in the coesite + melt field and then in the quartz + melt field, are concave up, indicating an increase in productivity with increasing melting. The significant drop in productivity of quartz melting relative to coesite melting at the triple point reflects the decrease in $(dT/dP)_{2\varphi}$ from the coesite to the quartz solidus (fig. 22B), which is only offset to a small degree by the decrease in ΔS_f that occurs at this point [see equation (14)].

This simple analysis makes an important general point: At this particular "cusp", the system partially crystallizes via the reaction coesite + melt = quartz; that is, the widely held notion (Presnall and others, 1979; Natland and Melson, 1980; Presnall, 1980; Flower, 1981; Presnall and Hoover, 1987; Wyllie, 1988; Salters and Hart, 1989) that cusps lead to enhanced melting is not likely to be universally valid. The reason for this is easy to understand using figure 22A. At the triple point, the solid phase changes from coesite to quartz. The specific entropy of quartz is higher than that of coesite (that is, in the coexistence of coesite + quartz at the triple point and lower pressures in figure 22A, coesite always plots to the left of quartz). The key point to understand here is that, because the specific entropy of the system as a whole is fixed by the constraint that the process is isentropic, the conversion from coesite to quartz (that is, from a low-specific-entropy phase to a high-specific-entropy phase) must be balanced by a decrease in entropy in another part of the system; this is achieved by decreasing the amount of melt, the phase with the highest specific entropy in the system. In other words, the reaction at the triple point is coesite + melt = quartz, and melt is consumed to balance the entropy required to convert the coesite in the system to quartz. That there is melt left after the complete conversion of coesite to quartz on this path reflects the fact that point *3* lies to the right of the specific entropy of quartz at the triple point (point *21* in fig. 22A); in words, this simply means that there is more entropy in the melt phase than is needed to convert fully the coesite to quartz.

If the vertical isentropic path passed right through point *21*, the position of quartz at the triple point (that is, the specific entropy of the system equals that of quartz at the P and T of the triple point), the coesite + melt present at a pressure infinitesimally higher than the triple point would be entirely consumed by the reaction occurring at the triple point, and the system would convert to 100 percent quartz (that is, the entropy stored in the liquid would precisely balance the amount needed to convert the coesite to quartz).

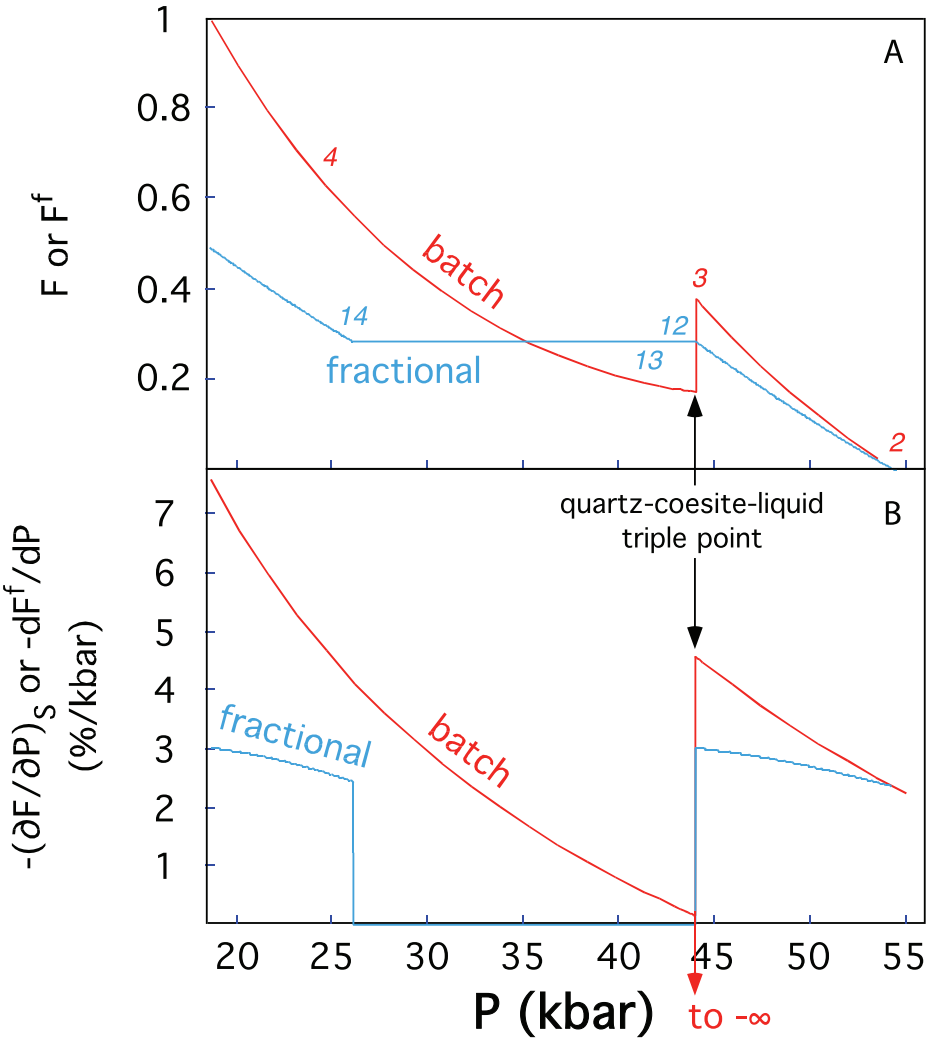

Fig. 24. (A) Melt fraction (F) vs. P and (B) productivity vs. P for the silica one-component system for batch (isentropic) and fractional (incrementally isentropic) decompression melting starting from the same initial entropy (that is, melting of coesite begins for both examples at *2* in fig. 22). Based on Asimow and others (1995).

For paths that intersect the triple point to the left of the position of quartz at the triple point (for example, the purple path *5*→*6*→*7*→*8*→*9*→*10* shown in fig. 22A), there is not enough melt to balance the entropy needed to convert fully the coesite to quartz, and the system crystallizes fully at the triple point (point *7*). With further isentropic decreases in pressure, the system follows an initially subsolidus path across the coesite + quartz field (*7*→*8*); after full subsolidus conversion of the coesite to quartz at point *8*, the system then traverses the quartz field until again reaching the solidus, this time the quartz solidus at point *9*, after which it melts normally with further decompression. The corresponding path in P-T space is shown in purple in figure 22B. This rather complex P-T path illustrates again the difficulty of understanding decompression melting using P-T coordinates alone.

For systems with specific entropy less than that of coesite at the P and T of the triple point (point *12* in fig. 22A), coesite converts directly to quartz without first partially melting: In P-T space, the isentropes crossing the coesite field for such systems reach the pressure of the triple point at temperatures lower than the triple point and intersect the coesite + quartz curve rather than the coesite + melt curve. An example of such a path is illustrated by *16→17→18→19* in figure 22; note that if the initial entropy were low enough, the system would traverse the quartz field and reach 1 atm without ever intersecting the quartz solidus.

The insights from this simple analysis of isentropic batch fusion can be generalized to systems of arbitrary complexity. Thus, when subsolidus reactions (whether discontinuous, by analogy with the example described here for a one-component system, or continuous) that convert low-specific-entropy phases to high-specific-entropy phases with decreasing pressure interact with the solidus, the entropy balance required by isentropic decompression will tend to consume (or at least diminish the production of) melt, generally the phase with the highest specific entropy in the system (this is not the case, however, in vapor-bearing systems). In natural systems where a large number of continuous reactions involving solids and liquid dominate, the entropy balance is less straightforward than in the one-component system analyzed here; nevertheless, if a solid-solid reaction is encountered (for example, garnet→spinel peridotite or spinel→plagioclase peridotite) and the solids involved are present in sufficient quantity to influence significantly the overall entropy balance, melt production on decompression will diminish in response to such reactions, and in extreme cases, crystallization (that is, a decrease in melt fraction during decompression, rather than the usual situation of progressive melting) can occur (see Asimow and others, 1995). Note that if the entropy required to convert from the high-pressure to low-pressure solids is small or the amounts of the phases involved are small, the influence on the overall entropy balance will also be small, leading only to minor influence on melt production and on the temperature decrease that accompanies isentropic decompression melting.

Since isentropic processes are reversible, these diagrams can also be used to understand the effects of isentropic compression, as opposed to decompression. Whereas decompression across a subsolidus phase change with positive Clapeyron slope induces crystallization or decreased melt production, compression across such a phase change has the opposite effect, leading to onset or enhancement of melt production. This may be relevant in subduction zones, where a network of metamorphic reactions take place upon pressure increase in the slab and also in the entrained downward flow of the mantle wedge. Such an effect has been invoked to drive melting at the breakdown of amphibole in hydrated peridotite, which produces a large cusp on the solidus (see Iwamori, 1998).

An important point is that crystallization or diminished melt production only occurs if the low-pressure solid(s) are higher in specific entropy than the high-pressure ones. This manifests itself in the P-T diagram by a positive slope on the subsolidus reactions among these solids (for example, fig. 22B); we can thus anticipate that if the solid-solid reaction has a negative P-T slope, the conversion of the high- to low-pressure phase will release rather than consume entropy, in which case melting will be enhanced at the cusp. This case will be discussed below (section 9.3), but it is important to emphasize that there is no general rule about whether melting will be enhanced or diminished by the presence of cusps: it depends on the entropy change of the solid-solid reaction, which can generally be read from its slope on a P-T diagram. Note, however, that the positive slopes of the plagioclase→spinel lherzolite and spinel→garnet lherzolite phase boundaries (fig. 21) suggest that for basalt production in the upper mantle, solid-solid transitions will lead to diminished melt production;

this has been confirmed by thermodynamic calculations (see Asimow and others, 1995, section 3).

9.2.2. Fractional fusion paths.—Figure 22A can also be used to analyze incrementally isentropic fractional fusion in the presence of a solid-solid phase change. Starting from the same initial specific entropy (point 1) as the first batch fusion path described above, the system undergoing fractional fusion follows the path 1→2→12→13→14→20: that is, since the liquid is removed instantaneously as it is produced, the specific entropy of the residual solid when melting is taking place is always at the solid edge of the two-phase solid + melt field. As a result, when the system reaches the triple point (that is, at point 12), it has the specific entropy of coesite coexisting with quartz and liquid, and on further decompression from this point (12→13→14), a substantial pressure interval must be traversed before the system intersects the solidus (14) and begins to melt again; note that since no melting occurs between 12 and 14, the total entropy of the source is fixed in this pressure interval. The corresponding P-T path is shown in figure 22B. The actual values of F vs. P and productivity versus P are compared in figure 24 with those for batch fusion for sources with the same starting entropy; except for the influence of the triple point, the differences in batch and fractional fusion are similar to those from our earlier analysis of diopside melting (fig. 12).

This analysis reveals what was an unanticipated result prior to the work of Asimow and others (1995): in a one-component system, fractional fusion from a pressure higher than a triple point (or solidus "cusp") results in a cessation of melting at the triple point and a substantial "barren" zone at lower pressure, provided the slope of the univariant solid-solid transition is positive. From a petrological standpoint this is an interesting result: decompression melting does not necessarily continue all the way to the surface once it is initiated; solid-solid transitions can, in principle, shut it off entirely, especially if fractional fusion is the dominant process. The situation in natural systems is more complex, but thermodynamic calculations (Asimow and others, 1995) suggest that melt production may actually cease at the spinel→plagioclase transition and slow noticeably at the garnet→spinel transition for conditions of incrementally isentropic fractional fusion, just as this simple system analysis suggests. Significant decreases in productivity related to this phenomenon may have petrogenetic importance: for example, a zone of low productivity overlying a deeper zone of higher productivity could serve as an impermeable cap, leading to melt accumulation and subsequent instabilities (Spiegelman, 1993). We note that the five-component models of Presnall and others (2002) have been interpreted to differ from this analysis at the spinel-plagioclase transition. The six-phase univariant solidus through the transition interval in their model has a positive slope (though the slope $(dT/dP)_{6\varphi}$ is lower than those of the five-phase solidus curves in either the plagioclase or spinel lherzolite melting intervals) and decompression melting is able to continue through this interval even for fractional fusion; that is, melting of plagioclase-bearing lherzolite is so productive that this interval produces a great deal of melt in their model despite the ongoing spinel→plagioclase transition. We emphasize, however, that the spinel→plagioclase transition, even in this case, is acting to suppress melting; that is, productivity is lower than at equal melt fraction in the spinel-free region.

9.3. The Case of a Solid-Solid Transition with a Negative dT/dP

9.3.1. Batch fusion paths.—For completeness, we now briefly consider the intersection of the solidus with a solid-solid transition with a negative P-T slope. An example of a possibly petrologically relevant one-component system with such a topology is in the system $MgSiO_3$, where the transition from the clinoenstatite (C2/c) phase to majorite has a negative slope and intersects the solidus at 2370 °C and 164 kbar (Presnall and Gasparik, 1990). The solidus still has a cusp, but isentropic melting behavior is different from the case considered above because the solid reaction at the triple point

releases rather than consumes entropy, and this extra entropy produces an enhancement rather than a diminishment in melting (that is, it provides the entropy of melting needed to convert solid to melt at constant P, T, and S). Three isentropes are shown in the P-S diagram in figure 25A and its companion P-T diagram in figure 25B. Note that while the P-S diagram for a system with positive P-T slope for the solid-solid transition looked like a binary T-X diagram with a peritectic, the one shown in figure 25A looks either like a binary eutectic (in the sense that there is only a single two-phase region in the lower part of the diagram and two such regions trending in opposite directions in the upper part) or like an upside-down peritectic (in the sense that the liquid at the triple point is not between the two solid phases), depending on how one looks at it.

For the isentrope shown as a red vertical line in figure 25A, phase β decompresses from *1* to *2*, at which point the system begins to melt, doing so continuously until the triple point is reached at *3*. At a pressure infinitesimally above the triple point, the system is about 10 percent melt and 90 percent β; however, at a pressure infinitesimally below the triple point, the diagram can be read to indicate that the system is about 30 percent melt and 70 percent α. In other words, the reaction at the triple point is β = α + melt. In this case, as previously anticipated, the low-pressure solid phase (α) has the lower specific entropy, so when the high-pressure solid phase, β, transforms at the triple point to α, the difference in entropy is balanced by making more of the high-entropy phase, that is, melt. Continued depressurization below the triple point (*3*→*4*) simply leads to further melting of α. The path in P-T space follows the solidus from *2*→*3*→*4*, with no indication of the discontinuous enhancement of melting at the triple point.

The second path shown is in purple, and it differs from the red path in that it has a specific entropy less than that of phase β at the P and T of the triple point. In this case, the system cools and depressurizes as phase β (*5*→*6*). As pressure decreases beyond point *6*, β converts to α. Note that this releases entropy since the specific entropy of α is less than that of β, but since there are no other phases present, the entropy balance is achieved by increasing the temperature of the system; this is shown in figure 25B as the path from *6* to *7* where, following the solid-solid univariant curve, the temperature of the system increases. When the pressure of the triple point is reached at point *7*, the system is a mixture of α and β; at the triple point, the remaining β converts to α + melt, leading to an instantaneous increase in melt fraction from 0 to about 8 percent for the example shown. Further depressurization leads to continuous melting of α (*7*→*8*). The P-T path of this isentrope is shown in purple in figure 25B. This case is of potential interest petrologically in that a system well below the solidus as it traverses the stability field of the high-pressure solid phase can receive a temperature boost to the solidus on conversion to the low-pressure phase, and produce a "burst" of melting at the cusp. Komatiites may require very deep melting (Miller and others, 1991) and high degrees of melting (Herzberg and O'Hara, 2002), and it is conceivable that the anomalously high degrees of melting inferred for them reflect enhanced melting associated with the interaction of negatively-sloped solid-solid phase boundaries in the transition zone (Verhoogen, 1965) and the solidus.

The final example shown in figure 25A is a case for which the specific entropy of the system is less than that of α at the triple point (that is, *10*). Starting from point *12*, the system cools and depressurizes as phase β (*12*→*13*). As pressure decreases beyond point *13*, T increases as β converts to α. Complete conversion of β to α occurs at *14* (that is, at a pressure higher than that of the triple point). If the specific entropy of the system were sufficiently low, on further decompression it would traverse the field for α, reaching 1 bar as phase α without ever beginning to melt. For the case shown in figure 25A, however, melting of α begins at *15* and continues (*15*→*16*) with further decompression. The equivalent path in P-T space is shown in figure 25B.

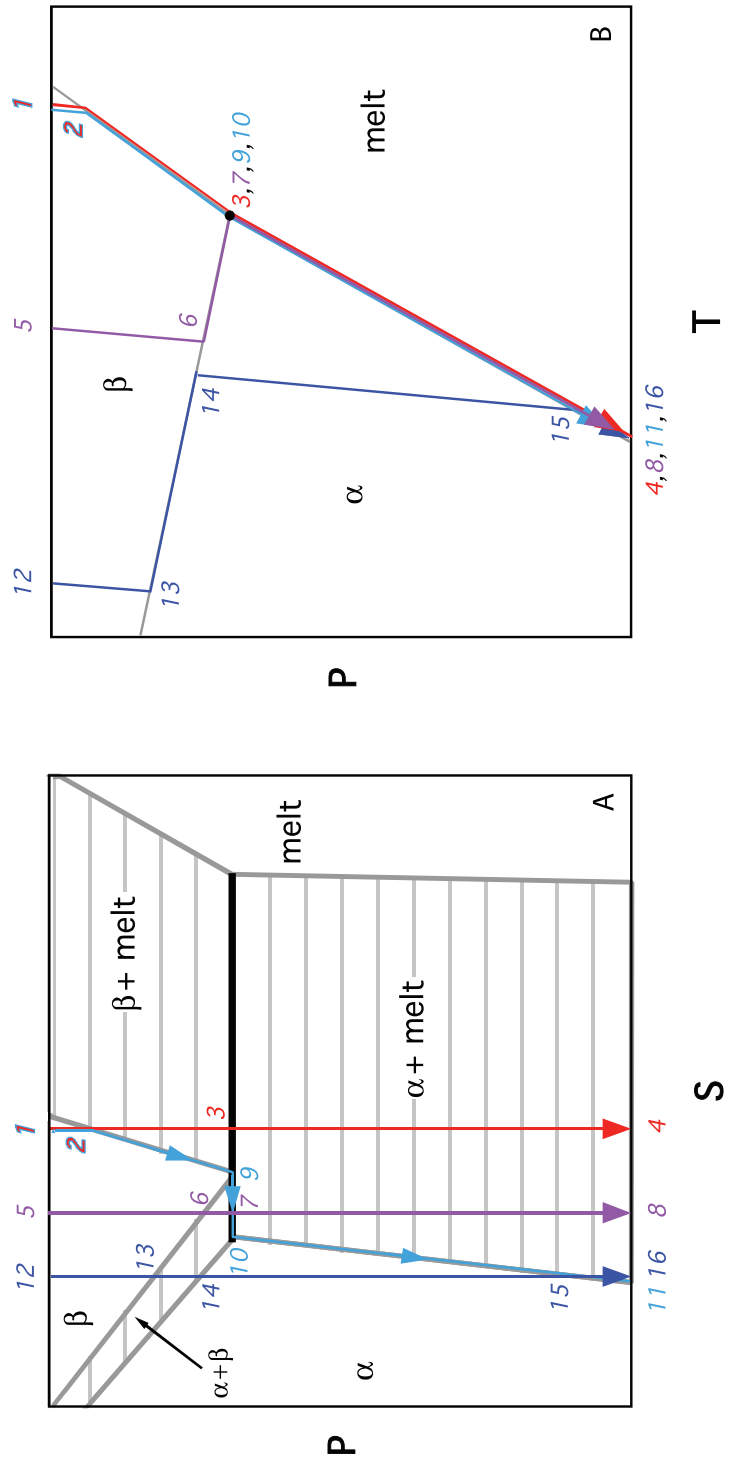

Fig. 25. Schematic (A) P-S and (B) P-T phase diagrams after Asimow and others (1995) for a one-component system with a triple point (α, β, melt) in which the univariant α + β coexistence has a negative slope in P-T space. The heavy black horizontal line in (A) is the triple point where α, β, and melt coexist; this same point is shown in (B) as the invariant point where these three phases coexist. Isentropic decompression paths are vertical lines in (A) and more complex paths in (B); three such paths are shown in various colors and described in the text. One fractional fusion path is shown (*1→2→9→10→11*) and described in the text.

9.3.2. Fractional fusion paths.—Fractional fusion paths can also be followed using figure 25A. Shown in cyan is such a path for the same starting entropy (1) as the red batch fusion isentrope. As the pressure is reduced from point 2 to the pressure at the triple point, β melts, and the residue tracks along the β-edge of the two-phase β + melt field to point 9. For a further infinitesimal decrease in pressure, all the β in the source converts to ~80 percent α plus ~20 percent melt (that is, the residue jumps from 9 to 10). Note that it is impossible to generate an infinitesimal increment of melt no matter how small the pressure decrement from point 9; the conversion from the high-entropy solid phase β to the low-entropy solid phase α in an infinitesimal isentropic decompression requires this discontinuous "burst" of melt production to achieve entropy balance regardless of the pressure step. Further pressure decreases produce melt continuously, and the residue tracks the α-edge of the two-phase α + melt field (10→11).

10. Melting of a "Plum-Pudding" Mantle

As described in section 8.3, melting of mantle sources with multiple rock types, each with its own melting behavior and chemical and isotopic properties, is believed to be an important factor in producing the range of magma types characteristic of individual igneous provinces. An important example of such a compound source would be a dominantly peridotitic mantle with minor eclogitic or pyroxenitic veins, on which there is a large and growing literature (for example, Wood, 1979; Allègre and others, 1984; Langmuir and Bender, 1984; Zindler and others, 1984; Allègre and Turcotte, 1986; Prinzhofer and others, 1989; Ben Othman and Allègre, 1990; Langmuir and others, 1992; Chabaux and Allègre, 1994; Lundstrom and others, 1995; Hauri, 1996; Hirschmann and Stolper, 1996; Hofmann and Jochum, 1996; Lassiter and Hauri, 1998; Jackson and others, 1999; Lassiter and others, 2000; Sobolev and others, 2000; Kogiso and Hirschmann, 2001; Norman and others, 2002; Reiners, 2002; Takahashi and Nakajima, 2002; Hirschmann and others, 2003; Pertermann and Hirschmann, 2003; Sobolev and others, 2005). In section 8.3, we considered briefly the limiting case of a heterogeneous mantle with an infinitesimal amount of a low-melting source rock. Here we develop in more detail the melting behavior of a heterogeneous source without the restriction that the low-melting source rock is present in infinitesimal quantities. As we shall see, this is another case in which consideration of a one-component system illustrates relatively simply several of the important behaviors that are likely to appear in more complex systems.

10.1. Graphical Analysis of Batch Melting of Mixed Sources

As we did in section 8.3, we treat the source as a mixture of two rock types, A and B, each of which is a one-component system. The solidus of A is taken to be at much higher temperature than that of B; schematic P-T diagrams for materials A and B are shown in figure 26. In thinking about this as a model for a mixed peridotite + pyroxenite mantle, A would typically represent the peridotite and B would represent the pyroxenite or eclogite. We assume that A and B are mixed on a scale such that they are always in thermal equilibrium but that chemical interactions between them are negligible (Sleep, 1984; Hirschmann and Stolper, 1996; Phipps Morgan, 2001). Kogiso and others (2004) examined this problem specifically for equilibration with respect to Os isotopes and found such thermal equilibrium and chemical isolation to be probable for heterogeneities larger than a scale of meters. We also assume that the ascent of the mixed source is adiabatic and sufficiently slow that the processes within it are reversible: that is, the process is approximated as isentropic (although as in previous cases, we will allow for melt removal, in which case each increment of ascent is isentropic). Note that although A and B are non-interacting one-component systems, they together can be viewed as what is known as a degenerate binary system; that is, the system as a whole has two components, but the end members, A and B in this case, are

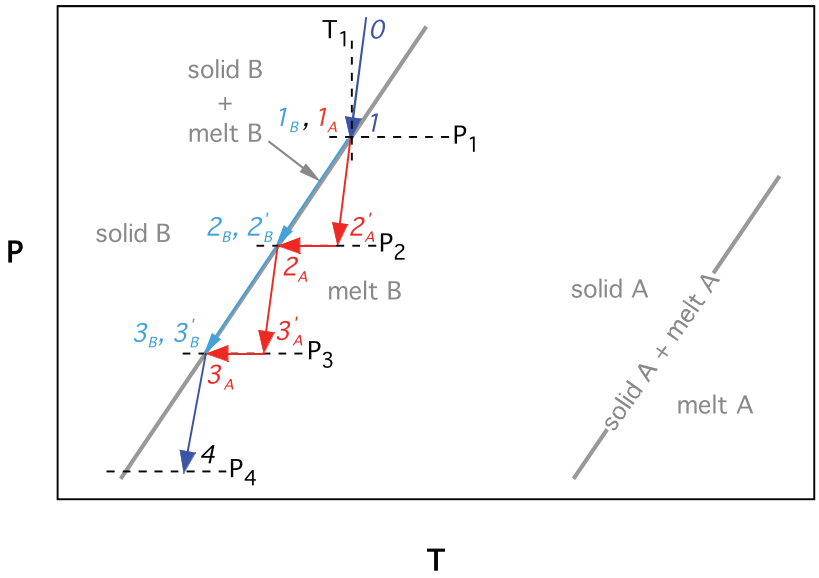

Fig. 26. Schematic P-T diagram illustrating isentropic melting of sources containing two one-component systems that interact thermally but not chemically. The base phase diagrams for the two one-component parts of the system, A and B, are from figure 18: at all pressures the solidus of B is at lower temperature than that of A. Melting of the mixed source is broken up into two isentropic steps: For example, starting at *1*, the A and B parts of the system are in equilibrium (that is, both are at P_1 and T_1). Then, the two parts of the system each undergo an isentropic pressure decrement from P_1 to P_2; the B part of the system partially melts, following its solidus (the cyan arrow from $1_B \rightarrow 2'_B$), while the A part of the system remains unmolten (the red arrow from $1_A \rightarrow 2'_A$). The temperatures of the two parts of the system at $2'_A$ and $2'_B$ now differ, and in the next step, they are allowed to reequilibrate thermally and at constant entropy, so the temperature of the A part of the system decreases to the solidus of B (the red arrow from $2'_A \rightarrow 2_A$), transferring entropy to B and resulting in an increase in the degree of melting of the B part of the system ($2'_B \rightarrow 2_B$; the temperature is the same in these two states). A finite isentropic decompression of the mixed lithology system can then be built up as a series of small isentropic steps as shown in the figure, until the B part of the system is totally molten. See the text and the companion diagram (fig. 28) for additional details.

one-component systems. We use ϕ^0_B, the mass fraction of B, to describe the compositions of sources described by such a binary system (that is, $\phi^0_B = m^0_B/(m^0_A + m^0_B)$, where m^0_A and m^0_B are the initial masses of lithologies A and B in the source).

In order to analyze graphically the process of decompression melting of such mixed sources, we introduce the diagrams shown in figure 27. Each panel maps the stable (minimum H) assemblages at a particular pressure as functions of the proportions of the two distinct lithologies (that is, ϕ^0_B) and the specific entropy of the mixed source. These isobaric phase diagrams for the degenerate A-B binary system are comparable to the S-X diagrams used by Asimow and others (1995, 1997) to analyze decompression melting of single lithology binary sources. Isotherms are shown as gray lines, except for the pink triangle, which represents the coexistence of solid A + solid B + liquid B at the temperature of the univariant solid B + liquid B coexistence for the pressure at which the diagram is drawn. When the system is pure A ($\phi^0_B = 0$), no melt is present for any of the conditions we will consider (note that only a portion of the phase relations are shown; there is another triangle, not shown, at higher entropy and temperature where the A-component melts). However, when the system is pure B ($\phi^0_B = 1$), the system can be either solid B at low entropy, a mixture of solid B + liquid B over a range of entropies equal to ΔS_f (at a single temperature defined by univariant coexistence of these two phases at this pressure), or liquid B at high entropy; this follows from our analysis of figure 4. At equilibrium, the A and B parts

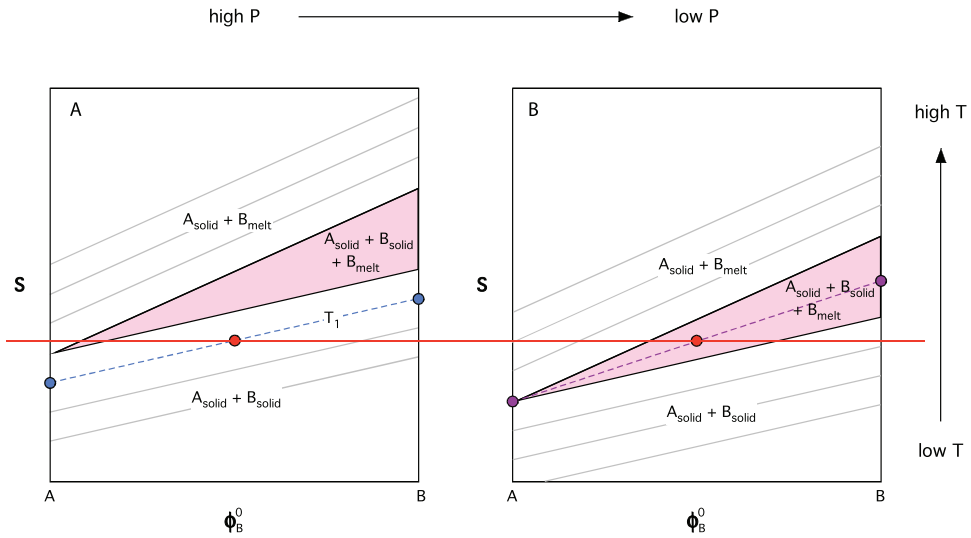

Fig. 27. Schematic isobaric S-ϕ_B^0 diagrams for analysis of isentropic melting of sources containing two one-component systems that interact thermally but not chemically. This diagram is a companion to figure 26 and portrays the system as a degenerate binary system. ϕ_B^0 is the initial mass fraction of B in the source [that is, $\phi_B^0 = m_B^0/(m_A^0 + m_B^0)$, where m_A^0 and m_B^0 are the initial masses of lithologies A and B in the source]. The left edge of the diagram ($\phi_B^0 = 0$) shows the phase relations of the A component as a function of S; it is solid under all conditions. The right edge of the diagram ($\phi_B^0 = 1$) shows the phase relations of the B component as a function of S; with increasing S, the stable assemblages for the B component are solid → solid + melt → melt. The gray tie lines are isotherms connecting coexisting solid A + solid B or solid A + molten B. The pink triangle represents the temperature at which solid A + solid B + molten B coexist. Each panel is isobaric, but panel (B) is drawn for a lower pressure than panel (A); the key difference between them is that the solid B + liquid B coexistence moves to lower S with decreasing pressure (for example, see fig. 5), so the three-phase triangle has moved down in panel (B) relative to panel (A). We assume C_P's in all phases are the same and that ΔS_f of B is constant, so the only difference between panels (A) and (B) is that the three-phase triangle and tie lines are all translated downward. For a particular S and ϕ_B^0, the temperature and phase assemblage at a given P can be read from the appropriate diagram. Consider for example the red dot at $\phi_B^0 = 0.5$. In panel (A), it plots on the solid A + solid B tie line at T_1 (dashed in blue), and consequently such a system will be 50% solid A and 50% solid B at T_1, represented by two blue dots at $\phi_B^0 = 0$ and 1. At the lower P of panel (B), the red dot falls within the three-phase triangle, and the level rule (applied to the purple dashed tie line between the solid A apex of the three-phase triangle and the red dot and extending to the right side of the diagram) can be used to determine that the system is now made up of 50% solid A (the purple dot at $\phi_B^0 = 0$) and 50% B (the purple dot at $\phi_B^0 = 1$), but that the B component is 50% molten (that is, the purple dot at $\phi_B^0 = 1$ plots halfway between entropies of solid and liquid B), so the stable assemblage is 50% solid A + 25% solid B + 25% liquid B. A sequence of these diagrams is used in figure 28 to analyze the isentropic decompression process shown in figure 26.

of the system will have the same temperature, so for a given total S and ϕ_B^0, we can read from this diagram the equilibrium assemblage, which will be a mixture of solid A and whatever assemblage is stable for B (that is, solid, solid + liquid, or liquid) in proportions given by ϕ_B^0, by identifying the isotherm that passes through the S-ϕ_B^0 coordinates of the mixed source. When the temperature is on the univariant solid B + liquid B curve (that is, the S-ϕ_B^0 coordinates of the system plot in the pink triangle), the stable assemblages will be solid A for the A part of the system and solid B + liquid B for the B part of the system. Note that we have arranged the two panels with decreasing pressure from (a) to (b), and since the temperature of the univariant curve for solid B + liquid B decreases with decreasing pressure, the vertices of the solid A + solid B + liquid B triangle move to lower S from panel (a) to panel (b). We can follow an isentropic decompression by monitoring the changing stable temperature and assemblage of a particular choice of S-ϕ_B^0 coordinates from panel to panel. Although these diagrams are schematic, the

isotherms in each of the two-phase fields (solid A + solid B and solid A + melt B) are parallel, implying that all of the phases have the same C_P, and the three-phase triangle is the same size in each panel (that is, it is simply translated downward without changing shape), implying that ΔS_f of B is independent of pressure.

As an illustration of how to read figure 27, consider as an example the point indicated by the red dot, which has an arbitrary S and $\phi_B^0 = 0.5$. At the higher pressure of panel (a), the isotherm for T_1 passes through this point, indicating that the stable assemblage is a mixture of solid A and solid B (shown as the blue dots at $\phi_B^0 = 0$ and $\phi_B^0 = 1$) at T_1 in the proportions given by ϕ_B^0 (50% of each for this example). At the lower pressure of panel (b), the red dot lies in the pink triangle, so the stable assemblage is 50 percent solid A (shown as a purple dot at $\phi_B^0 = 0$) and 50% solid B + liquid B (shown as a purple dot at $\phi_B^0 = 1$), and the bulk source (represented by the red dot) lies on a line between the purple dots at $\phi_B^0 = 0$ and $\phi_B^0 = 1$ representing the A and B parts of the system. Note that the purple dot at $\phi_B^0 = 1$ is midway between the entropy of solid and liquid B at this pressure, so the lever rule tells us for this particular example that the B part of the system is 50 percent molten.

It is now a relatively simple matter to evaluate decompression melting for any mixture of A and B using figure 26 and figure 28, where figure 28 shows from panels (A)→(D) a series of S-ϕ_B^0 diagrams at progressively lower pressures. We break each decompression into two steps: in the first step, the A and B portions of the system decompress on separate isentropes (that is, each portion decompresses isentropically, but the two portions do not equilibrate thermally); in the second step, the two portions equilibrate thermally at constant pressure and total entropy. Starting at state *1*, which is right at the solidus of B, the system is fully solid. On the P-T diagram in figure 26, both parts of the system are solid and at the same temperature (T_1) on the univariant curve for coexistence of solid B and liquid B. Figure 28A shows the S-ϕ_B^0 diagram at P_1. The model bulk source is represented in figure 28A by the red dot, which for convenience we have again arbitrarily chosen to be 50 percent A and 50 percent B. The red dot plots on the lower edge of the solid A + solid B + liquid B triangle in figure 28A; that is, it is at the temperature (T_1) of the solidus of B, but the equilibrium assemblage, shown by the end points of the dashed purple tie line, is solid A (state 1_A; shown by the purple dot at $\phi_B^0 = 0$) plus solid B (state 1_B; shown by the purple dot at $\phi_B^0 = 1$); note that the specific entropies of A and B differ even though the two parts of the system are in thermal equilibrium.

We next allow the system to undergo a reversible adiabatic decompression from P_1 (fig. 28A) to P_2 (fig. 28B). In this step, A and B are not allowed to equilibrate thermally: that is, that part of the source that is A follows an isentropic path from state 1_A to state $2'_A$, while that part of the source that is B follows an isentropic path from state 1_B to state $2'_B$. The B component of the source partially melts during this decompression (since state *1* was right on the solidus of B), so its temperature decreases along the solidus of B during this decompression; in contrast, the A component of the source is below its solidus, so its temperature is assumed to decrease much less, along the isentrope of solid A. The temperatures of A and B thus differ after the decompression from P_1 to P_2. This decompression is illustrated in both figure 26 and figure 28 by the arrows from state 1_A to state $2'_A$ and from state 1_B to state $2'_B$.

There are several interesting points that can be seen on figure 28, which contains significantly more information than figure 26. State 1_A, as explained in the previous paragraph, is represented by the purple dot at $\phi_B^0 = 0$ in panel (A), which is one vertex of the solid A + solid B + liquid B three-phase triangle, and thus is at the temperature of the solidus of B at P_1. We represent the isentropic transformation to state $2'_A$ simply by translating the purple dot for state 1_A horizontally to the same position in panel (B);

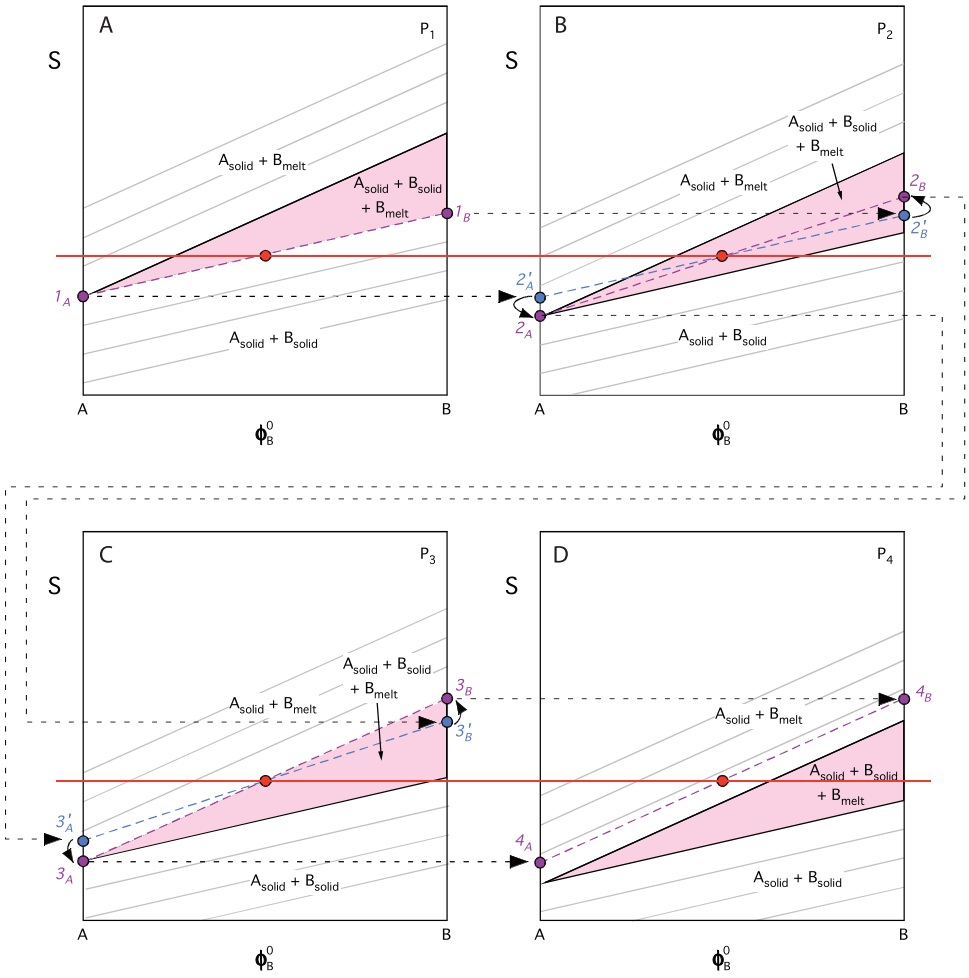

Fig. 28. A sequence of four schematic isobaric S-ϕ^0_B diagrams at progressively lower P ($P_1 > P_2 > P_3 > P_4$). As described in the caption to figure 27, the tie lines and three-phase triangles are the same in each panel, except for having been moved down together by a constant amount in each successive panel. The construction of the diagrams is arbitrary, but was chosen for illustration purposes such that red dot at $\phi^0_B = 0.5$ (a 50% mixture of A and B) is at the solidus of B in (A), such that B is 50% molten in (B), and such that B has just reached 100% melting in (C). See the text and the related P-T diagram in figure 26 for a description of how such a sequence of S-ϕ^0_B diagrams can be use to visualize and analyze quantitatively isentropic batch melting of sources containing two one-component systems that interact thermally but not chemically.

that is, the entropy or S coordinate of the A part of the system is unchanged in this decrease of pressure to P_2. But whereas A with this entropy was at one vertex of the three-phase triangle at P_1, we can read from figure 28B that at P_2 it is at a temperature higher than that of the three-phase triangle that defines the temperature of the solidus of B. We can similarly see that the transformation from state 1_B to state $2'_B$ is simply a horizontal translation of the purple dot at $\phi^0_B = 0$ from panel (A) to panel (B). And whereas the B part of the system at P_1 was totally solid, we can read from panel (B) that it is about ¼ of the way up the right edge of the three-phase triangle, signifying that it is partially molten, made up of 25 percent liquid B and 75 percent solid B, and the temperature is defined by the solid B + liquid B univariant curve at this pressure (that is, lower than that of solid A at state $2'_A$).

The next step is to allow an isentropic thermal equilibration of A and B at P_2.[2] Taking note of the gray isotherms in figure 28B, the temperature of A at $2'_A$ is greater than that of B at $2'_B$, so heat flows from A to B. As long as B is partially molten, the temperature of B will be defined by the univariant solid + liquid curve for B, so as heat flows from A to B, the temperature of B remains unchanged, but the heat flow results in increased melting; the flow of heat from A to B will continue until the temperature of A reaches that of B (that is, on the solidus of B). When the system has equilibrated thermally at P_2, component A is at state 2_A and component B is at state 2_B. All we can see from figure 26 is that both the A and B parts of the system have the same temperature on the solidus of B, but figure 28B conveys significantly more information. As described in the previous paragraph, after decompression but prior to thermal equilibration, the two parts of the system are indicated in figure 28B by the blue dots representing states $2'_A$ and $2'_B$. Although together they have the correct total entropy (that is, the line between them passes through the red dot representing the S-ϕ^0_B coordinates of the system), they are at different temperatures. Thermal equilibrium at the same total entropy will be defined by an isothermal tie line between the A and B parts of the system at P_2 that passes through the red dot. The unique tie line that satisfies this condition is shown in panel (B) by the dashed purple line that joins purple dots at $\phi^0_B = 0$ (representing state 2_A) and at $\phi^1_B = 1$ (representing state 2_B). We can see that the entropy of A decreased during this process (that is, from the blue dot representing state $2'_A$ to the purple dot representing state 2_A) and the entropy of B increased during this process (that is, from the blue dot representing state $2'_B$ to the purple dot representing state 2_B). Moreover, we can see by comparing the blue dot representing state $2'_B$ to the purple dot representing state 2_B not just that the amount of melting of the B component increases during this thermal reequilibration, but that it doubles, from 25 percent to 50 percent molten. We will return in the next paragraph to the significance of the fact that the amount of melting precisely doubles given our construction, but the key conceptual point here is that the thermal equilibration of A and B after their initial decompression releases heat from A (resulting in a decrease in its specific entropy) until it reaches the temperature of the B solidus, and flow of this heat into B (resulting in an increase in its specific entropy at constant temperature) produces extra melt related to its entropy increase. Thus, because it is embedded in A, which is well below its own solidus, low-melting component B undergoes enhanced melting relative to what it would experience were it to decompress isentropically on its own. This is, of course, of petrogenetic importance since it leads (1) to elevated degrees of melting (that is, higher productivity) of the fertile (that is, low-solidus) components of a mixed mantle relative to what would be produced were it not present as veins or pods in a mixed mantle, and (2) to "refrigeration" (and thus ultimately lower melt production) of the refractory (that is, high-solidus) components of the mixture.

The quantitative increase in melting of low-solidus component B is of critical importance yet simple to understand by referring back to the approach to analyzing isentropic melting explored in section 7. In the initial decompression step ($1_B \rightarrow 2'_B$), the B component of the system starts at its solidus and partially melts isentropically but without thermal equilibration with the A component of the system. But, as described in

[2] As we have emphasized several times, an isobaric, *adiabatic* equilibration would be isenthalpic, not isentropic. However, for the present discussion, we will force the reequilibration to occur at constant entropy (in effect, by extracting heat from it to keep the entropy constant). The reason for this is that the actual process we are envisioning will take place continuously and reversibly as the source ascends, and thus the true process can be approximated by a series of infinitesimal, reversible (and therefore isentropic) steps. However, for the purposes of illustration, we have made the decompression step large enough to be able to visualize what is going on graphically.

section 7, we can break this isentropic decompression melting of B into two steps, a metastable isentropic decompression of solid B without melting, followed by an irreversible isentropic transformation to the stable partially molten assemblage; we showed previously that the amount of melting in the second step is defined by the amount of entropy released by the cooling of metastable solid B to the temperature of the solidus; that is, the integral on the left-hand side of equation (20). Now consider the thermal equilibration between A and B after the initial decompression step. Solid A has decompressed from the solidus of B at state 1_A, but if we assume that the V, α, and C_P, of solid A and solid B are the same, then its temperature prior to the thermal equilibration step will be identical to the temperature of metastable solid B prior to its irreversible conversion to a partially molten state. In other words, the amount of entropy per mass transferred to the B part of the system on cooling of solid A to the solidus of B in the thermal equilibration step will be identical (for the assumptions we have made) to that which led to the partial melting of B in the previous step (that is, $1_B \rightarrow 2'_B$). Consequently, if as in our example the system is 50 percent A and 50 percent B, the amount of melting of B during the second (that is, thermal reequilibration) step must be the same as during the first (that is, isentropic decompression) step, thereby explaining what we concluded from our graphical analysis that the thermal reequilibration step between A and B leads to a doubling of the amount of melting. The same principles apply when the masses of the two parts of the system differ, except that the entropy transfer from A to B and leading to enhanced melting has to take into account their different masses.

The quantitative aspects of this example illustrate another point of petrological importance. If the source were made only of solid B, on decompressing isentropically from P_1 to P_2, it would melt by 25 percent (that is, this is described fully by the isentropic transformation from state 1_B to state $2'_B$ in fig. 28). Thus, 100 g of source B would produce 25 g of melt in this step. Now consider the mixture of 50 percent B and 50 percent A melting as described in the previous paragraphs. In the first step of the decompression (that is, isentropic decompression of solid B without thermal interaction with solid A), B melts by 25 percent, and in the next step (that is, the thermal equilibration with A), the amount of melt doubles to 50 percent. However, again considering a 100 g source, although the B component of the source melts by 50 percent, since it only comprises 50 percent of the source, it only produces 25 g of melt. This is a very important point: although embedding a component with a lower solidus than the enclosing mantle leads to enhanced melting of the low-solidus component, the total amount of melt coming from the source will not be enhanced. The explanation for this is simple: if the melting process is isentropic, the amount of melting is controlled by the entropy made available by cooling the total source to the solidus of whatever is melting [that is, as described by the integral in equation (20)]; and all other things being equal (that is, C_P, α, V of all solid phases), the available entropy and consequently the amount of melting is similar whether the source is dominantly composed of the low- or high-solidus material. Based on analysis of this same process in compositionally more complex systems, including pyroxenite-peridotite mixtures (Smith and others, 2003) and models of natural peridotite (Phipps Morgan, 2001), this simple insight can be generalized to natural systems. This therefore leads to a very specific petrological prediction that could in principle be used to recognize this process: the partial melts of the low-solidus component of the source will show geochemical and petrological evidence of high degrees of melting, but the mass of magma produced will not be correspondingly high.

We have thus far only considered a single finite pressure decrement of the mixed source, but this process can be imagined to proceed in a succession of such pressure decrements, each of which we break up into two steps, the first of which is on an

isentrope individually for each of the two components of the source, and the second of which equilibrates them thermally while keeping the total entropy of the system constant. Figure 26 and figure 28 show two such additional steps, and for this schematic example, component B is fully molten after the increment from P_2 to P_3 (fig. 28C) after which (that is, from P_3 to P_4; fig. 28D), the system simply decompresses with A fully solid and B fully molten. Inspection of figure 28 shows that if the solidus and liquidus of the B component are linear and parallel in P-S space (and assuming that C_P and $V\alpha$ for all the phases are the same), the productivity of the melting of the B component, although enhanced, is independent of pressure and the degree of melting (as was the case for isentropic melting described using fig. 8, with its linear and parallel solidus and liquidus).

It is important to reemphasize that although our treatment of this process dealt with finite pressure decrements so as to allow the process to be readily visualized, for the process as a whole to be isentropic (that is, adiabatic and reversible), it would have to be constructed by integration of infinitesimal pressure decrements over a finite pressure interval. In a natural process in which a source made up of two lithologies underwent a finite decompression in which the two lithologies first decompressed adiabatically and without interaction and then a step in which they equilibrated thermally, the thermal equilibration step would reach an equilibrium state of constant enthalpy and increased entropy, and thus the enhancement of melting of the low-solidus component would be even greater than we have described. We emphasize, however, that since decompression melting of a mixed lithology mantle source would typically involve slow ascent (see section 3), the actual process is probably close to reversible, and thus our treatment of the process in terms of two isentropic steps reaches an equilibrium state that correctly approaches what would occur in nature, even though the two-step path by which this equilibrium state was reached in our modeling would not be followed in nature.

The analysis presented so far in this section only applies until the low-solidus component is completely melted, after which the solid A and completely molten B components ascend together (assuming batch melting and that liquid B does not escape even after complete melting; fractional fusion of the low-solidus material is considered in the next section) without further phase changes until the source reaches the solidus of A at much lower pressure. Note again, however, that the extra melting of component B was accompanied by refrigeration of solid A, and thus the solidus of A will be reached at lower pressure and the total amount of melting of component A at any stage in the process will be less than or equal to the case where the source is entirely composed of A. This result is also quite general (that is, it also occurs in models of more complex systems, Smith and others, 2003), and thus another feature of the output of such a system will be degrees of melting of the peridotitic component of the mixed source that are lower than would be expected for similar starting conditions (that is, similar P and T prior to the initiation of melting) of a peridotite-only source.

The pressure interval required to melt fully the low-melting component depends on the proportions of A and B in the source. If, as described in section 8.3, the amount of B in the source is infinitesimal (that is, $\phi_B^0 \rightarrow 0$), the productivity of melting of B approaches infinity, and the pressure interval approaches zero. If the amount of A in the source is infinitesimal (that is, $\phi_B^0 \rightarrow 1$), the productivity of melting approaches that of isentropic decompression of B alone, and the pressure interval approaches that defined by melting of B alone (ΔP_B in fig. 29). For intermediate amounts of B in the source, the P-T path of the mixed source follows the solidus of B until the B component is fully molten, after which the isentrope diverges from the solidus and decompresses further as a thermally equilibrated mixture of liquid B and solid A until the solidus of A is encountered at much lower pressures. The pressure interval over which mixed

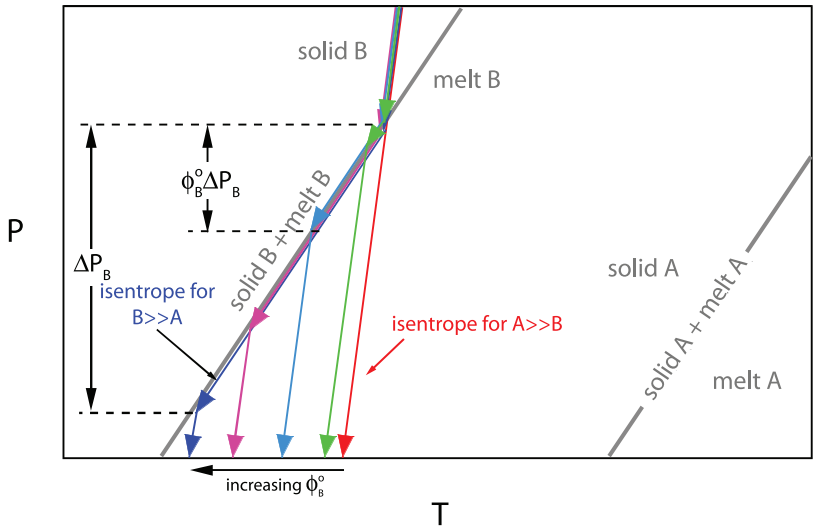

Fig. 29. Schematic P-T diagram summarizing the results of isentropic batch melting of sources containing two one-component systems that interact thermally but not chemically. The base phase diagrams for the two one-component parts of the system, A and B, are from figure 18 and figure 26. The colored lines/curves show the isentropic paths for mixed sources with different values of ϕ_B^0, the mass fraction B in the source, all starting from the same subsolidus (T, P) point. Each source begins to melt when the solidus of B is reached and follows this solidus in P-T space until the B component is completely molten, after which the mixed source follows an isentropic path across the molten B + solid A field. As developed in the text, the pressure interval over which the B component of the mixed source reaches complete melting is simply $\phi_B^0\Delta P_B$, where ΔP_B is the pressure interval over which a source containing only solid B would melt completely. The two end members of B $\gg$ A ($\phi_B^0 = 1$) and B $\ll$ A ($\phi_B^0 = 0$) are the same as shown in figure 18.

sources remain on the solidus of B (that is, the pressure interval required to melt fully the B component) can be readily inferred based on our analysis. Suppose that the pressure decrement is sufficient to melt 1 g of the B component by 25 percent in the isentropic first step of the two-step process we have modeled. As we explained above, the amount of melting is proportional to the entropy released on cooling B from the metastable adiabat to its solidus [see equation (20)] which, to first order, is also the amount of melt produced on cooling the same amount of solid A to the solidus of B. Thus, 3 g of A must be cooled to the solidus of B in order to melt the B component by an additional 75 percent, such that it would be completely molten. So for $\phi_B^0 = 0.25$, the pressure at which B would reach 100 percent melting is that at which a source composed only of B reaches 25 percent melting. Similarly, if the pressure decrement is such that the B component reaches 50 percent melting in the first step of the process, an equal amount of A must be cooled to melt the remainder of the B component, and so forth. So the pressure interval required for complete melting of the B component can be approximated by $\phi_B^0\Delta P_B$; this is only an approximation since it assumes that the productivity is constant, which we know not to be the case (see section 6). This is shown schematically in figure 29, where the pressure interval over which the isentrope of the mixed system follows the solidus of B varies with the proportion of B.

10.2. Graphical Analysis of Fractional Fusion of Mixed Sources

It is also relatively simple to evaluate fractional fusion during decompression of a mixture of A and B by approximating the melting that occurs in each decompression step as an increment of isentropic batch fusion as in the previous section, and then removing the melt prior to the next increment of decompression. We do this using

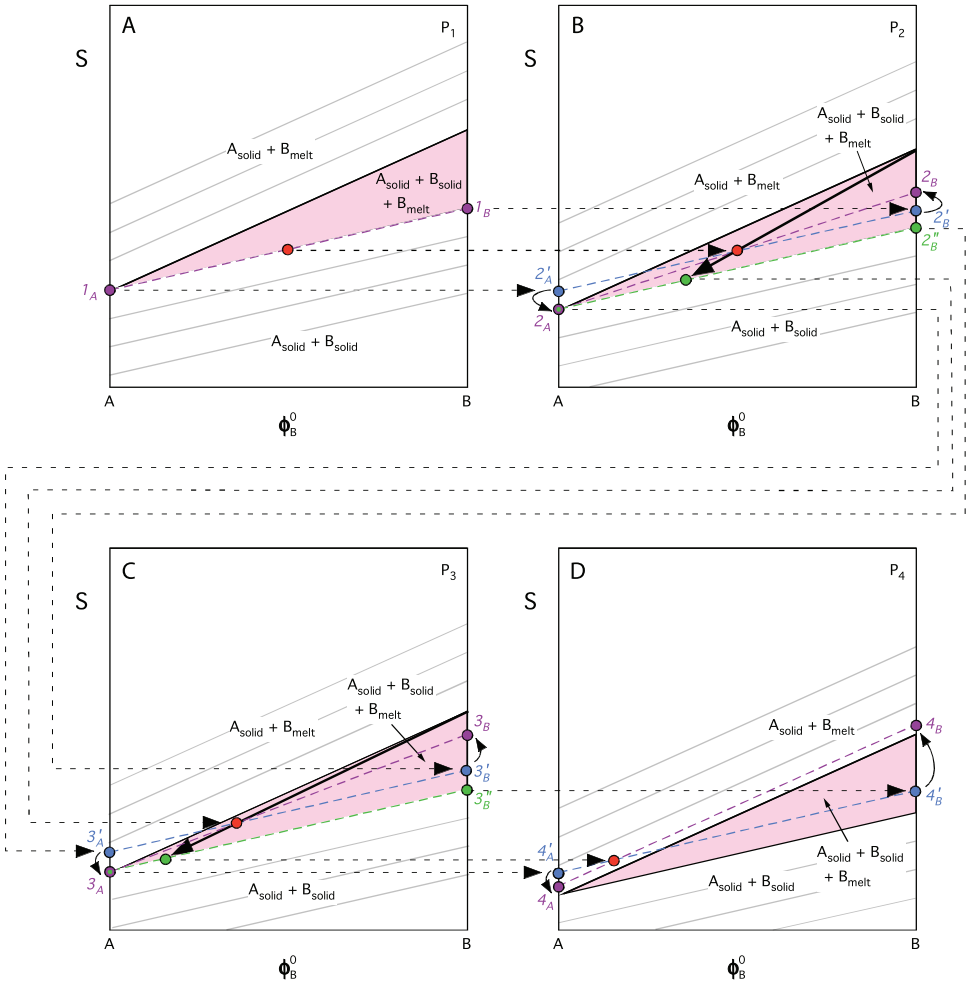

Fig. 30. The same sequence of four schematic isobaric S-ϕ_B^0 diagrams at progressively lower P ($P_1 > P_2 > P_3 > P_4$) shown in figure 28 applied to incrementally isentropic fusion of a mixed lithology system. The analysis differs from that of batch fusion developed using figure 28 in that after each decrement of pressure and thermal equilibration between A and B, the melt in the B part of the system is removed. This melt-removal step is illustrated by the heavy black arrows in panels (B) and (C). The S-ϕ_B^0 coordinates of the residue move to the solid A + solid B edge of the three-phase triangle [that is, to the green dots in (B) and (C)] and each progressive decompression steps operates on this residue rather than the initial bulk S-ϕ_B^0 point (that is, the red dot in panel (A), which remained fixed in each panel for analysis of batch melting in figure 28). See the text for a description of how such a sequence of S-ϕ_B^0 diagrams can be used to visualize and analyze quantitatively incrementally isentropic melting and incrementally isentropic fractional fusion of sources containing two one-component systems that interact thermally but not chemically.

figure 30, which shows from panels (A)→(D) the same series of schematic S-ϕ_B^0 diagrams at progressively lower pressures shown in figure 28.

The melting that occurs in the first decompression step from P_1 to P_2 is identical to that for batch fusion: (1) the model bulk source is represented in figure 30A by the red dot at 50 percent A and 50 percent B, and it is right at the solidus at P_1; (2) the system undergoes a reversible adiabatic decompression from P_1 to P_2 during which that part of the source that is A remains solid following an isentropic path from state 1_A (fig. 30A) to state $2'_A$ (fig. 30B), while that part of the source that is B partially melts by

25 percent following an isentropic path from state 1_B (fig. 30A) to state $2'_B$ (fig. 30B); and (3) we then allow an isentropic thermal equilibration of A and B at P_2 which results in the still solid component A decreasing in entropy from $2'_A$ to 2_A component B increasing in entropy from $2'_B$ to 2_B and increasing its melt fraction from 25 to 50 percent (fig. 30B). At this point, the fractional fusion path differs from that of batch fusion in that we remove the melt from the system. This is represented in figure 30B by the heavy black arrow extending from the liquid B apex of the three-phase triangle through the bulk composition represented by the red dot, leaving a residue on the solid A + solid B edge of the three-phase triangle (represented by the green dot). Assuming we have 100 g of A and B at the start of the process, after extraction of the partial melt (50% of the B part of the system, or 25 g) from the B component of the system, all that is left in the system is 50 g of solid A + 25 g solid B. This green dot representing the residue therefore plots at $\phi_B^0 = 0.33$ on the solid A (at 2_A) + solid B (at $2''_B$) edge of the three-phase triangle and has a lower entropy than the initial bulk composition.

The next step is an isentropic decompression of this residue from P_2 to P_3, which can be followed on figures 30B and 30C. In this step, the A part of the system remains solid, going from 2_A to $3'_A$, and the B part of the system goes from $2''_B$ to $3'_B$, melting by an additional 25 percent. Note that the 25 percent increase in melting of the B component is the same as occurred for the equivalent step in the batch fusion example described using figure 28; this is dictated by the distance moved downward by the three-phase triangle in going from P_2 to P_3. However, as was the case for the simple analysis of incrementally isentropic fusion of a one-component system, the mass of B in the system decreases in the fractional fusion case and therefore the actual amount of melt in this increment is smaller than in the batch fusion case. In going from P_2 to P_3 for the batch fusion case, the 50 g of B melts by 25 percent, producing 12.5 g of melt, but for fractional fusion, only 25 g of B is left in the residue, so it only produces 6.25 g of melt in this step. The next step is isentropic thermal equilibration between the A and B parts of the system (shown graphically in panel (c) by the $3'_A \rightarrow 3_A$ and $3'_B \rightarrow 3_B$ changes to the A and B parts of the system) such that the equilibrium tie line between these two parts of the system is isothermal and passes through the bulk S-ϕ_B^0 coordinates of the bulk residue from the previous melting and melt extraction step (that is, shown as the red dot in fig. 30C). The amount of melting of the B component of the system again increases in this step, but with a crucial difference; whereas in the equivalent step at P_2 the A and B parts of the system had the same mass, in this case the mass of A is twice that of B. As a consequence, whereas previously, the amount of heat flowing from A to B was enough to generate an additional 25 percent melting (or 12.5 g, for the initial 100 g we are considering), in the fractional fusion case, the same amount of heat flows from A to B, generating the same 12.5 g of melt; but the 2:1 ratio of A to B means that this same 12.5 g of melt represents an additional 50 percent melting of the 25 g of B in the residue. Therefore, the total amount of melting of B in this step is 18.75 g of the 25 g in the source, amounting to 75 percent of the mass of B in the source at this point in the process; this is less than the total of 25 g of melt produced in the batch melting P_2 to P_3 step. The total amount of melt of B is thus the 25 g from the P_1 to P_2 step plus the 18.75 g from the P_2 to P_3 step, or 43.75 g of melt, equivalent to 87.5 percent melting of the 50 g of B in the source prior to melting at P_1; this is less than the 50 g of melt (that is, 100% melting) in the equivalent batch fusion example. It is, however, exactly the same amount of melt that would have been produced by the same two increments of incrementally isentropic fusion of a source made up only of B; that is, a 100 g source would generate 25g of melt (that is, 25% melting of the 100 g source) in the first step and 18.75 g (25% melting of the 75 g residue) in the second step, yielding the same 43.75 g (or 43.75% melting relative to the initial mass of the

source) as from the two increments of melting of the mixed source. As the final stage in the P_2 to P_3 step, we extract the 18.75 g of liquid B from the source; this step is shown by the black arrow in figure 30C, leaving a residue at $\phi_B^0 = 0.11$ (50 g of solid A and 6.25 g of solid B; the green dot) on the solid A + solid B edge of the three-phase triangle in this panel.

The final step is an isentropic decompression of this residue from P_3 to P_4, which can be followed on figures 30C and 30D. In this step, the A part of the system remains solid, going from 3_A to $4'_A$, and the B part of the system goes from $3''_B$ to $4'_B$, melting by an additional 25 percent (but producing only 1.56 g of melt). The next step is isentropic thermal equilibration between the A and B parts of the system, shown graphically in panel (D) by the $4'_A \rightarrow 4_A$ and $4'_B \rightarrow 4_B$ changes to the A and B parts of the system such that the equilibrium tie line between these two parts of the system is isothermal and passes through the bulk S-ϕ_B^0 coordinates of the bulk residue from the previous melting and melt extraction step (that is, the red dot in fig. 30D). The amount of melting of the B component of the system again increases in this step, but now the overwhelming mass of A relative to residual B resulting from the heat flow from A to B during this step (sufficient to melt 12.5 g of B) results in complete melting and then superheating of the remaining $<$ 5 g of B in the source. Finally, extraction of the remaining melt leaves a residue of pure A composition at point 4_A.

Although this sequence of isentropic decompression melting and thermal equilibration increments of a mixed lithology followed by melt extraction after each step has relatively large, finite pressure decrements and amounts of melting in each step, we can, as we did in section 5.2, easily apply it to continuous fractional fusion by making these pressure decrements infinitesimal. This analysis illustrates once again how relatively complex melting processes can be visualized and analyzed once the critical variables are identified and used to construct simple phase diagrams. The results of this analysis also highlight key similarities and differences between fractional and batch fusion for mixed lithology sources and between fractional melting in single and multilithological sources. The first is that just as for the batch melting mixed lithology case considered above in section 10.1, cooling of the A part of the system to the solidus of B results in a transfer of heat and entropy from A to B and an enhancement of melting of the B component relative to the case of fractional fusion of a single lithology source developed in section 5.2; for example, after the second increment of melting (at P_3), a source composed of B alone has melted only 43.75 percent, compared to the 87.5 percent of the B component for the mixed lithology. However, as we showed for the batch fusion of the mixed lithology, the total mass of melt generated by fractional fusion is the same whether the source is a mixed lithology or entirely the low-solidus component; that is, the melt fraction relative to the total mass of the source is the same for both cases. Moreover, the reason is also the same for both the batch and fractional fusion examples; that is, the entropy available to go into partial melting is related to the total mass that is cooled to the B solidus regardless of whether it is A and/or B that undergoes this cooling. The second important result is that the total amount of melt produced by fractional melting in such a mixed system is lower than that produced by batch fusion for precisely the same reason as in the single lithology case developed in section 5.2; that is, because of the progressively decreasing mass of the partially melting B component of the system. Finally, in contrast to incrementally isentropic fusion in single lithology systems, in which the source can never reach complete melting, incrementally isentropic fusion in a mixed lithology system will inevitably do so if the pressure interval over which partial melting occurs is large enough. The reason is simple given the example analyzed above with figure 30: The amount of B in the residue decreases progressively, so the amount of melt generated in the B component of the system in the first step of the two-stage process we have envisioned (that is, the

isentropic decompression of the two parts of the system without thermal equilibration) does go down progressively for our example; but the amount of A stays constant. Thus, although the amount of entropy released from A in cooling to the solidus of B in the second step of the process (that is, in the thermal equilibration step) also remains constant in our example[3], it is delivered to a progressively smaller amount of B, and thus although the mass of melt generated in the second step remains constant, the degree of melting (that is, the fraction of the remaining residue melted) in the second step becomes progressively larger and will eventually become so large that the B fraction of the system melts fully. We emphasize that this only occurs because of the thermal equilibration in the second step of the process. Note that B will melt 100 percent instantaneously as the pressure of the B solidus is crossed when the ratio of A to B is infinite whether the melting process is batch or fractional for essentially the same reason (see section 8.3).

10.3. Analytic Treatment of the Melting of Mixed Sources

It is straightforward to develop analytic expressions to describe the isentropic melting of a source comprising mixed one-component systems, and although they do not provide insights greater than those we have developed based on graphical analysis alone (at least with respect to the points we have chosen to emphasize), for completeness we present the relevant expressions for productivity of the same mixed A + B sources described earlier in this section. Phipps Morgan (2001) derived analytic expressions to describe the isentropic melting of mixed sources of arbitrary compositional complexity, and they reduce to our expressions with appropriate simplifications and approximations.

We first consider the case of batch melting of the B component (that is, the liquid does not escape from the source). We define the melt fraction, F, as the amount of liquid B divided by the total mass of B in the system[4]. The productivity for isentropic batch melting of a mixture of A and B is

$$-\frac{dF}{dP}=\frac{1}{\Delta S_{f,B}}\left\{\left[\overline{\frac{C_{P,B}}{T}}\left(\frac{dT}{dP}\right)_{2\varphi,B}-\overline{V_B\alpha_B}\right]+\frac{m_A^0}{m_B^0}\left[\frac{C_{P,A}^s}{T}\left(\frac{dT}{dP}\right)_{2\varphi,B}-V_A^s\alpha_A^s\right]\right\}. \qquad (25)$$

This is equation (55) derived in section 14.3. The notation and all of the parameters in this equation have been defined previously, with the exception that the subscripts A and B on C_P, α, and V refer to phases in the A and B parts of the system. If we assume that C_P and $V\alpha$ are the same for all phases in the system (that is, for solid A and solid and liquid B), equation (25) simplifies to:

$$-\frac{dF}{dP}\approx\left(1+\frac{m_A^0}{m_B^0}\right)\frac{1}{\Delta S_{f,B}}\left[\frac{C_P}{T}\left(\frac{dT}{dP}\right)_{2\varphi,B}-V\alpha\right]$$

$$=\frac{1}{\phi_B^0\Delta S_{f,B}}\left[\frac{C_P}{T}\left(\frac{dT}{dP}\right)_{2\varphi,B}-V\alpha\right]=\frac{1}{\phi_B^0}\left[-\left(\frac{\partial F_B}{\partial P}\right)_S\right], \qquad (26)$$

where $-(\partial F_B/\partial P)_S$ is the isentropic productivity of a source made up only of B [equation (14)]. Phipps Morgan (2001) obtained a similar result (his equation 19) that reduces to equation (26) for the case of a one-component system.

[3] Note that this will not in fact be constant; that is, the effect will be enhanced because the entropy transfer during the second step increases as the integral in equation (20) and this will typically increase with progressive decompression as T decreases and $(dT/dP)_{2\varphi}$ increases with progressive decompression; see section 7).

[4] Note that it is also possible to define the melt fraction relative to the total mass of the system (m_A^0 + m_B^0); this is done below.

Equation (26) is a very simple result. It states that for isentropically upwelling sources that are mixtures of two one-component materials with different solidi, the productivity of melting of the low-melting component is approximately the isentropic productivity of a source composed of the low-melting component alone, scaled by the reciprocal of the mass fraction of the low-melting component in the mixed source. In the limit of $\phi_B^0 \rightarrow 1$, the source consists only of B, and the productivity reduces to that of pure B. In the limit of $\phi_B^0 \rightarrow 0$, the productivity becomes infinite; this is the result developed in section 8.3 and shown in figure 18, where B melts entirely at a single temperature as the isentrope for solid A crosses the solidus of B. Equation (26) also confirms our result from the end of section 10.1 and shown in figure 29 that in the case of constant productivity (that is, the solidus and liquidus in P-S space are straight and parallel), the pressure interval over which B melts is simply that for a source composed of B scaled by ϕ_B^0. Note that the only approximations involved in deriving equation (26) were that C_P and $V\alpha$ are the same for all phases.

We can also define the melt fraction, $\tilde{F}$, as the amount of liquid B divided by the total mass of the system. In this case, $\tilde{F} = \phi_B^0 F$, and after differentiating this definition with respect to pressure and then substituting into equation (26), we obtain

$$\frac{d\tilde{F}}{dP} = \phi_B^0 \frac{dF}{dP} \approx \phi_B^0 \left[\frac{1}{\phi_B^0} \left(\frac{\partial F_B}{\partial P} \right)_S \right] = \left(\frac{\partial F_B}{\partial P} \right)_S . \tag{27}$$

This is equation (58) derived in section 14.3. Phipps Morgan (2001) obtained a similar result (his equation 20) that reduces to equation (27) for the case of a one-component system. Equation (27) demonstrates that when it is normalized to the total mass of the system, the productivity of the B component of the isentropically ascending mixed source is essentially unchanged from the isentropic productivity of a source consisting of the B component alone (again, the differences reflect only the generally small differences between C_P and $V\alpha$ of solid A and B and liquid B). This analytical result confirms our conclusion based on the graphical analysis: that is, although veins and pods of a component with a lower solidus temperature embedded in a component that remains unmelted produce liquid at a higher rate per unit mass in an increment of upwelling than a source consisting of the vein material alone, the total mass of melt from a given mass of the mixed source will be similar to that of a source consisting of the vein material alone, until the vein material is fully molten, at which point no more melt is produced until the solidus of the less fusible source component is reached. As emphasized above, to the degree that these insights from a one-component system extend to more complex mantle systems, this result signifies that although the chemical signature from melting of the vein material can reflect a high degree of melting relative to what would be expected for the same amount of upwelling of a homogeneous source, the actual total mass of melt generated will not be enhanced.

We finally present the expressions for fractional fusion of a mixed source. The complete expression for productivity of fractional fusion is

$$-\frac{dF^f}{dP} = \frac{1}{\Delta S_{f,B}} \left\{ \frac{m_B^s}{m_B^0} \left[\frac{C_{P,B}^s}{T} \left(\frac{dT}{dP} \right)_{2\varphi,B} - V_B^s \alpha_B^s \right] + \frac{m_A^0}{m_B^0} \left[\frac{C_{P,A}^s}{T} \left(\frac{dT}{dP} \right)_{2\varphi,B} - V_A^s \alpha_A^s \right] \right\}, \tag{28}$$

where the melt fraction for fractional fusion, F^f, is again defined as the amount of liquid B divided by the initial mass of B in the system and m_B^s is the remaining mass of solid B. This is equation (62) given in section 14.4. If we assume as in the equivalent derivation for the batch melting case that C_P and $V\alpha$ are the same for solid A and B, equation (28) simplifies to:

$$-\frac{dF^f}{dP} \approx \Delta S_{f,B}\left(\frac{m_B^s}{m_B^0}+\frac{m_A^0}{m_B^0}\right)\left[\frac{C_P^s}{T}\left(\frac{dT}{dP}\right)_{2\varphi,B} - V^s\alpha^s\right]$$
$$= \left(\frac{1}{\phi_B^0} - F^f\right)\left\{\frac{1}{\Delta S_{f,B}}\left[\frac{C_P^s}{T}\left(\frac{dT}{dP}\right)_{2\varphi,B} - V^s\alpha^s\right]\right\}. \quad (29)$$

Equation (29) is closely related to the expression for the productivity for incrementally isentropic fractional fusion of a source consisting only of component B [equation (15)]: that is, the $(1–F^f)$ term in equation (15) is replaced here by $(1/\phi_B^0–F^f)$. In the limit of $\phi_B^0 \rightarrow 1$, the source consists only of B, and the productivity reduces to that for fractional fusion of pure B [that is, equation (15)]. As ϕ_B^0 decreases, the productivity increases as the $(1/\phi_B^0–F^f)$ term increases. In the limit of $\phi_B^0 \rightarrow 0$, the productivity becomes infinite and B melts entirely at a single temperature as the isentrope for solid A crosses the solidus of B; this is the result developed in section 8.3, and it applies whether B melts by a fractional or a batch process [that is, equation (26) also has a $1/\phi_B^0$ term that goes to infinity as $\phi_B^0 \rightarrow 0$].

Although equation (29) is closely related to equation (15), these equations quantify a key difference between fractional fusion of mixed sources and that of homogeneous sources discussed at the end of section 10.2. The first factor in equation (29) is $(1/\phi_B^0 – F^f)$, whereas the equivalent factor in equation (15) is $(1- F^f)$. The important point is that $(1/\phi_B^0 - F^f) > 0$ at $F^f = 1$ and thus the productivity does not go to zero as the melt fraction goes to 1; this contrasts with the case of fractional fusion of a homogeneous source, for which $(1- F^f) \rightarrow 0$ as $F^f \rightarrow 1$ and thus the productivity also approaches zero as $F^f \rightarrow 1$. This difference means that whereas (as emphasized previously) a homogeneous source undergoing incrementally isentropic fractional fusion can never be melted completely by this process, a low-melting component embedded in a less fusible component will always fully melt given a sufficient amount of decompression. The reason for this difference is, as described above, that although the amount of melting of B in the first step of the two-stage process we envisioned in the previous section (that is, the isentropic decompression melting of B without thermal equilibration with the solid A) goes to zero as $F^f \rightarrow 1$ (that is, as the mass of the residue goes to 0), the amount of melting in the second step (that is, the thermal equilibration step between A and B) is independent of F^f and represents a constant increment for each pressure decrement and consequently will eventually lead to the complete melting of the B component.

Equation (29) is also closely related to the expression for productivity for batch fusion of a mixed source: that is, the $1/\phi_B^0$ term in equation (26) is replaced here by $(1/\phi_B^0 - F^f)$. Consequently, as for melting of a source consisting only of component B, fractional fusion is always less productive than batch fusion (except at $F^f = 0$, where equation (29) reduces to equation (26), such that as emphasized previously in the comparison of batch and fractional fusion, the productivities of these two processes are identical right at the solidus of B). However, when ϕ_B^0 is small, the effect of F^f on $(1/\phi_B^0 - F^f)$ is small, so the decrease in productivity of the fractional process relative to the batch process is not as large as in the case of a homogeneous source. We can estimate the overall impact of the lower productivity of fractional fusion on melt production by integrating the fractional and batch fusion expressions for a mixed source, as done previously for a homogeneous source [equation (11)]. The equivalent to equation (11) for a mixed source is

$$F^f = \frac{1}{\phi_B^0}\left[1 - \exp(-\phi_B^0 F)\right]. \quad (30)$$

When the low-melting component of a mixed source is completely melted by batch melting (that is, $F = 1$), $F^f = 0.63$, 0.79, and 0.95 for $\phi_B^0 = 1.0$, 0.5, and 0.1. Thus, when the amount of the low-melting component in the source (for example, as veins or pods) is less than several tens of percent, the difference in melt production between batch and fractional fusion is small.

We can also estimate the pressure interval required for complete melting of the low-melting component by fractional fusion. As described above, if the pressure interval over which a source composed of B alone goes from 0→100 percent batch melting is ΔP_B, the pressure interval required to melt fully by batch fusion component B from a mixed source is approximately $\phi_B^0 \Delta P_B$. Integrating the reciprocal of equation (29) (assuming the term in brackets on the right-hand side is a constant), we obtain that for fractional fusion, the pressure interval required to melt fully component B from a mixed source is $-\ln(1 - \phi_B^0)\Delta P_B$. For $\phi_B^0 = 0.9$, 0.5, and 0.1, the pressure interval required for complete melting of the low-melting component by fractional fusion is $2.3\Delta P_B$, $0.69\Delta P_B$, and $0.11\Delta P_B$. As expected, at low ϕ_B^0 the pressure interval is close to that for batch fusion, because the difference in productivity between these processes diminishes with decreasing ϕ_B^0. However, at high ϕ_B^0 the pressure interval can be greater than ΔP_B, which is not surprising since in the limit of $\phi_B^0 \rightarrow 1$ the pressure interval goes to infinity.

Finally, as we did above for batch melting, we can also define for fractional fusion the melt fraction, $\tilde{F}^f$, relative to the total mass of the mixed source. Differentiating $\tilde{F}^f = \phi_B^0 F^f$ [equation (57)] with respect to P and substituting equation (29) for dF^f/dP, we obtain

$$-\frac{d\tilde{F}^f}{dP} = -\phi_B^0 \frac{dF^f}{dP} \approx \left(\frac{m_B^0}{m_A^0 + m_B^0}\right)\left\{\frac{1}{\Delta S_{f,B}}\left(\frac{m_B^s}{m_B^0} + \frac{m_A^0}{m_B^0}\right)\left[\frac{C_P^s}{T}\left(\frac{dT}{dP}\right)_{2\varphi,B} - V^s\alpha^s\right]\right\}$$

$$= \left(\frac{m_B^s + m_A^0}{m_A^0 + m_B^0}\right)\left\{\frac{1}{\Delta S_{f,B}}\left[\frac{C_P^s}{T}\left(\frac{dT}{dP}\right)_{2\varphi,B} - V^s\alpha^s\right]\right\} = \frac{(1 - \tilde{F}^f)}{\Delta S_{f,B}}\left[\frac{C_P^s}{T}\left(\frac{dT}{dP}\right)_{2\varphi,B} - V^s\alpha^s\right]. \quad (31)$$

As for the case of batch fusion of a mixed source, when melt fraction is defined relative to the total mass of the mixed source, the productivity expression reduces to that of a homogeneous source (except for the approximation that C_P and $V\alpha$ are the same for solid A and B). Thus, although the low-melting component melts more than if it made up the entire source, and the liquids generated from it can have the chemical signatures of relatively high degrees of melting, the mass of liquid relative to that of the entire source is not enhanced. As emphasized previously, this is because the total mass of melt reflects the entropy balance done over the entire source; although the mixed source can concentrate melting into the low-melting component, when taken as a whole, an entropy balance of the entire source [for example, equation (20)] defines the total mass of melt that is produced.

11. ADVECTION OF HEAT BY ASCENDING MAGMAS

The final process we explore in this paper is illustrated schematically by the one-component T-P diagram shown in figure 31. Initially solid material (at point *0*) decompresses isentropically, and begins to melt when the isentrope intersects the solidus at point *1*(P_1, T_1). It then undergoes isentropic batch melting, following the solidus to point *2* [that is, from (P_1, T_1) to (P_2, T_2)]. At this point, we remove the melt from the residue, and the melt ascends separately to point *3* (P_3, T*) without interacting thermally. While the melt ascends isentropically to P_3, cooling very little because it is a single phase, the residue continues to melt and thus to cool as it ascends isentropically to point *4*, reaching P_3 at a lower temperature, T_3, than that of the melt

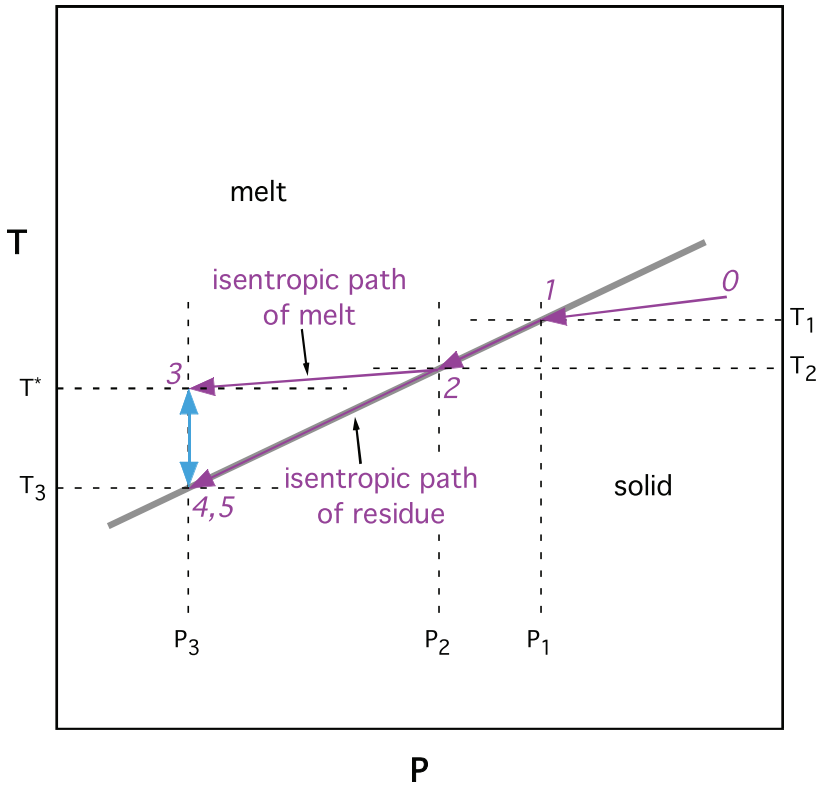

Fig. 31. Schematic P-T diagram for analyzing in a one-component system the advection of heat by ascending magma and how additional melting is induced in the residue if magma thermally interacts with it on ascent. A source at *0* begins to melt at *1*. At *2*, the partial melt and the residue are separated and each ascends isentropically (that is, to *3* and *4*, respectively). At this point, the superheated melt at *3* and the residue at *4* (which has melted further on ascent from *2*→*4*) interact thermally. During this interaction, the temperature of the melt decreases to the solidus, and the heat released is absorbed by the partially molten residue, leading to additional melting (although P-T coordinates of the final state of the melt + partially molten residue remain on the univariant solidus at P_3). This process is developed in more detail in the text and using figures 32 – 34. Point *5* refers to the state at P_3 of a source undergoing isentropic batch melting of a source starting at point *1* (that is, it differs from the above-described process in that melt and residue are not separated at point *2*).

that ascended separately. Note that the melt at (P_3, T*) is above its liquidus and is thus described as "superheated". If we now allow the superheated melt at (P_3, T*) and the partially molten residue at (P_3, T_3) to interact thermally, heat will flow from the melt to the residue, leading to additional melting of the residue; equilibrium is reached when the melt has cooled to T_3, at which point the melt and the partially molten residue are at the same temperature. This process is closely related to the melting of the mixed lithology (see section 10.1 and fig. 26) where solid A and partially melting B diverge thermally as they cross the solidus of B, but when they are reequilibrated, cooling of A to the solidus of B results in additional melting. And, as for the multilithology case, if the process is adiabatic and the pressure decrements are infinitesimal, the process can be approximated as reversible and isentropic; but if the pressure decrement is finite, adiabatic isobaric thermal reequilibration between melt and residue at P_3 is irreversible, and it proceeds at constant H with S increasing until it reaches a maximum.

This type of process is thought to be important in mantle igneous processes. In particular, if fractional fusion occurs (that is, melts are removed from their sources),

they will likely ascend in channels (Hart, 1993) or cracks (that is, dikes) (Nicolas, 1986; 1990) or by enhanced porous flow in high-permeability zones (Kelemen and others, 1997), and although under some circumstances it can be imagined that they will interact minimally with their surroundings on ascent, it is plausible that thermal and chemical interactions between ascending melt and residual mantle country rocks could be significant, particularly in the cases of porous flow or narrow channels. Indeed, chemical characteristics of some erupted basalts have been attributed to such interactions (Lundstrom and others, 1995), and some chemical and structural characteristics of mantle peridotites have been explained in these terms (Dick and Natland, 1996; Asimow, 1999; Lundstrom, 2000; Lundstrom and others, 2000]. For example, the occurrence of high-SiO_2 tholeiites in Hawaii has been explained by interaction between low-SiO_2 magmas from depth with depleted harzburgites or lherzolites near the base of the lithosphere (Eggins, 1992; Wagner and Grove, 1998; Stolper and others, 2004). And the elevated SiO_2 contents of a major class of lherzolite nodules from the Kaapvaal craton in South Africa have been explained by interactions between silica-rich melts from depth and overlying peridotites (Kelemen and others, 1992; Kelemen and others, 1998). Finally, dunite channels in ophiolites have been interpreted as high-permeability zones through which flow of melts from depth has been concentrated, and their olivine-rich nature is regarded as a consequence of the chemical and thermal interactions between melt and residue in a fashion similar to that described using figure 31 (Kelemen and others, 1995).

In natural, compositionally complex systems, these interactions will be both chemical and thermal, although the higher diffusivity of heat compared to chemical components means that there could be some cases in which melts and country rock could interact thermally with only minimal chemical interaction. Some of the most important aspects of this process in nature probably relate to the chemical interactions and in particular to the fact that the compositions of melt coexisting with lherzolites and harzburgites tend to be more silica-rich at low pressure than at high pressure. Consequently, interaction at lower pressure between peridotite and superheated melt from depth will typically lead to resorption of pyroxene from the peridotite and precipitation of olivine, thereby making the melt more silica-rich so that it can come into equilibrium with the peridotite and at the same time generating pyroxene-depleted, olivine-enriched residues (for example, dunites such as are observed in ophiolite bodies). This aspect of the process cannot be modeled with a one-component system, but the thermal aspects can be, and this is the emphasis of this final section of the paper.

11.1. Isentropic Reequilibration of Melt and Residue

We first analyze the particular example shown in figure 31 by recasting it using the now familiar P-S diagram (fig. 32). The process can be readily visualized with this diagram: The solid source (point *0*) decompresses isentropically and begins to melt at point *1* (P_1, T_1), and isentropic batch melting of the source from P_1 to P_2 follows a vertical path through the solid + liquid field to point *2*. At (P_2, T_2), residual solid is on the solidus at point *6*, melt is on the liquidus at point *7*, and the melt fraction, F, can be read from the diagram using the lever rule. For the example we have shown, $F \approx 0.33$ at this point. If we now separate the solid and melt at P_2 and allow them to ascend separately down to P_3, they each follow distinct vertical paths: the residual solid continues to cross the solid + liquid field, and at P_3 it is represented by point *4* and composed of solid (at point *8*) and melt (at point *9*), and its degree of melting can be read from the diagram to be $F \approx 0.42$; the isentropically decompressed melt is at point *3* in the liquid field, and although it has cooled slightly on decompression (from T_2 to T*), it is well to the right of the liquidus and therefore superheated. The total amount of melt in the system (assuming 100 g of the original solid source) is ≈ 61 g (33 g of

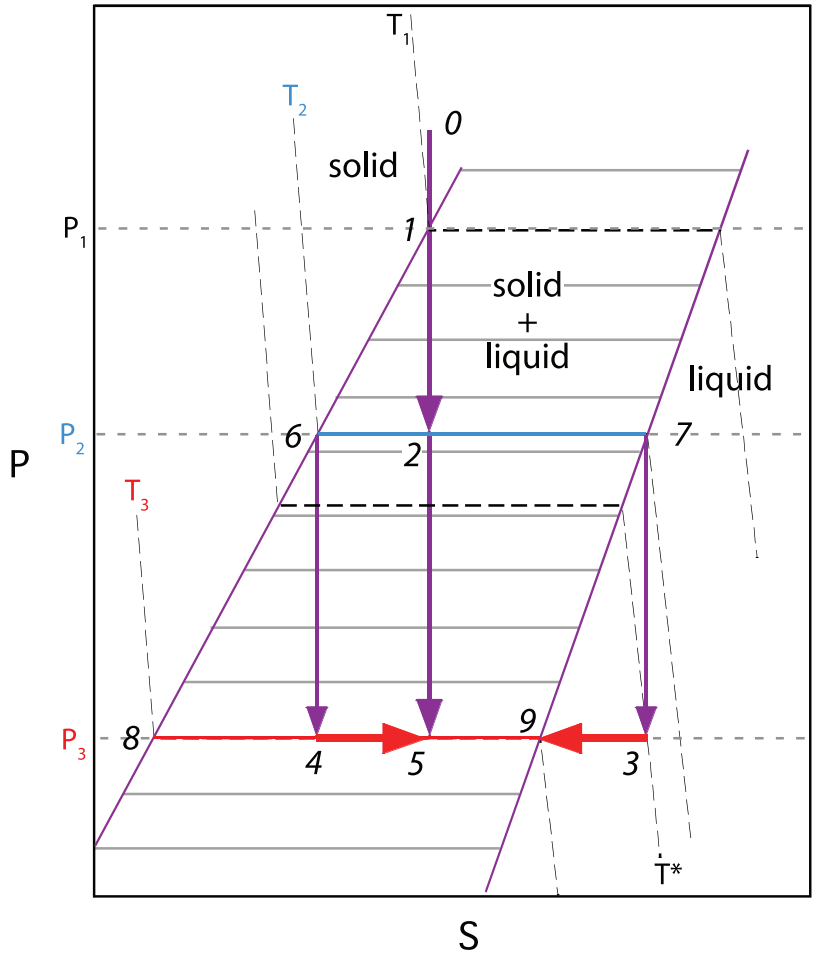

Fig. 32. Schematic P-S diagram for analyzing the advection of heat by ascending magma and how additional melting is induced in the residue if magma thermally interacts with it on ascent; this figure is a companion to figure 31 and considers the case in which the process is isentropic. Isotherms are shown at T_1, T_2, T_3, and T* as dashed black lines; isobars are shown at P_1, P_2, and P_3 as horizontal, dashed, light gray lines. As described for figure 31, the solid source at *0* decompresses isentropically and begins to melt at *1* (P_1). At *2* (P_2), it divides into solid residue (*6*) and melt (*7*). The residue decompresses isentropically from *6*→*4* (P_2→P_3), melting further in the process, resulting in solid at *8* and melt at *9*. The melt decompresses isentropically from *7*→*3* (also P_2→P_3); at *3* it is fully molten and at a temperature higher than the liquidus at the same pressure (that is, it is superheated). The thermal equilibration step at P_3 requires the melt at *3* to cool to the temperature of the liquidus (the left-pointing red arrow from *3*→*9*); if the process is isentropic, the entropy released on cooling the superheated melt to the liquidus is transferred to the residual solid at *8*, resulting in additional melting of the residue (the right-pointing red arrow from *4*→*5*). Note that the left- and right-pointing arrows differ in length because they represent changes in specific entropy, which depends on the relative masses of melt at *3* and residual solid at *8*. Note also that although the melt fraction of the residue increases as a result of this process, the total amount of melt in the system is the same as if the source had continued to melt isentropically from *2*→*5*, without the intermediate steps of melt-residue segregation, separate isentropic ascent, and isentropic reequilibration at lower pressure. See the text for further details.

melt at point *3* and 0.42 x 67 g ≈ 28 g at point *9*). Note that this is less than the amount of melting that the source would have at P_3 if melt and solid had not separated at P_2 (point *5*; F ≈ 0.71, or 71 g of melt); this is simply an example of the lower amount of melting for incremental isentropic fusion relative to batch fusion analyzed in some detail in section 5.2 (see the discussion of fig. 9).

At P_3, we now allow the melt at T* to equilibrate thermally with the partially molten residue at T_3. As emphasized previously, since the process is adiabatic and isobaric, it should be treated as isenthalpic with an increase in entropy. However, let us first consider an isentropic thermal equilibration; if we actually wanted to achieve this, we would have to extract heat from the system after bringing the two parts of the system into thermal equilibrium so as to keep the entropy constant. There are two different ways of thinking about this process using figure 32:

- The first is to realize that if we mix the two parts of the system back in the same proportions as when we separated them into states *6* and *7* at P_2 (that is, retrieving the same total entropy as we started with), the final state and total amount of melting will be the same as if we simply continued batch melting of the original, unseparated source. In other words, the thermally equilibrated isentropic system corresponds to point *5*, with residual solid at point *8* and all the melt at point *9* (rather than in two batches, at *9* and *3* prior to thermal equilibration). As stated in the previous paragraph, the amount of melt can be read from the lever rule to be $F \approx 0.71$, higher that the total F of 0.61 prior to thermal reequilibration.
- The second approach is slightly different, although it leads to the same result. Here we focus on the entropy released on cooling the superheated melt from T* to the solidus at T_3. As we developed in connection with equation (20), the entropy released in this cooling step is $m_l \int_{T^*}^{T_3} (C_P^l/T)dT$, where m_l is the mass of liquid undergoing the cooling; this decrease in entropy of the superheated liquid is represented by the heavy, left-pointing arrow at P_3 in figure 32. Since the system is constrained to be isentropic, this entropy decrease in the melt must be accompanied by an increase in entropy of the residue, and this entropy increase generates additional melt, where the entropy consumed by this melting ($m_s \Delta S_f \Delta F$, where m_s is the mass of solid in the residue and ΔF is the amount by which this residual solid melts) is equal to that released on cooling of the superheated melt. This increase in entropy of the residue is represented by the heavy, right-pointing arrow at P_3 in figure 32. If the masses of solid and superheated melt prior to reequilibration were identical, the two arrows would be the same length, and they are indeed similar in this example because the mass of melt at *3* per 100 g of source (33 g) is similar to the mass of solid (39 g) at *8* prior to reequilibration. However, if the masses are very different, the arrows will differ according to their ratio; for example, if the mass of melt is 1/10 of the unmelted residue, the length of the left-pointing arrow will be 10 times that of the right-pointing arrow. The importance of this second approach is that it emphasizes that the additional melting in this process is driven by the entropy transferred from melt to residue on cooling of the melt to the solidus and is proportional to the entropy of fusion (weighted by the ratio of the masses of the superheated melt and unmelted residue). However, the end point must in this case come precisely to the same amount of melting as would be achieved by isentropic batch melting of the original source.

This example highlights two important points. The first is that, as expected, when the ascending melt and country rock equilibrate thermally at low pressure, additional melt is generated, and the amount can be calculated by balancing the entropy released on cooling of the melt and absorbed by melting of the solid. The second is that if the residue is, as we have constructed in this case, derived from the source of the ascending melt and the system is isentropic, the extra melting at high levels equals the deficit in melting related to the decrease in mass of the source due to extraction of melt at depth. So in a system obeying these rules, although the advection of heat will indeed produce enhanced melting at lower pressures, in effect exaggerating even further the

progressive increase in productivity with decreasing pressure emphasized in section 6.1, it will not lead to extra melt flux from the top of the magmatic system. Thus, as with the case of a multilithologic mantle considered in section 10, if the system is isentropic, although entropy can be distributed in interesting ways — leading to extra melting of the low-solidus component at high pressure but less melting of the high-solidus component at low pressure in that case, or extra melting at low pressure and less melting at high pressure in this case — the amount of melting is fixed by the balance of entropy release on cooling and the entropy of fusion of the solid, and to the degree that they are not highly variable in mantle materials, this constraint is hard to violate in the absence of significant irreversible entropy production.

Under what conditions might the isentropic approximation developed in this example be appropriate? As we have emphasized previously, if the pressure decrements become infinitesimal, these processes can approach true reversibility. So, if the process described in figure 31 and figure 32 applied over an infinitesimal pressure decrement, the isentropic approximation would be valid, but in effect, this is just another way of describing batch melting, since the melt and solid effectively move upward together, reaching equilibrium at each step. But any process involving relative motion of melt and solid will also satisfy this requirement of being capable of being broken up into infinitesimal equilibrium steps, in each of which entropy is conserved, provided that the melt and solid are always in local equilibrium. Consider, for example, an idealized system in which after an infinitesimal isentropic increment of melting, the melt is removed from the residue and placed adjacent to it in a pipe. If the melt moves up in the pipe at the same speed as the residue, thermally equilibrating in each increment of ascent, then there is no entropy production and we simply reproduce batch fusion again. But even if the melt moves more rapidly than the solid and all the melt at each step is collected into the pipe (that is, true fractional fusion), as long as the residue and the melt in the adjacent pipe are in thermal equilibrium at each depth, the total entropy flux up the column is unchanged, except for a term due to separation of different density fluids in a gravity field, which McKenzie (1984) and Asimow (2002) have analyzed and found to be negligible even in the infinite permeability limit. And thus, although quantities such as the average depth of melt production may change, the total amount of melt emerging from the column is unchanged for any such process. This relates to the point made in section 5.2 that simply removing the melt from the solid does not actually change the entropy of the system. If all parcels of melt are removed fractionally and travel upward separately and isentropically, then simply adding up the total entropy emerging from the top of the system yields the initial entropy entering the bottom of the system. If, instead of going all the way to the surface isentropically, we insist that all parcels of ascending melt equilibrate thermally with the residue continuously (that is, in infinitesimal increments) as they ascend, then each increment of melt production, ascent, and thermal equilibration can be treated as an isentropic step as we have done in figure 32. To the extent that all porous flow processes presumably maintain thermal equilibrium in all parts of the system, they can always be treated in this way.

This imposed conservation of entropy flux explains why treatments of steady-state, adiabatic ascending porous-flow melting columns have a flux and composition of melt emerging from the top of the column identical to that produced by isentropic batch melting (Ribe, 1985; Richter, 1986; Spiegelman and Elliott, 1993; Iwamori and others, 1995; Asimow and Stolper, 1999). Asimow and Stolper (1999) showed how this simplification could be used to study the process of melt focusing into reactive conduits through transformation of the bulk composition modeled as undergoing batch melting. This kind of analysis is more general in that any overall adiabatic system — whether one-, two-, or three-dimensional and either steady or time-dependent – can

be tracked using conservation of entropy for the whole system provided thermal equilibrium is achieved locally and instantaneously at all parts of the system. Spatial divergence of entropy flux can be balanced by changes in entropy density with time, leading to local variations in melt production, but total melt production from such a system will equal that of a system with equal entropy flux into the bottom boundary undergoing simple batch melting.

11.2. Isenthalpic Reequilibration of Melt and Residue

What if the process proceeds in finite increments such that the thermal equilibration step in figure 31 and figure 32 is truly irreversible? An example might be a case in which melt gets into cracks or conduits sufficiently large that thermal equilibration is not possible during ascent, but then ponds or reestablishes porous flow at shallow levels and consequently thermally reequilibrates irreversibly. In such a case, we need to treat the thermal equilibration step as isenthalpic rather than isentropic and to evaluate the effects of an increase in entropy on melt production. This is relatively simple in principle given the tools we have developed. Instead of the P-S diagram in figure 32, we consider instead the isobaric H-S construction shown in figure 33 (see figs. 2 – 5 and the associated discussion in section 4). At P_2, stable states of solid and liquid each are represented by concave up curves (remember that the slope of the curve is the temperature), and the coexistence of solid and liquid is represented by the common tangent to the two curves. As in figure 32, points *6* and *7* represent the H-S coordinates of coexisting solid and liquid at P_2. At P_3 there is another set of curves for stable solid and liquid, and points *8* and *9* represent coexisting solid and liquid at this pressure. Points *2* and *5* both have the bulk entropy of the model source we are considering, and this figure shows that this source is partially molten on isentropic decompression melting at both P_2 and P_3.

In the process we envision, at P_2 the system divides into liquid and solid that decompress separately and isentropically to P_3, as illustrated in figure 34. The decompression of the residual solid is represented by the vertical arrow from point *6* to point *4*, which is the equilibrium (that is, minimum H) assemblage of the residue at P_3 on the tie line between coexisting solid (point *8*) and melt (point *9*) at T_3. As we read from the equivalent decompression in figure 32, the lever rule can be applied to this diagram as well to determine that the degree of melting of the residue at P_3 is about 42 percent. Decompression of the liquid portion of the partially molten system from P_2 to P_3 is represented by the vertical arrow from point *7* to point *3*. The minimum H state for this part of the system at P_3 is homogeneous melt at point *3*, and the higher slope of the tangent to the curve at *3* relative to the tie line between points *8* and *9* indicates that the temperature of melt (T*) is higher than that of the solid + melt coexistence (T_3).

If we mix the melt at point *3* (T*) with the partially molten residue (point *4*) in their original proportions ($\sim$ 33:67), the mixture has H and S represented by point *10*. The equilibrium assemblage at constant entropy is that with minimum H at the value of S given by point *10*. This is point *5*, the same constant isentropic equilibrium assemblage with $\sim$ 71 percent melting that we analyzed in the previous section (that is, this is the same amount of melt that would have been obtained from a simple isentropic decompression, without the division into residue and melt at P_2). To evaluate the isenthalpic equilibrium state, we need to find the stable assemblage with the same H as *10* but with maximum S representing a stable assemblage. This is point *11*, to the right of *10*, at the same H but with higher S, on the solid + liquid tie line at P_3. The lever rule can again be used to determine the melt fraction of this assemblage, $\sim$ 80 percent. Although the amount of melt in this example is entirely arbitrary, the geometry of the diagram requires that the isenthalpic approximation has a higher melt fraction than the isentropic approximation.

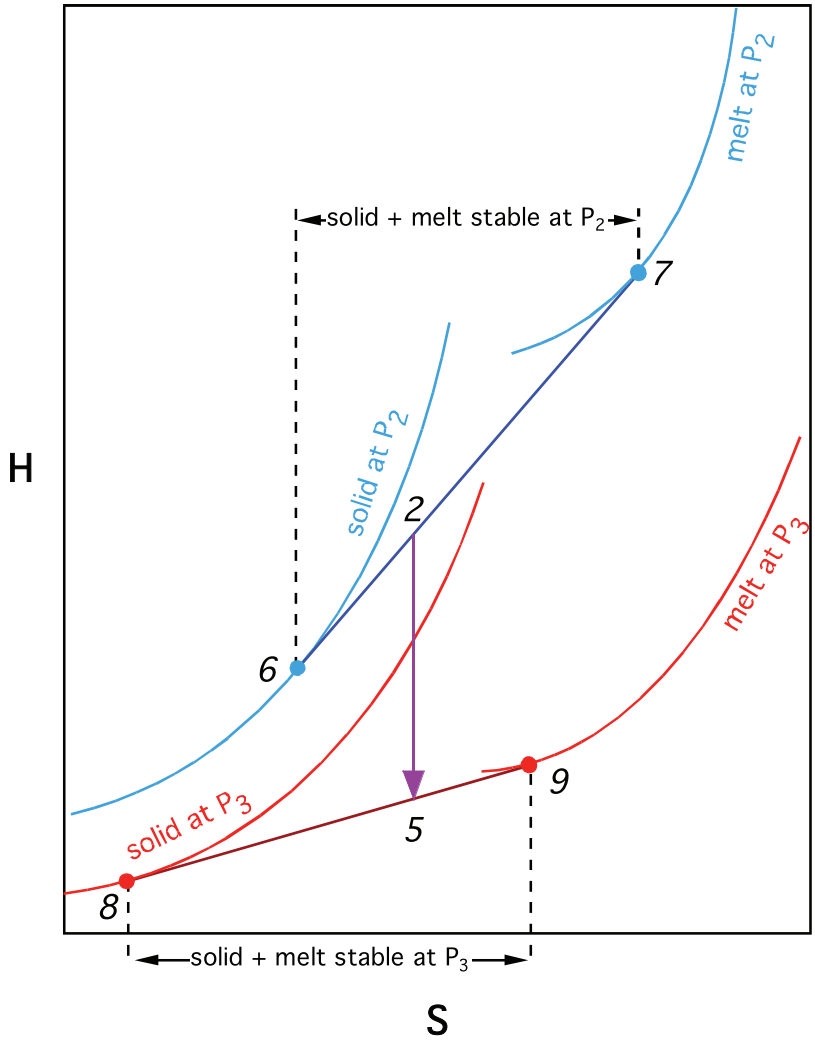

Fig. 33. Schematic H-S diagram (the curves are reproduced from figure 5; $P_2 > P_3$) for analyzing the advection of heat by ascending magma and how additional melting is induced in the residue if magma thermally interacts with it on ascent. This figure illustrates isentropic decompression from the partially molten state *2* at P_2 (with coexisting solid and melt at *6* and *7*) to the partially molten state 5 at P_3 (with coexisting solid and melt at *8* and *9*).

We can use the diopside one-component system used to construct figure 11 to estimate the actual difference between the isentropic and isenthalpic approximations to the thermal equilibration step in the process we have envisioned. We assume that the source is 20 percent partially molten at 30 kbar (~2026 K), and then decompress the melt and solid residue to 10 kbar. The temperature of the superheated melt at 10 kbar is ~1968 K, and the residue is at the 10 kbar solidus (~1807 K) and 30.0 percent molten. The system as a whole is 44.0 percent molten (20.0% superheated melt + 30.0% of the 80% residual source). We can now estimate the increased amount of melting either (1) by determining the total S or H in a 20:80 mixture of these two components and then, using the equivalent of figure 33, determine the equilibrium

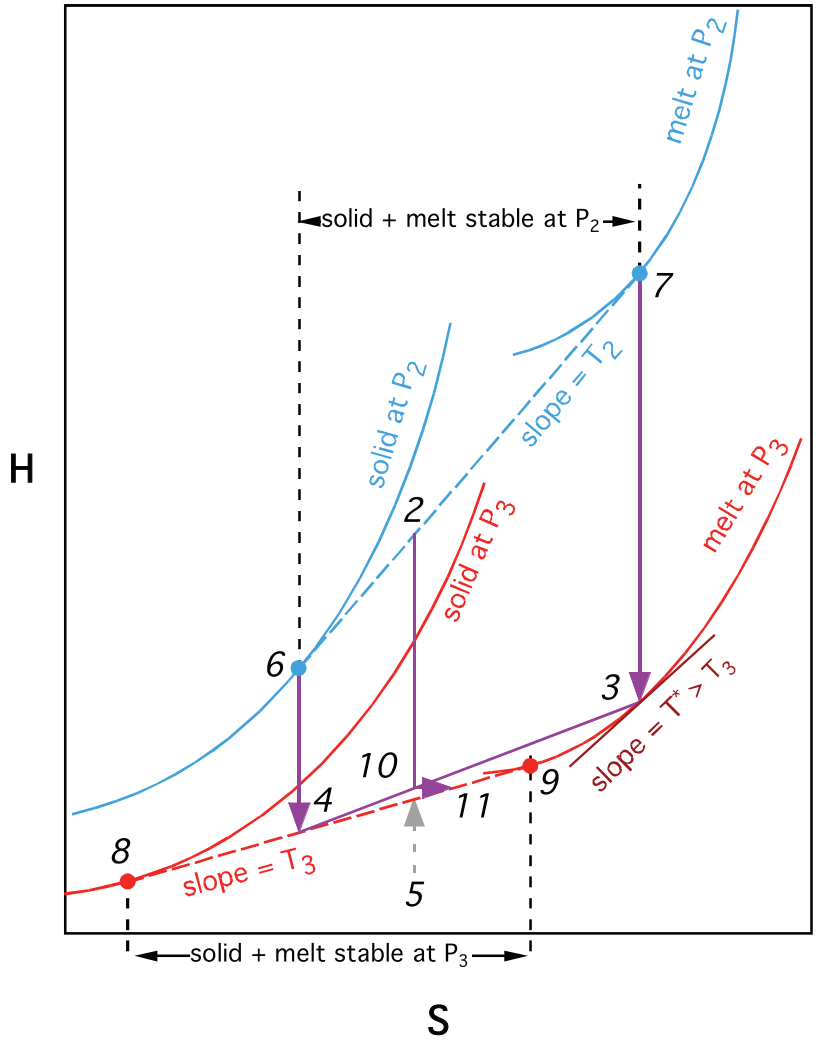

Fig. 34. Schematic H-S diagram for analyzing advection of heat by ascending magma and how additional melting is induced in the residue if ascending magma thermally interacts with it on ascent. State *2* at pressure P_2 is partially molten, consisting of coexisting solid residue at *6* and melt at *7*. As described in the text, segregated melt decompresses isentropically to P_3 on the path *7→3*, at which point the melt is superheated at temperature T*. Over the same pressure range, the residue decompresses isentropically on path *6→4*, at which point the residue consists of residual solid at *8* and melt at *9*, both at temperature $T_3 <$ T*. Mixing the partially molten residue (*4*) and superheated melt (*3*) back together at P_3 while conserving H and S yields point *10*. The isentropic equilibrium state for material at *10* is the one with the same value of S but minimum H; this is the same state *5* as shown in figure 33 — that is, this process (despite its intermediate steps of melt-residue segregation, separate isentropic ascent of melt and residue, and isentropic reequilibration at lower pressure) recovers the state and degree of partial melting for isentropic batch melting of the original source. In contrast, the equilibrium state at constant H for the mixture at *10* is reached via the horizontal arrow from *10→11*, which maximizes S for the fixed value of H. It is clear from this construction that isenthalpic thermal equilibration between melt at *3* and residue at *4* yields a higher melt fraction (at *11*) than an isentropic thermal equilibration (at *5*). See the text for details and for an estimate of the magnitude of the difference between melt fraction at *5* and *11*.

amounts of the melt and solid at 10 kbar; or (2) integrate either the entropy or enthalpy released on cooling the superheated diopside melt from 1968 K to 1807 K, and then, using either the ΔS_f or ΔH_f for diopside at 10 kbar, determine the amount of melting this entropy or enthalpy release will produce. The two approaches are, of course, equivalent. For the isentropic case, the total amount of melting increases by about 6.9 percent on thermal equilibration between superheated melt and residue to 51.0 percent. For isenthalpic melting, the total amount of melting increases by about 7.2 percent to 51.3 percent. Although the difference can be made larger or smaller by varying the initial amount of melting, the pressure drop between the initial or final states, or by focusing melt (that is, increasing the melt:residue ratio prior to reequilibration), this difference is small. Thus, although conceptually the difference between the isenthalpic and isentropic approximations is important, quantitatively, the entropy increase for the irreversibility represented by the isenthalpic process relative to the isentropic approximation (that is, to continuous, local thermal equilibrium at every stage of advection of heat by the ascending melt) is unlikely to be significant. McKenzie (1984) and Asimow (2002) reached similar conclusions in analysis of multi-component systems undergoing fractional fusion and porous flow: the additional melt production due to cooling the escaping melt into thermal equilibrium with the residue is negligible. McKenzie (1984) found this extra melt production to be negligible compared to the uncertainties in melting models (particularly due to poor constraints on the value and definition of the entropy of fusion of a multi-component system, Hirschmann and others, 1999a), whereas Asimow (2002) found it to be negligible compared to the chemically-driven difference between batch and fractional fusion in multi-component systems. Consequently, the generalizations from the end of the last section regarding the isentropic advection of heat by ascending magma are likely to be generally valid, and most importantly, although this process can redistribute melt production to lower pressures, it is unlikely to enhance significantly the melt production of ascending mantle. Note that we reached a similar conclusion in section 7, in which we compared the amount of melting resulting from isentropic conversion of metastable solid to a partially molten assemblage [using the entropy balance of equation (20)] to the amount of melting that results from an isenthalpic conversion [using the enthalpy balance of equation (19)]; that is, although the conceptual difference is important, the quantitative distinction between these two processes would generally be small.

12. FINAL COMMENTS

The larger goals of igneous petrology are to infer from study of igneous rocks (including observations such as their compositional variations in space and time; their volumes and distributions, regional contexts, and connections to geophysical and other geological patterns and phenomena; and their eruptive or emplacement mechanisms) how they formed and evolved and what this can tell us about processes and conditions in the earth's interior. This is a tall order given the necessity of integrating insights from physical chemistry, physics, and geology and the complexity and variability of the materials and processes involved. Increasingly, and appropriately, the discipline has been moving towards models of these processes that can capture ever more of the complexity and details of the characteristics of igneous rocks and therefore extract useful constraints on these processes by comparing observations with the output of these models. Thus, for example, efforts to understand compositional variations of magmas, whether due to variability of melting processes and sources or to higher level fractionation processes, are relying increasingly on computer programs that can model quantitatively the behavior of compositionally complex magmatic systems. The increasing utilization of the MELTS model and programs (Ghiorso and Sack, 1995; Ghiorso and others, 2002; Smith and Asimow, 2005), which are based on a

rigorous thermodynamic model of igneous systems, is an excellent example of this trend in igneous petrology.

This evolution of the discipline toward greater ability to model and understand the complexities of natural igneous systems is exciting and appropriate. But at the same time, it is important that we have simple, comprehensible frameworks for understanding these processes without having to refer at each step to the output of these complex models. For example, there may be patterns that emerge from such frameworks that allow the behaviors of complex systems to be relatively simply understood, systematized, and taught; and without these patterns the natural phenomena can become a bewildering array where almost anything seems possible simply by invoking ever more complexity. Likewise, there are certain "rules" that can be inferred from analysis of simple systems that could be difficult to tease out of or understand from study of more complex systems, and yet they carry over largely intact to such systems, and thus study of simple systems can provide the necessary framework for thinking about complex natural systems, can calibrate people's intuition on what is possible or likely, and can even in some cases prevent errors or incorrect generalizations or inferences.

The point of this paper has been to provide such a framework for thinking about partial melting of the earth's mantle based on phase equilibria in one-component systems. We have shown that when the independent variables are properly identified (that is, generally P-S or P-H) and phase diagrams are constructed based on this choice of variables, a wide range of insights into melting phenomena is possible. These include variations in the productivity of melting as a function of pressure, the differences between batch and fractional fusion, why the mantle partially rather than fully melts, the effects of solid-solid phase changes on melting, what to expect from melting of a mantle composed of more than one lithology, and the effects on melting of the advection of heat by ascending magmas. Some of these insights are surprising (such as the increase in productivity of melting of a parcel of mantle as it ascends, or the lower productivity of melting at most "cusps" on the solidus), yet are so readily understood and visualized with the appropriate phase diagrams in a one-component system that it is surprising in hindsight that they are not basic parts of the lexicon of igneous petrology that have been known for a long time. And even things that are well known, such as the lower productivity of fractional fusion relative to batch fusion, can be more clearly explained and visualized than has been previously possible. To be sure, as we have emphasized frequently, there are key aspects of these processes that are not captured fully (if at all) in a one-component system. Interestingly, although it is important to explore each of these phenomena using programs such as MELTS to understand the extent to which the insights from analysis of one-component systems carry over to complex natural systems, it can be shown that many of these additional complexities only require going to binary systems to illustrate the importance of additional components (Asimow and others, 1995, 1997; Hirschmann and others, 1999b; Smith and others, 2003). The key point, however, is that many of the insights from one-component systems presented here apply to a large extent to natural systems and therefore do indeed provide a framework for thinking about and understanding such systems.

The reason for the success of the one-component system analysis as a framework for understanding many aspects of melting in more complex natural systems is a relatively simple one, and we conclude by reemphasizing it. The key to the treatment we have presented is the identification of the independent variables in the melting process: If the process of decompression melting can be approximated as adiabatic, and if it proceeds reversibly (that is, if it can be broken up into a series of infinitesimal equilibrium steps), then the independent variables are specific entropy, S, and

pressure, P, and the equilibrium state is one in which for a given choice of S and P, the specific enthalpy, H, reaches a minimum. This statement is true regardless of the compositional complexity of the system, and thus the insights that derive from this choice of variables will be largely independent of the number of components in the system. And as we have emphasized, many of the critical insights do indeed derive from this choice of independent variables (rather than the more familiar choice of P and T and the achievement of minimum G at equilibrium). Basically, the problem reduces to partitioning an overall fixed amount of entropy among the various phases in the system at a given pressure in such a way that enthalpy is minimized. In a one-component system, there is usually a liquid phase and a single solid phase (although several of the examples we considered had an additional solid), and only a small number of thermochemical parameters (that is, those required to specify H as a function of S and P) are needed for each phase to solve for the system's equilibrium state, which can be fully characterized by its T and the proportions of solid(s) and liquid for the given choice of P and S. In more compositionally complex systems, there are usually more phases and most are compositionally variable, so determination of the equilibrium state for a given S, P, and bulk composition of the system requires distribution of more than a single chemical component among the various phases so as to minimize H, and characterization of the equilibrium state requires the compositions of all the phases in addition to T and their proportions. However, despite this greater complexity, the problem is still the same one of distributing entropy and mass among the various phases at a given pressure so as to minimize enthalpy. The compositional effects can, of course, lead to interesting and important phenomena not present or anticipated by analysis of one-component systems, but it is the fact that it is fundamentally the same problem with the same key variables — whether the system has one, two, or n components — that leads to the robustness and utility of the analysis and insights into melting processes presented here for one-component systems and makes them such a useful framework for thinking about natural igneous systems and processes.

13. Acknowledgments

This manuscript is an outgrowth of various lectures and classes given by the authors over several years, including especially the Ingerson lecture of the Geochemical Society (1996), a series of Bateman lectures given at Yale (2005), and the Crosby lectures at MIT (2006) by EMS. We are particularly grateful to Marc Hirschmann for his many contributions to the material presented here over the past decade; to Paula Smith for her more recent help and advice; to Peter Reiners for suggesting that we put it together into a manuscript for publication in this journal; and to reviewers John Longhi and S. A. Morse for their helpful suggestions. Finally, EMS wishes to acknowledge Professor J.B. Thompson's influence on his thinking about many of the issues presented in this paper and particularly, as pointed out by S. A. Morse, Professor Thompson's "emphasis on the felicitous choice of thermodynamic variables in petrology, and in choosing the variable to fit the problem" and his use of P-S diagrams in his two remarkable Harvard courses, "Phase equilibrium in mineral systems" and "Metamorphism".

14. Appendix

14.1. Derivation of the Expression for Isentropic Productivity for Batch Melting in a One-Component System

There are several ways to derive the equation for isentropic productivity for batch melting in a one-component system. We provide here a simple one following Miller and others (1991). Verhoogen (1965) presented a similar, generic analysis for the progress of any univariant reaction in a one-component system undergoing isentropic decompression.

For a partially molten assemblage, we have the following expression for the total specific entropy of the system:

$$S = FS^l + (1 - F)S^s, \tag{32}$$

where S^l and S^s are the specific entropies of the liquid and solid phases and F is the mass fraction of melt. On differentiation, this becomes

$$dS = FdS^l + S^l dF + (1 - F)dS^s - S^s dF = FdS^l + (1 - F)dS^s + \Delta S_f dF. \tag{33}$$

The expressions for dS^l and dS^s in a one-component system can be obtained from their total differentials, taking T and P as the dependent variables. For dS^l the expression is:

$$dS^l = \left(\frac{\partial S^l}{\partial T}\right)_P dT + \left(\frac{\partial S^l}{\partial P}\right)_T dP = \frac{C_P^l}{T} dT - V^l \alpha^l dP, \tag{34}$$

The analogous expression for dS^s is

$$dS^s = \left(\frac{\partial S^s}{\partial T}\right)_P dT + \left(\frac{\partial S^s}{\partial P}\right)_T dP = \frac{C_P^s}{T} dT - V^s \alpha^s dP. \tag{35}$$

Because the solid + liquid assemblage is restricted to the univariant curve on which they coexist, we can replace dT in these equations with

$$dT = \left(\frac{dT}{dP}\right)_{2\varphi} dP. \tag{36}$$

Substitution of equations (34) - (36) into (33) and using $\overline{C_P} = FC_P^l + (1 - F)C_P^s$ and $\overline{V\alpha} = FV^l\alpha^l + (1 - F)V^s\alpha^s$ to indicate mean values, we obtain the following for the total specific entropy change:

$$dS = \left[\frac{\overline{C_P}}{T}\left(\frac{dT}{dP}\right)_{2\varphi} - \overline{V\alpha}\right] dP + \Delta S_f dF \tag{37}$$

Since the process is by definition isentropic, this entire expression must equal zero, so by rearrangement we obtain the following expression for productivity in a one-component system:

$$-\left(\frac{\partial F}{\partial P}\right)_S = \frac{1}{\Delta S_f}\left[\frac{\overline{C_P}}{T}\left(\frac{dT}{dP}\right)_{2\varphi} - \overline{V\alpha}\right] \tag{38}$$

This is the expression given as equation (14) in the text.

14.2. Derivation of the Expression for the Productivity of Incrementally Isentropic Fractional Fusion in a One-Component System

Asimow and others (1997) derived a single expression for the productivity of a one-component system that applied for batch fusion, fractional fusion, and what is often referred to as "continuous melting" (that is, where all melt above a certain critical melt fraction is removed continuously). We are concerned here only with fractional fusion, so the derivation is simpler, requiring only some minor manipulation of the relations presented in section 14.1 to account for the continuously changing mass of the residue undergoing increments of isentropic melting. As described in the text, we treat fractional fusion as a series of infinitesimal increments of isentropic batch fusion, after each of which the liquid is removed.

We define the initial, unmelted mass of the system as m_0 and the mass of solid in the source as m_s; m_0 is a constant, but m_s decreases continuously as melt is generated and instantaneously extracted from the source. If we define the melt fraction produced by fractional fusion, F^f, relative to m_0, we have

$$F^f = \frac{m_0 - m_s}{m_0} = 1 - \frac{m_s}{m_0}, \tag{39}$$

and since m_0 is a constant,

$$dF^f = -\frac{dm_s}{m_0}. \tag{40}$$

At any point in the process of fractional fusion, the mass of the source is simply m_s, the mass of solid, since all the liquid has been removed. Starting from such a point in the fractional fusion process, we can decrement the pressure on the source by an infinitesimal amount and use equation (38), the expression for

the melt production for an increment of batch melting, to determine the amount of melt produced. However, the increment in F calculated using equation (38) in this case is the amount of melt produced ($-dm_s$) relative to the current mass of the source (m_s). Thus, equation (38) can be rewritten as follows for this pressure decrement on the residual solid in the source region:

$$-\frac{dm_s}{m_s} = \frac{1}{\Delta S_f}\left[\frac{C_P^s}{T}\left(\frac{dT}{dP}\right)_{2\varphi} - V^s\alpha^s\right]dP \tag{41}$$

Multiplying both sides by m_s/m_0 and rearranging using equation (40), we obtain

$$-\frac{dm_s}{m_s}\left(\frac{m_s}{m_0}\right) = -\frac{dm_s}{m_0} = -dF^f = \left(\frac{m_s}{m_0}\right)\frac{1}{\Delta S_f}\left[\frac{C_P^s}{T}\left(\frac{dT}{dP}\right)_{2\varphi} - V^s\alpha^s\right]dP \tag{42}$$

Noting from equation (39) that $m_s/m_0 = 1 - F^f$, equation (42) can be rearranged to yield the following expression for the productivity of incrementally isentropic fractional fusion:

$$-\frac{dF^f}{dP} = \frac{(1 - F^f)}{\Delta S_f}\left[\frac{C_P^s}{T}\left(\frac{dT}{dP}\right)_{2\varphi} - V^s\alpha^s\right]. \tag{43}$$

This is the expression given as equation (15) in the text.

If we assume that C_P^s and $V^s\alpha^s = V^1\alpha^1$, the expressions in brackets on the right-hand sides of equations (38) and (43) are identical and thus at any given pressure

$$\frac{dF^f}{(1 - F^f)} = dF. \tag{44}$$

Assuming that fractional fusion and batch fusion start from the same initial point on the solidus in P-S space, we can integrate both sides of equation (44) from the solidus (that is, from $F = 0$ and $F^f = 0$) to obtain

$$F^f = 1 - \exp(-F), \tag{45}$$

where F and F^f are the melt fractions for isentropic batch fusion and incrementally isentropic fractional fusion after the same amount of decompression. This is equation (11) in the text.

14.3. Batch Melting of a Mixed Source

We consider the case of isentropic (that is, reversible and adiabatic) batch melting of a source composed of the B component (which partially melts) and the A component (which does not melt). The A and B components are assumed to interact thermally but there is no mass transfer between them. As described in the text (section 10.1), the process is broken into two steps. In the first step, each of the two components decompresses isentropically, without thermal equilibration with the other component (for example, $2_A \rightarrow 3'_A$ and $2_B \rightarrow 3'_B$ in going from P_2 to P_3 in fig. 26 and fig. 28). The temperatures of A and B are the same before the decompression, but after the decompression, the temperature of solid phase A has decreased by

$$dT_A = \frac{TV_A^s\alpha_A^s}{C_{P,A}^s}\,dP, \tag{46}$$

while the temperature of component B, which is a mixture of solid and liquid and is thus confined to the solid + liquid univariant curve for B, has decreased according to

$$dT_B = \left(\frac{dT}{dP}\right)_{2\varphi,B} dP, \tag{47}$$

where $(dT/dP)_{2\varphi,B}$ is the slope of the solidus of B. Throughout this section, the subscripts A or B refer to the component of the source to which the properties apply if they differ for the two components. We define the melt fraction, F, as the amount of liquid B divided by the total mass of B in the system, such that

$$1 - F = \frac{m_B^s}{m_B^0}, \tag{48}$$

and

$$dF = -\frac{dm_B^s}{m_B^0}. \tag{49}$$

Note that it is also possible to define the melt fraction relative to the total mass of the system ($m_A^0 + m_B^0$); this is done below. The change in the amount of melt accompanying the isentropic decompression of B in this first step, dF′, is simply the previously derived isentropic productivity [equation (38)] times the size of the pressure decrement, dP:

$$dF' = \frac{dm_B^{s'}}{m_B^0} = -\frac{1}{\Delta S_{f,B}}\left[\overline{\frac{C_{P,B}}{T}\left(\frac{dT}{dP}\right)}_{2\varphi,B} - \overline{V_B\alpha_B}\right]dP, \tag{50}$$

where $\Delta S_{f,B}$ is the entropy of fusion of solid B at the solidus at this pressure and $dm_B^{s'}$ is the change in the mass of solid B during this first step.

In the next step, A and B equilibrate thermally at constant pressure and total entropy. The cooling of A from T_A to T_B (dT) results in a decrease in the entropy (note that this is the entropy, an extensive property, not specific entropy) of solid A from equation (20):

$$dS_A = m_A^0 \frac{C_{P,A}^s}{T}(dT_B - dT_A). \tag{51}$$

This entropy decrease in A is compensated by an entropy increase in B accommodated by an increase in the melt fraction. The entropy increase in B is given by

$$dS_B = \Delta S_{f,B}(-dm_B^{s''}) = \Delta S_{f,B}\left(\frac{-dm_B^{s''}}{m_B^0}\right)m_B^0 = \Delta S_{f,B}dF''m_B^0, \tag{52}$$

where dF″ is the increase in melt fraction due to the entropy transfer in this step, $dm_B^{s''}$ is the change in the mass of solid in B due to this entropy transfer, and $\Delta S_{f,B}$ is the entropy of fusion of solid B at the solidus at this pressure. Equating dS_A [equation (51)] and dS_B [equation (52)], and then substituting equations (46) and (47) for dT_A and dT_B, we obtain after minor rearrangement the following expression for the amount of melt generated in the second step:

$$dF'' = -\frac{C_{P,A}^s(dT_B - dT_A)}{T\Delta S_{f,B}}\frac{m_A^0}{m_B^0} = -\frac{C_{P,A}^s}{T\Delta S_{f,B}}\frac{m_A^0}{m_B^0}\left[\left(\frac{dT}{dP}\right)_{2\varphi,B} - \frac{TV_A^s\alpha_A^s}{C_{P,A}^s}\right]dP. \tag{53}$$

The total melt production on isentropic decompression of the A+B mixture is the sum of equations (50) and (53):

$$dF = dF' + dF'' = -\frac{1}{\Delta S_{f,B}}\left[\overline{\frac{C_{P,B}}{T}\left(\frac{dT}{dP}\right)}_{2\varphi,B} - \overline{V_B\alpha_B}\right]dP - \frac{C_{P,A}^s}{T\Delta S_{f,B}}\frac{m_A^0}{m_B^0}\left[\left(\frac{dT}{dP}\right)_{2\varphi,B} - \frac{TV_A^s\alpha_A^s}{C_{P,A}^s}\right]dP. \tag{54}$$

Upon rearrangement, we obtain the following expression for the productivity:

$$-\frac{dF}{dP} = \frac{1}{\Delta S_{f,B}}\left\{\left[\overline{\frac{C_{P,B}}{T}\left(\frac{dT}{dP}\right)}_{2\varphi,B} - \overline{V_B\alpha_B}\right] + \frac{m_A^0}{m_B^0}\left[\frac{C_{P,A}^s}{T}\left(\frac{dT}{dP}\right)_{2\varphi,B} - V_A^s\alpha_A^s\right]\right\}. \tag{55}$$

This is equation (25) in the text. If we assume that C_P and $V\alpha$ are the same for all phases in the system (that is, for solid A and solid and liquid B), equation (55) simplifies to:

$$-\frac{dF}{dP} \approx \left(1 + \frac{m_A^0}{m_B^0}\right)\frac{1}{\Delta S_{f,B}}\left[\frac{C_P}{T}\left(\frac{dT}{dP}\right)_{2\varphi,B} - V\alpha\right] = \frac{1}{\phi_B^0\Delta S_{f,B}}\left[\frac{C_p}{T}\left(\frac{dT}{dP}\right)_{2\varphi,B} - V\alpha\right] = \frac{1}{\phi_B^0}\left[-\left(\frac{\partial F_B}{\partial P}\right)_S\right], \tag{56}$$

where $-(\partial F_B/\partial P)_S$ is the isentropic productivity of a source made up only of B [equation (38)].

We also consider the productivity of melting in this same system if melt fraction is defined relative to the total mass of the system. We define $\tilde{F}$ as the total mass of liquid generated from B divided by the total mass of the system:

$$\tilde{F} = \frac{m_B^0 - m_B^s}{m_A^0 + m_B^0} = \frac{m_B^0}{m_A^0 + m_B^0}\frac{m_B^0 - m_B^s}{m_B^0} = \phi_B^0 F. \tag{57}$$

We differentiate equation (57) with respect to pressure and then substitute from equation (26) to obtain

$$\frac{d\tilde{F}}{dP} = \phi_B^0 \frac{dF}{dP} \approx \phi_B^0 \left[\frac{1}{\phi_B^0} \left(\frac{\partial F_B}{\partial P} \right)_S \right] = \left(\frac{\partial F_B}{\partial P} \right)_S . \tag{58}$$

This is equation (27) in the text.

14.4. Fractional Melting of a Mixed Source

We follow the same approach as in the previous section to evaluate the productivity of a mixed source region in which the low-melting component is undergoing incrementally isentropic fractional fusion. We again break each infinitesimal increment of isentropic decompression into two steps: in the first step, the two components, A and B, ascend isentropically without thermal equilibration; in the second step, the two components equilibrate thermally at constant entropy, after which all of the melt is removed from the system. Melt fraction, F^f, is defined relative to the initial mass of the B component:

$$1 - F^f = \frac{m_B^s}{m_B^0} . \tag{59}$$

This expression is analogous to equation (48) for batch melting.

Melt production in component B during the first step (dF') is the previously derived productivity for incrementally isentropic fractional fusion [equation (43)] times the size of the pressure decrement, dP, where we substitute equation (59) for ($1–F^f$) in equation (43):

$$dF' = - \frac{m_B^s}{m_B^0} \frac{1}{\Delta S_{f,B}} \left[\frac{C_{P,B}^s}{T} \left(\frac{dT}{dP} \right)_{2\varphi,B} - V_B^s \alpha_B^s \right] dP. \tag{60}$$

The amount of melt produced during the thermal equilibration step, dF'', is identical to that produced in the equivalent step for batch fusion of a mixed source [equation (53)], and the total melt production is given by the following equivalent to equation (54):

$$dF^f = dF' + dF'' = - \frac{m_B^s}{m_B^0} \frac{1}{\Delta S_{f,B}} \left[\frac{C_{P,B}^s}{T} \left(\frac{dT}{dP} \right)_{2\varphi,B} - V_B^s \alpha_B^s \right] dP - \frac{C_{P,A}^s}{T \Delta S_{f,B}} \frac{m_A^0}{m_B^0} \left[\left(\frac{dT}{dP} \right)_{2\varphi,B} - \frac{T V_A^s \alpha_A^s}{C_{P,A}^s} \right] dP \tag{61}$$

This simplifies to

$$- \frac{dF^f}{dP} = \frac{1}{\Delta S_{f,B}} \left\{ \frac{m_B^s}{m_B^0} \left[\frac{C_{P,B}^s}{T} \left(\frac{dT}{dP} \right)_{2\varphi,B} - V_B^s \alpha_B^s \right] + \frac{m_A^0}{m_B^0} \left[\frac{C_{P,A}^s}{T} \left(\frac{dT}{dP} \right)_{2\varphi,B} - V_A^s \alpha_A^s \right] \right\}. \tag{62}$$

This is equation (28) in the text.

15. References

Ahrens, T. J., 1987, Shock wave techniques for geophysics and planetary physics, *in* Sammis, C. G., and Henyey, T. L., editors, Methods of Experimental Physics: New York, Academic Press, p. 185–235.

Allègre, C. J., and Turcotte, D. L., 1986, Implications of a two-component marble-cake mantle: Nature, v. 323, p. 123–127.

Allègre, C. J., Hamelin, B., and Dupré, B., 1984, Statistical-analysis of isotopic ratios in MORB: the mantle blob cluster model and the convective regime of the mantle: Earth and Planetary Science Letters, v. 71, p. 71–84.

Asimow, P. D., 1999, A model that reconciles major- and trace-element data from abyssal peridotites: Earth and Planetary Science Letters, v. 169, p. 303–319.

——— 2002, Steady-state mantle-melt interactions in one dimension: II. Thermal interactions and irreversible terms: Journal of Petrology, v. 43, p. 1707–1724.

Asimow, P. D., and Stolper, E. M., 1999, Steady-state mantle-melt interactions in one dimension: I. Equilibrium transport and melt focusing: Journal of Petrology, v. 40, p. 475–494.

Asimow, P. D., Hirschmann, M. M., Ghiorso, M. S., O'Hara, M. J., and Stolper, E. M., 1995, The effect of pressure-induced solid-solid phase transitions on decompression melting of the mantle: Geochimica et Cosmochimica Acta, v. 59, p. 4489–4506.

Asimow, P. D., Hirschmann, M. M., and Stolper, E. M., 1997, An analysis of variations in isentropic melt productivity: Philosophical Transactions of the Royal Society of London A, v. 355, p. 255–281.

Asimow, P. D., Hirschmann, M. M., and Stolper, E. M., 2001, Calculation of peridotite partial melting from thermodynamic models of minerals and melts. IV. Adiabatic decompression and the composition and mean properties of mid-ocean ridge basalts: Journal of Petrology, v. 42, p. 963–998.

Basaltic Volcanism Study Project, 1981, Basaltic Volcanism on the Terrestrial Planets: New York, Pergamon Press, 1286 p.
Basu, A. R., Hannigan, R. E., and Jacobsen, S. B., 1998, Melting of the Siberian mantle plume: Geophysical Research Letters, v. 25, p. 2209–2212.
Ben Othman, D., and Allègre, C. J., 1990, U-Th isotopic systematics at 13°N East Pacific ridge segment: Earth and Planetary Science Letters, v. 98, p. 129–137.
Bergantz, G. W., 1989, Underplating and partial melting: Implications for melt generation and extraction: Science, v. 245, p. 1093–1095.
——— 1992, Conjugate solidification and melting in multicomponent open and closed systems: International Journal of Heat and Mass Transfer, v. 35, p. 533–543.
Bowen, N. L., 1928, The Evolution of the Igneous Rocks: Princeton, New Jersey, Princeton University Press, 334 p.
Boyd, F. R., and England, J. L., 1963, Effect of pressure on the melting of diopside, $CaMgSi_2O_6$, and albite, $NaAlSi_3O_8$, in the range up to 50 kilobars: Journal of Geophysical Research, v. 68, p. 311–323.
Campbell, I. H., and Griffiths, R. W., 1990, Implications of mantle plume structure for the evolution of flood basalts: Earth and Planetary Science Letters, v. 99, p. 79–93.
Cawthorn, R. G., 1975, Degrees of melting in mantle diapirs and the origin of ultrabasic liquids: Earth and Planetary Science Letters, v. 27, p. 113–120.
Chabaux, F., and Allègre, C. J., 1994, ^{238}U-^{230}Th-^{226}Ra disequilibria in volcanics: A new insight into melting conditions: Earth and Planetary Science Letters, v. 126, p. 61–74.
Dick, H. J. B., and Natland, J. H., 1996, Late-stage melt evolution and transport in the shallow mantle beneath the East Pacific Rise, *in* Mével, C., Gillis, K. M., Allan, J. F., and Meyer, P. S., editors: College Station, Texas, Ocean Drilling Program, Proceedings of the Ocean Drilling Program, Scientific Results, v. 147, p. 103–134.
Domb, C., 1996, The Critical Point: London, Taylor and Francis, Ltd., 376 p.
Eggins, S. M., 1992, Petrogenesis of Hawaiian tholeiites: 2. Aspects of dynamic melt segregation: Contributions to Mineralogy and Petrology, v. 110, p. 398–410.
Flower, M. J. F., 1981, Thermal and kinematic controls on ocean-ridge magma fractionation: contrasts between Atlantic and Pacific spreading axes: London, Journal of the Geological Society, v. 138, p. 695–712.
Galer, S. J. G., and O'Nions, R. K., 1986, Magmagenesis and the mapping of chemical and isotopic variations in the mantle: Chemical Geology, v. 56, p. 45-61.
Gallagher, K., and Hawkesworth, C. J., 1992, Dehydration melting and the generation of continental flood basalts: Nature, v. 358, p. 57-59.
Ganguly, J., 2005, Adiabatic decompression and melting of mantle rocks: An irreversible thermodynamic analysis: Geophysical Research Letters, v. 32, doi:10.1029/2005GL022363.
Ghiorso, M. S., and Sack, R. O., 1995, Chemical mass transfer in magmatic processes IV. A revised and internally consistent thermodynamic model for the interpolation and extrapolation of liquid-solid equilibria in magmatic systems at elevated temperatures and pressures: Contributions to Mineralology and Petrology, v. 119, p. 197–212.
Ghiorso, M. S., Hirschmann, M. M., Reiners, P. W., and Kress, V. C., 2002, The pMELTS: A revision of MELTS for improved calculation of phase relations and major element partitioning related to partial melting of the mantle to 3 GPa: Geochemistry Geophysics Geosystems, v. 3, doi:10.1029/2001GC000217.
Gibbs, J. W., 1961, The Scientific Papers of J. Willard Gibbs: New York, Dover Publications, 434 p.
Hart, S. R., 1993, Equilibration during mantle melting: A fractal tree model: Proceedings of the National Academy of Sciences, v. 90, p. 11914–11918.
Hauri, E., 1996, Major-element variability in the Hawaiian mantle plume: Nature, v. 382, p. 415–419.
Herzberg, C. T., and O'Hara, M. J., 2002, Plume-associated ultramafic magmas of Phanerozoic age: Journal of Petrology, v. 43, p. 1857–1883.
Hess, P. C., 1989, Origins of Igneous Rocks: Cambridge, Massachusetts, Harvard University Press, 336 p.
——— 1992, Phase equilibria constraints on the origin of ocean floor basalt, *in* Phipps Morgan, J., Blackman, D. K., and Sinton, J. M., editors, Mantle Flow and Melt Generation at Mid-Ocean Ridges: Washington, D. C., American Geophysical Monograph, v. 71, p. 67–102.
Hirschmann, M. M., and Stolper, E. M., 1996, A possible role for garnet pyroxenite in the origin of the "garnet signature" in MORB: Contributions to Mineralogy and Petrology, v. 124, p. 185–208.
Hirschmann, M. M., Baker, M. B., and Stolper, E. M., 1998a, The effect of alkalis on the silica content of mantle-derived melts: Geochimica et Cosmochimica Acta, v. 62, p. 883–902.
Hirschmann, M. M., Ghiorso, M. S., Wasylenki, L. E., Asimow, P. D., and Stolper, E. M., 1998b, Calculation of peridotite partial melting from thermodynamic models of minerals and melts. I. Methods and comparison to experiments: Journal of Petrology, v. 39, p. 1091–1115.
Hirschmann, M. M., Asimow, P. D., Ghiorso, M. S., and Stolper, E. M., 1999a, Calculation of peridotite partial melting from thermodynamic models of minerals and melts. III. Controls on isobaric melt production and the effect of water on melt production: Journal of Petrology, v. 40, p. 831–851.
Hirschmann, M. M., Ghiorso, M. S., and Stolper, E. M., 1999b, Calculation of peridotite partial melting from thermodynamic models of minerals and melts. II. Isobaric variations in melts near the solidus and owing to variable source composition: Journal of Petrology, v. 40, p. 297–313.
Hirschmann, M. M., Kogiso, T., Baker, M. B., and Stolper, E. M., 2003, Alkalic magmas generated by partial melting of garnet pyroxenite: Geology, v. 31, p. 481–484.
Hofmann, A. W., and Jochum, K. P., 1996, Source characteristics derived from very incompatible trace elements in Mauna Loa and Mauna Kea basalts, Hawaii Scientific Drilling Project: Journal of Geophysical Research, v. 101, p. 11831–11839.
Huppert, H. E., and Sparks, R. S. J., 1988a, Melting the roof of a chamber containing a hot, turbulently convecting fluid: Journal of Fluid Mechanics, v. 188, p. 107–131.

——— 1988b, The generation of granitic magmas by intrusion of basalt into continental-crust: Journal of Petrology, v. 29, p. 599–624.
Ito, G., and Mahoney, J. J., 2005, Flow and melting of a heterogeneous mantle: 1. Method and importance to the geochemistry of ocean island and mid-ocean ridge basalts: Earth and Planetary Science Letters, v. 230, p. 29–46.
Iwamori, H., 1998, Transportation of H_2O and melting in subduction zones: Earth and Planetary Science Letters, v. 160, p. 65–80.
Iwamori, H., McKenzie, D. P., and Takahashi, E., 1995, Melt generation by isentropic mantle upwelling: Earth and Planetary Science Letters, v. 134, p. 253–266.
Jackson, M. C., Frey, F. A., Garcia, M. O., and Wilmoth, R. A., 1999, Geology and geochemistry of basaltic lava flows and dikes from the trans-Koolau tunnel, Oahu, Hawaii: Bulletin of Volcanology, v. 60, p. 381–401.
Johnson, K. T. M., Dick, H. J. B., and Shimizu, N., 1990, Melting in the oceanic upper mantle: An ion microprobe study of diopsides in abyssal peridotites: Journal of Geophysical Research, v. 95, p. 2661–2678.
Kelemen, P. B., Dick, H. J. B., and Quick, J. E., 1992, Formation of harzburgite by pervasive melt/rock reaction in the upper mantle: Nature, v. 358, p. 635–641.
Kelemen, P. B., Shimizu, N., and Salters, V. J. M., 1995, Extraction of mid-ocean-ridge basalt from the mantle by focused flow of melt in dunite channels: Nature, v. 375, p. 747–753.
Kelemen, P. B., Hirth, G., Shimizu, N., Spiegelman, M., and Dick, H. J. B., 1997, A review of melt migration processes in the adiabatically upwelling mantle beneath oceanic spreading ridges: Philosophical Transactions of Royal Society of London A, v. 355, p. 283–318.
Kelemen, P. B., Hart, S. R., and Bernstein, S., 1998, Silica enrichment in the continental upper mantle via melt/rock reaction: Earth and Planetary Science Letters, v. 164, p. 387–406.
Kieffer, S. W., 1989, Geologic nozzles: Reviews of Geophysics, v. 27, p. 3–38.
Kieffer, S. W., and Delany, J. M., 1979, Isentropic decompression of fluids from crustal and mantle pressures: Journal of Geophysical Research, v. 84, p. 1611–1620.
Kinzler, R. J., and Grove, T. L., 1992, Primary magmas of mid-ocean ridge basalts 2. Applications: Journal of Geophysical Research, v. 97, p. 6907–6926.
Klein, E. M., and Langmuir, C. H., 1987, Global correlations of ocean ridge basalt chemistry with axial depth and crustal thickness: Journal of Geophysical Research, v. 92, p. 8089–8115.
Kogiso, T., and Hirschmann, M. M., 2001, Experimental study of clinopyroxenite partial melting and the origin of ultra-calcic melt inclusions: Contributions to Mineralogy and Petrology, v. 142, p. 347–360.
Kogiso, T., Hirschmann, M. M., and Reiners, P. W., 2004, Length scales of mantle heterogeneities and their relationship to ocean island basalt geochemistry: Geochimica et Cosmochimica Acta, v. 68, p. 345–360.
Kushiro, I., 1972, Determination of liquidus relations in synthetic silicate systems with electron probe analysis: The system forsterite-diopside-silica at 1 atmosphere: American Mineralogist, v. 57, p. 1260–1271.
Langmuir, C. H., and Bender, J. F., 1984, The geochemistry of oceanic basalts in the vicinity of transform faults: observations and implications: Earth and Planetary Science Letters, v. 69, p. 107–127.
Langmuir, C. H., Klein, E. M., and Plank, T., 1992, Petrological systematics of mid-ocean ridge basalts: Constraints on melt generation beneath ocean ridges, *in* Phipps Morgan, P., Blackman, D. K., and Sinton, J. M., editors, Mantle Flow and Melt Generation at Mid-Ocean Ridges: Washington, D. C., American Geophysical Union, Geophysical Monograph, v. 71, p. 183–280.
Lassiter, J. C., and Hauri, E. H., 1998, Osmium-isotope variations in Hawaiian lavas: Evidence for recycled oceanic lithosphere in the Hawaiian plume: Earth and Planetary Science Letters, v. 164, p. 483–496.
Lassiter, J. C., Hauri, E. H., Reiners, P. W., and Garcia, M. O., 2000, Generation of Hawaiian post-erosional lavas by melting of a mixed lherzolite/pyroxenite source: Earth and Planetary Science Letters, v. 178, p. 269–284.
Longhi, J., 1992, Origin of green glass magmas by polybaric fractional fusion: Proceedings of Lunar and Planetary Sciences Conference, v. 22, p. 343–353.
Lundstrom, C. C., 2000, Rapid diffusive infiltration of sodium into partially molten peridotite: Nature, v. 403, p. 527–530.
Lundstrom, C. C., Gill, J., Williams, Q., and Perfit, M. R., 1995, Mantle melting and basalt extraction by equilibrium porous flow: Science, v. 270, p. 1958–1961.
Lundstrom, C. C., Gill, J., and Williams, Q., 2000, A geochemically consistent hypothesis for MORB generation: Chemical Geology, v. 162, p. 105–126.
McKenzie, D. P., 1984, The generation and compaction of partial melts: Journal of Petrology, v. 25, p. 713–765.
McKenzie, D. P., and Bickle, M. J., 1988, The volume and composition of melt generated by extension of the lithosphere: Journal of Petrology, v. 29, p. 625–679.
——— 1990, A eutectic parameterization of mantle melting: Journal of Physics of the Earth, v. 38, p. 511–515.
McKenzie, D. P., and O'Nions, R. K., 1991, Partial melt distributions from inversion of rare earth element concentrations: Journal of Petrology, v. 32, p. 1021–1091.
——— 1995, The source regions of ocean island basalts: Journal of Petrology, v. 36, p. 133–159.
Miller, G. H., Stolper, E. M., and Ahrens, T. J., 1991, The equation of state of a molten komatiite 2. Applications to komatiite petrogenesis and the Hadean mantle: Journal of Geophysical Research, v. 96, p. 11849–11864.
Morse, S. A., 1994, Basalts and Phase Diagrams (reprint, with corrections): Malabar, Florida, Krieger Publishing Company, 493 p.
Natland, J. H., and Melson, W. G., 1980, Compositions of basaltic glasses from the East Pacific Rise and Siqueiros fracture zone, near 9°N: Initial Reports of the Deep Sea Drilling Project, v. 54, p. 705–725.
Nicolas, A., 1986, A melt extraction model based on structural studies in mantle peridotites: Journal of Petrology, v. 27, p. 999–1022.

——— 1990, Melt extraction from mantle peridotites: hydrofracturing and porous flow, with consequences for oceanic ridge activity, *in* Ryan, M. P., editor, Magma Transport and Storage: Chichester, John Wiley and Sons, p. 159–174.
Niu, Y., and Batiza, R., 1991, An empirical method for calculating melt compositions produced beneath mid-ocean ridges: Application to axis and off-axis (seamounts) melting: Journal of Geophysical Research, v. 96, p. 21753–21777.
Norman, M. D., Garcia, M. O., Kamenetsky, V. S., and Nielsen, R. L., 2002, Olivine-hosted melt inclusions in Hawaiian picrites: Equilibration, melting, and plume source characteristics: Chemical Geology, v. 183, p. 143–168.
Pertermann, M., and Hirschmann, M. M, 2003, Anhydrous partial melting experiments on MORB-like eclogite: Phase relations, phase compositions and mineral/melt partitioning of major elements at 2-3 GPa: Journal of Petrology, v. 44, p. 2173–2201.
Phipps Morgan, J., 2001, The thermodynamics of pressure-release melting of a veined plum-pudding mantle: Geochemistry Geophysics Geosystems, v. 2, doi:10.1029/2000GC000049.
Plank, T., and Langmuir, C. H., 1988, An evaluation of the global variations in the major element chemistry of arc basalts: Earth and Planetary Science Letters, v. 90, p. 349–370.
Presnall, D. C., 1969, The geometrical analysis of partial fusion: American Journal of Science, v. 267, p. 1178–1194.
——— 1980, A double partial-melt zone beneath mid-ocean ridges: Physics of the Earth and Planetary Interiors, v. 23, p. 103–111.
Presnall, D. C., and Gasparik, T., 1990, Melting of enstatite ($MgSiO_3$) from 10 to 16.5 GPa and the forsterite (Mg_2SiO_4) – majorite ($MgSiO_3$) eutectic at 16.5 GPa: Implications for the origin of the mantle: Journal of Geophysical Research, v. 95, p. 15771–15777.
Presnall, D. C., and Hoover, J. D., 1987, High pressure phase equilibrium constraints on the origin of mid-ocean ridge basalts, *in* Mysen, B. O., editor, Magmatic Processes: Physicochemical Principles: University Park, Pennsylvania, Geochemical Society Special Paper No. 1, p. 75-89.
Presnall, D. C., Dixon, J. R., O'Donnell, T. H., and Dixon, S. A., 1979, Generation of mid-ocean ridge tholeiites: Journal of Petrology, v. 20, p. 3–35.
Presnall, D. C., Gudfinnsson, G. H, and Walter, M. J., 2002, Generation of mid-ocean ridge basalts at pressures from 1 to 7 GPa: Geochimica et Cosmochimica Acta, v. 66, p. 2073–2090.
Prigogine, I., and Defay, R., 1954, Chemical Thermodynamics: London, Longmans, Green and Company, 543 p.
Prinzhofer, A., Lewin, E., and Allègre, C. J., 1989, Stochastic melting of the marble cake mantle: evidence from local study of the East Pacific rise at 12°50'N: Earth and Planetary Science Letters, v. 92, p. 189–206.
Qin, Z. W., 1992, Disequilibrium partial melting model and its implications for trace-element fractionations during mantle melting: Earth and Planetary Science Letters, v. 112, p. 75–90.
Ramberg, H., 1971, Temperature changes associated with adiabatic decompression on geological processes: Nature, v. 234, p. 539–540.
——— 1972, Mantle diapirism and its tectonic and magmagenic consequences: Physics of the Earth and Planetary Interiors, v. 5, p. 45–60.
Reiners, P. W., 2002, Temporal-compositional trends in intraplate basalt eruptions: Implications for mantle heterogeneity and melting processes: Geochemistry Geophysics Geosystems, v. 3, doi:10.1029/2001GC000250.
Ribe, N. M., 1985, The generation and composition of partial melts in the earth's mantle: Earth and Planetary Science Letters, v. 73, p. 361–376.
Richards, M. A., Duncan, R. A., and Courtillot, V. E., 1989, Flood basalts and hot-spot tracks: Plume heads and tails: Science, v. 246, p. 103–107.
Richter, F. M., 1986, Simple models for trace element fractionation during melt segregation: Earth and Planetary Science Letters, v. 77, p. 333–344.
Rigden, S. M., Ahrens, T. J., and Stolper, E. M., 1989, High pressure equation of state of molten anorthite and diopside: Journal of Geophysical Research, v. 94, p. 9508–9522.
Salters, V. J. M., and Hart, S. R., 1989, The hafnium paradox and the role of garnet in the source of mid-oceanic-ridge basalts: Nature, v. 342, p. 420–422.
Scott, D. R., and Stevenson, D. J., 1989, A self-consistent model of melting, magma migration and buoyancy-driven circulation beneath mid-ocean ridges: Journal of Geophysical Research, v. 94, p. 2973–2988.
Sigurdsson, H., 2000, The history of volcanology, *in* Sigurdsson, H., editor, Encyclopedia of Volcanoes: San Diego, Academic Press, p. 15–37.
Sisson, T. W., and Bronto S., 1998, Evidence for pressure-release melting beneath magmatic arcs from basalt at Galunggung, Indonesia: Nature, v. 391, p. 883–886.
Sleep, N. H., 1984, Tapping of magmas from ubiquitous mantle heterogeneities: An alternative to mantle plumes: Journal of Geophysical Research, v. 89, p. 10029–10041.
Smith, P. M., and Asimow, P. D., 2005, Adiabat_1ph: A new public front-end to the MELTS, pMELTS, and pHMELTS models: Geochemistry Geophysics Geosystems, v. 6, doi:10.1029/2004GC000816.
Smith, P. M., Asimow, P. D., and Stolper, E. M., 2003, Thermodynamic modelling of melting in chemically heterogeneous mixtures of peridotite and pyroxenite: Geochimica et Cosmochimica Acta, v. 67, p. A440.
Sobolev, A. V., Hofmann, A. W., and Nikogosian, I. K., 2000, Recycled oceanic crust observed in 'ghost plagioclase' within the source of Mauna Loa lavas: Nature, v. 404, p. 986-990.
Sobolev, A. V., Hofmann, A. W., Sobolev, S. V., and Nikogosian, I. K., 2005, An olivine-free mantle source of Hawaiian shield basalts: Nature, v. 434, p. 590–597.
Solomatov, V. S., and Stevenson, D. J., 1994, Can sharp seismic discontinuities be caused by nonequilibrium phase-transformations: Earth and Planetary Science Letters, v. 125, p. 267–279.

Sparks, D. W., and Parmentier, E. M., 1991, Melt extraction from the mantle beneath spreading centers: Earth and Planetary Sciences Letters, v. 105, p. 368–378.
Spiegelman, M., 1993, Flow in deformable porous media. Part 2: Numerical analysis — the relationship between shock waves and solitary waves: Journal of Fluid Mechanics, v. 247, p. 39–63.
Spiegelman, M., and Elliott, T., 1993, Consequences of melt transport for uranium series disequilibrium in young lavas: Earth and Planetary Science Letters, v. 118, p. 1-20.
Spiegelman, M., and Kenyon, P., 1992, The requirements for chemical disequilibrium during magma migration: Earth and Planetary Science Letters, v. 109, p. 611–620.
Stolper, E., Garcia, M., Seaman, C., Baker, M. B., and Sherman, S., 2004, Glass in the submarine section of the HSDP2 drill core, Hilo, Hawaii: Geochemistry Geophysics Geosystems, v. 5, doi:10.1029/2003GC000553.
Takahashi, E., and Nakajima, K., 2002, Melting processes in the Hawaiian plume: An experimental study, *in* Takahashi, E., Lipman, P. W., Garcia, M. O., Naka, J., and Aramaki, S., editors, Hawaiian Volcanoes: Deep Underwater Perspectives: Washington, D.C., American Geophysical Union, Geophysical Monograph, v. 128, p. 403–418.
Thompson, R. N., and Gibson, S. A., 2000, Transient high temperatures in mantle plume heads inferred from magnesian olivines in Phanerozoic picrites: Nature, v. 407, p. 502–506.
Turcotte, D. L., and Ahern, J. L., 1978, A porous flow model for magma migration in the asthenosphere: Journal of Geophysical Research, v. 83, p. 767–772.
Turner, S., Sandiford, M., and Foden, J., 1992, Some geodynamic and compositional constraints on postorogenic magmatism: Geology, v. 20, p. 931–934.
Turner, S., Arnaud, N., Liu, J., Rogers, N., Hawkesworth, C., Harris, N., Kelley, S., Van Calsteren, P., and Deng, W., 1996a, Post-collision, shoshonitic volcanism on the Tibetan plateau: Implications for convective thinning of the lithosphere and the source of ocean island basalts: Journal of Petrology, v. 37, p. 45–71.
Turner, S., Hawkesworth, C., Gallagher, K., Stewart, K., Peate, D., and Mantovani, M., 1996b, Mantle plumes, flood basalts, and thermal models for melt generation beneath continents: Assessment of a conductive heating model and application to the Parana: Journal of Geophysical Research, v. 101, p. 11503–11518.
Van Orman, J. A., Grove, T. L., and Shimizu, N., 1998, Uranium and thorium diffusion in diopside: Earth and Planetary Science Letters, v. 160, p. 505–519.
Verhoogen, J., 1954, Petrological evidence on temperature distribution in the mantle of the earth: Transactions of the American Geophysical Union, v. 35, p. 85–92.
——— 1965, Phase changes and convection in the Earth's mantle: Philosophical Transactions of the Royal Society of London A, v. 258, p. 276–283.
Waff, H. S., and Bulau, J. R., 1979, Equilibrium fluid distribution in an ultramafic partial melt under hydrostatic stress conditions: Journal of Geophysical Research, v. 84, p. 6109–6114.
Wagner, T. P., and Grove, T. L., 1998, Melt/harzburgite reaction in the petrogenesis of tholeiitic magma from Kilauea volcano, Hawaii: Contributions to Mineralogy and Petrology, v. 131, p. 1–12.
Waldbaum, D. R., 1971, Temperature changes associated with adiabatic decompression in geological processes: Nature, v. 232, p. 545–547.
Walker, D., Agee, C. B., and Zhang, Y., 1988, Fusion curve slope and crystal/liquid buoyancy: Journal of Geophysical Research, v. 93, p. 313–323.
Watson, S., and McKenzie, D., 1991, Melt generation by plumes: A study of Hawaiian volcanism: Journal of Petrology, v. 32, p. 501–537.
Wood, D. A., 1979, A variably veined suboceanic upper mantle - Genetic significance for mid-ocean ridge basalts from geochemical evidence: Geology, v. 7, p. 499–503.
Wyllie, P. J., 1988, Solidus curves, mantle plumes, and magma generation beneath Hawaii: Journal of Geophysical Research, v. 93, p. 4171–4181.
Zindler, A., Staudigel, H., and Batiza, R., 1984, Isotope and trace-element geochemistry of young Pacific seamounts: implications for the scale of upper mantle heterogeneity: Earth and Planetary Science Letters, v. 70, p. 175–195.